Investigating the Near-Infrared Properties of Planetary Nebulae II. Medium Resolution Spectra

Joseph L. Hora
Smithsonian Astrophysical Observatory, 60 Garden Street MS/65, Cambridge, MA 02138

William B. Latter
SIRTF Science Center/Infrared Processing and Analysis Center, MS 100-22, Caltech, Pasadena, CA 91125

Lynne K. Deutsch
Astronomy Department, Boston University, 725 Commonwealth Avenue, Boston, MA 02215

ABSTRACT

We present medium-resolution (R$\sim$700) near-infrared ($\lambda = 1 - 2.5$ μm) spectra of a sample of planetary nebulae (PNe). A narrow slit was used which sampled discrete locations within the nebulae; observations were obtained at one or more positions in the 41 objects included in the survey. The PN spectra fall into one of four general categories: H I emission line-dominated PNe, H I and H_2 emission line PNe, H_2 emission line-dominated PNe, and continuum-dominated PNe. These categories correlate with morphological type, with the elliptical PNe falling into the first group, and the bipolar PNe primarily in the H_2 and continuum emission groups. The catagories also correlate with C/O ratio, with the O-rich objects falling into the first group and the C-rich objects in the groups. Other spectral features were observed in all catagories, such as continuum emission from the central star, and warm dust continuum emission towards the long wavelength end of the spectra.

H_2 was detected in four PNe in this survey for the first time. An analysis was performed using the H_2 line ratios in all of the PN spectra in the survey where a sufficient number of lines were observed to determine the ortho-to-para ratio and the rotational and vibrational excitation temperatures of the H_2 in those objects. One unexpected result from this analysis is that the H_2 is excited by absorption of ultraviolet photons in most of the PNe, although there are several PNe in which collisional excitation plays an important role. The correlation between bipolar morphology and H_2 emission has been strengthened with the new detections of H_2 in this survey.

Subject headings: planetary nebulae: general – ISM: molecules – ISM: structure – infrared: ISM: continuum – infrared: ISM: lines and bands – molecular processes

1. Introduction

This is the second of two papers describing the results of surveys of the properties of planetary nebulae (PNe) in the near-infrared ($\lambda = 1 - 2.5$ μm). The first paper (Latter et al. 1995; hereafter Paper I) presented an infrared imaging survey; here we present the results of a near-infrared spectral survey.

There are several reasons why knowledge of the near-infrared (near-IR) characteristics of PNe is important, as described in Paper I. In order to interpret the imaging results, we must examine the spectra of these objects to understand the processes responsible for the emission. There are many emission lines present in the 1 - 2.5 μm spectral region, most notably those due to recombination lines of H I, and lines from vibrationally excited H_2. Also present are atomic lines of He I and [Fe II], and emission from other molecular species such as CO and C_2. These lines can act as diagnostic tools to probe the physical conditions inside the nebula, sampling different regions and ranges of temperature, density, and excitation than is seen by observing the optical line emission. Some PNe also exhibit strong continuum emission in the near-IR from hot dust. This emission becomes significant longward of $\lambda = 2$ μm in many of the PNe, requiring near-IR spectroscopy to detect it and to differentiate between line and continuum emission sources. Finally, the lower optical depth of the PNe in the IR as compared to optical wavelengths allows us to potentially see into regions of the nebula that are obscured by dust.

There have been several previous surveys that have explored the properties of PNe in the infrared. Early spectroscopic and photometric surveys (e.g., Gillett, Merrill, & Stein 1972, Cohen & Barlow 1974) determined that there was an excess of IR emission over what was expected from reflected continuum emission from the central star. Other photometric surveys in the following years (Whitelock 1985; Persi et al. 1987) determined the primary sources of IR emission to be stellar continuum, thermal dust emission, and thermal & line emission from the nebula itself. The near-IR color characteristics of most PNe are unique and can be used to identify new PNe and post-AGB objects (Garcia-Lario et al. 1990).

More recently there have been more detailed spectral observations of PNe in the near- IR. Hrivnak, Kwok, & Geballe (1994) surveyed a set of proto-PNe in the H and K bands. In these objects the H I Brackett lines were observed in absorption, and most objects had CO absorption or emission, indicating recent mass loss events. Rudy et al. (1992, and references therein) and Kelly & Latter (1995) have surveyed several PNe and proto-PNe in the $\lambda = 0.5 - 1.3$ μm range. Dinerstein & Crawford (1998) have completed a survey of a set of PNe in the K-band, focusing on excitation of molecular hydrogen.

There are several unique aspects of the survey results we present here that was made possible by the KSPEC spectrograph (see the instrument description below). First, because of KSPEC's high sensitivity and simultaneous sampling of the full spectral range, we were able to obtain data on a comparatively large number of objects (41) in a short period of time. Using the spectrograph's relatively narrow and short slit, we sampled different regions of the PNe to examine the emission throughout the nebula. In most of the other surveys described above, larger beams were used which included much or all of the object. Another aspect of the data presented here is that due to the cross-dispersed design of the instrument, the entire $\lambda = 1.1 - 2.5$ μm range is obtained at once, eliminating the possibility of telescope pointing errors or other fluctuations affecting the relative line strengths in the spectra. Finally, the slit-viewing detector allowed precise positioning and guiding, so the region of the PN being observed was well known for each spectrum. The PNe observed in this survey were chosen to overlap with the near-IR imaging survey (Paper I), along with several other optically-bright PNe and unresolved objects that were not included in the imaging survey.

2. Observations and Data Reduction

The observations were performed on several runs during the period 1992 October through 1994 September at the University of Hawaii 2.2m telescope on Mauna Kea, using the near-IR KSPEC spectrograph (Hodapp et al. 1994). KSPEC is a $\lambda = 1 - 2.5$ μm cross-dispersed spectrograph that has a separate slit-viewing IR array for acquiring the source and guiding. The full spectral range is obtained in a single exposure, resulting in accurate relative line measurements and highly efficient data acquisition. The diffraction orders are well- matched to the atmospheric transmission windows, with the K band in 3rd order (1.9 - 2.5 μm), H in 4th order (1.45 - 1.8 μm) and J in 5th order (1.15 - 1.32 μm). The 1×6 arcsecond slit

provides a small aperture that was used to sample different spatial regions of the nebula to search for spectral variations.

Table 1 lists the nebulae observed and details of the observations. Integration times for each exposure ranged from a few seconds for the extremely bright sources to 5 minutes for faint sources. The off-axis guider was used to keep a consistent on-source slit position. Multiple "Fowler" sampling was used to reduce the read noise. The number of samples for a particular integration ranged from 4 to 16, with more samples used for the longer integration times. The spectra were reduced using IRAF; the extraction and processing of the spectral data were done using the functions in the noao.twodspec and noao.onedspec packages. Alternating source and sky integrations of the same length were taken and differenced to remove sky and telescope background flux. Dome flats were used to correct for pixel-to-pixel gain variations in the array. Stars of known spectral type (either G0 or A0) were observed at the same airmass as the nebulae immediately before and after the PNe observations and were used for correction of the instrumental response and sky transmission. Individual lines were removed from the stellar spectra, and then normalized using a blackbody function of T = 5920 K for the G0 stars and T = 10800 K for the A0 standards. The spectra were wavelength-calibrated using observations of an Argon reference lamp. The wavelength values used for lines greater than 1.1 μm are from Rao et al. (1966); for lines less than 1.1 μm, the wavelengths were taken from Wiese, Smith, & Miles (1969) and corrected to vacuum wavelengths. The average 1σ error in the measured wavelengths of the lines is about 5 Å.

Infrared photometric standard stars were observed in the same way as the PNe and used to flux calibrate the spectra. Absolute calibration is difficult with these spectra because not all of the flux from the star enters the narrow slit during a single integration, and the amount differs for each integration depending on how well the star is centered on the slit (the seeing at 2 μm during typical observations was $0\farcs5$ – $1\farcs0$). The amount of light lost was estimated by the following method: the full width at half maximum (FWHM) brightness of the standard star was measured along the spatial direction of the slit, in the spectrum with maximum flux for that star. It was then assumed that the point spread function (PSF) is well represented by a two-dimensional Gaussian distribution with the measured FWHM, and the amount of flux falling outside of the slit was then calculated. This was typically 20 – 30% of the total light for a single integration. The calibration for each star was corrected by this factor, along with corrections for airmass. Comparing results from different standard stars taken throughout the night indicated that this method is accurate to approximately 20%. For the observations of the PNe, no correction was applied for the slit width. The length along the slit of the extracted regions was typically 3″ for point sources. For extended sources, there are overlapping regions of the spectral orders that cannot be properly extracted, so these regions were masked off. In these spectra, the extracted slit lengths were as follows for the three bands: $2\farcs0$ (J), $3\farcs5$ (H), and $4\farcs0$ (K).

3. Results

The spectra are presented in Figures 1 – 31. One to three PNe spectra are plotted in each figure. Various line identifications are given at the bottom of each plot. These are the same for all plots of a given PN spectral grouping (see below) for means of comparison; they do not necessarily indicate that the lines were detected in any or all of the spectra plotted in that figure. When several spectra are plotted in one figure, an offset was added and/or the spectrum was scaled by a constant to prevent overlap for clarity of display. The spectra are identified by the object name, and if several spectra of the same PN are shown, the position in the nebula is also indicated (see Table 1). The spectral data points between $\lambda = 1.32 - 1.42$ μm and 1.8 – 1.9 μm are in regions of poor atmospheric transmission and are not plotted. Tables 2, 3, and 4 list the line identifications and extracted fluxes.

The PNe spectra are separated into four groups that share common characteristics. These are H I recombination line-dominated, H I recombination line + H_2 emission, H_2 - dominated, and continuum-dominated. A fifth group of objects is included that contains two objects that were at one time classified as PNe, but are now generally regarded as being H II regions (M 1-78 and K4-45; Acker et al. 1992). We do not discuss these objects further, but include them for comparison. Within each group, the NGC objects are listed first, followed by the remaining PNe in alphanumeric order. The morphological classifications are given according to Balick (1987), unless otherwise noted.

3.1. H I - line dominated

The line emission in these PNe is dominated by lines of H I and He I. In the J-band, the Paschen β (Paβ) line is the most intense, with contributions from lines of He I, [Fe II], and O I. In the H band, the Brackett series of H I dominate, with emission from the 1.7002 μm line of He I and 1.6440 μm line of [Fe II] present in some PNe. In the K band, the brightest line is usually Brackett γ (Brγ), with strong lines of He I at 2.058 and 2.112 μm. When the H I lines are strong enough, one begins to see the Pfund series lines starting near 2.35 μm where they are just beginning to be separated at this resolution. There are also two unidentified infrared (UIR) lines at 2.199 and 2.287 μm (Geballe et al. 1991) that appear in several PNe in this category. (Note that these UIR lines are different from the broad near- and mid-IR UIR lines usually attributed to PAHs). A few of the spectra shown here have contributions from central star continuum flux that is larger towards shorter wavelengths, or warm dust continuum that gets stronger at longer wavelengths.

3.1.1. NGC 1535

NGC 1535 is classified as early round, and its near-IR spectrum is dominated by emission lines of H I. It has a bright ionized shell of emission which is surrounded by a fainter halo (e.g., see Schwarz, Corradi, & Melnick 1992). Near-IR images were presented in Paper I. This PN has previously been observed to have H_2 lines in absorption in the far-UV (Bowers et al. 1995). Recent observations by Luhman et al. (1997) failed to detect H_2 in emission in the $v = 1 \rightarrow 0$ S(1) line. They attribute the detection in absorption at shorter wavelength to the interstellar medium, or a region in the PN itself of a much smaller size than the ionized zone.

The spectrum of NGC 1535 shown in Figure 1 was obtained at a position centered on the brightest part of the ring directly W of the central star. We also fail to detect the H_2 emission in the $v = 1 \rightarrow 0$ S(1) line, at a 1 σ level of about 5×10^{-17} ergs cm^{-2} s^{-1} Å^{-1}. There is some indication of emission from the $v = 1 \rightarrow 0$ Q(1) and $v = 1 \rightarrow 0$ Q(3) lines at the long wavelength end of the spectrum. However, the spectrum is noisier in this region and the lines are not detected above the 3 σ level.

3.1.2. NGC 2022

NGC 2022 is an early elliptical PN, but is morphologically very similar to NGC 1535 in optical images (e.g., Schwarz et al. 1992). The main difference is a different relative outer halo size as compared to the inner ring (the halo is relatively smaller in NGC 2022). Zhang & Kwok (1998) also find similar parameters in their morphological fits of these two PNe. Near-IR images of this PN were presented in Paper I.

NGC 2022 is also spectrally similar to NGC 1535, as seen in Figure 1. The spectrum of NGC 2022 was taken centered on the ring directly E of the central star. The dominant lines are those of neutral hydrogen.

3.1.3. NGC 2392

The PN NGC 2392 (the "Eskimo nebula") is another double-shell nebula; however, this PN has a significant amount of structure in the inner ring and outer shell. Spectrophotometric (Barker 1991) and kinematical studies (Reay, Atherton, & Taylor 1983; O'Dell, Weiner, & Chu 1990) that have been carried out with optical imaging and spectroscopy have revealed the abundances and ionization states and the velocities of the various components. Near-IR images of this PN were presented in Paper I.

The spectrum of NGC 2392 in Figure 1 was taken centered on the brightest part of the ring directly E of the central star. This third early-type round PN differs from the other two in Figure 1 primarily from the bright He I line at 2.058 μm, and the [Fe II] lines in the J and H bands of the spectrum.

3.1.4. NGC 3242

NGC 3242 is an early elliptical with several interesting morphological features. In addition to the bright elliptical ring, there are several filaments and knots of emission in the central region, and two ansae that are placed roughly along the major axis of the elliptical emission. Also, there is a larger faint halo that envelopes the inner structure.

Spectra acquired at three different positions on the nebula are shown in Figure 2, on the SE knot (NGC 3242SE), on the E section of the bright ring (NGC 3242E), and on the SW halo (NGC 3242H). The spectra are similar in all locations; the bright H I lines are present in all positions, along with stellar continuum at the shorter wavelengths. One difference is that the

He II lines at 1.206 and 2.189 μm are much brighter in the E ring than in the SE knot or halo position.

3.1.5. NGC 6210

NGC 6210 is a fairly compact PN with a core/halo morphology similar to other ellipticals. Phillips & Cuesta (1996) performed a visible wavelength spectroscopic study that revealed a complex velocity structure which suggests multiple shells and possibly "jets" at various position angles. The near-IR image presented in Paper I does not reveal much of the structure. This PN is one of several in which Geballe et al. (1991) detected UIR emission at 2.286 μm (but not at 2.199 μm).

Three spectra are presented for this PN, and shown in Figure 3. They were acquired with the slit centered on the core (Core), 1″ east (E1), and 3″ east (E3). The core position shows a contribution from stellar continuum in the $\lambda = 1-1.8$ μm region that decreases successively in the E1 and E3 positions. The UIR feature at 2.287 μm is detected at the E1 position, but not the 2.199 line, similar to Geballe et al. (1991).

3.1.6. NGC 6543

NGC 6543 (the "Cat's Eye") has a complex morphology, with a high degree of symmetry. Recent HST imaging (Harrington & Borkowski 1994) has shown more clearly the structure of rings, shock fronts, jets, and fast, low-ionization emission-line regions (FLIERS) present in this PN.

The spectrum shown in Figure 4 was taken at the position S of the central star and slightly E, where the two emission arcs cross and create a local emission maximum (see Paper I). The spectra is similar to the other PN in the H I/He I – dominated class, and also show the unidentified lines at 2.199 and 2.286 μm.

3.1.7. NGC 6572

This young PN has a bipolar morphology in the near-IR, with its major axis in the N-S direction, and a bright ring structure closer to the central star (Paper I). The near-IR spectrum from 0.77 to 1.33 μm was measured by Rudy et al. (1991), and the UV and optical spectrum was recently obtained by Hyung, Aller, & Feibelman (1994), who found evidence of variability.

Figure 5 shows two positions in the PN, one on the nebula center, and one on the brightest location on the E lobe of the PN. Both the core and E lobe spectra show a strong contribution from stellar continuum flux. There is strong H I and He I line emission, and relatively strong unidentified line emission at 2.19 and 2.29 μm.

3.1.8. NGC 6790

This PN has been shown by radio continuum observations to be an elliptically-shaped nebula with a diameter on order of an arcsecond (Aaquist & Kwok 1990). Aller, Hyung, & Feibelman (1996) obtained UV and optical spectra and suggest that NGC 6790 is a relatively young object, slightly more evolved than Hb 12. Kelly & Latter (1995) obtained a 0.9 – 1.3 μm spectrum and find similarities to Hb 12 and AFGL 618.

The spectrum of NGC 6790 in Figure 4 shows a stellar contribution because the slit was centered on the object, and includes the star as well as the nebular emission that is typical of this class of PN.

3.1.9. NGC 6803

This compact elliptical PN has a uniformly bright disk with no apparent structure in the optical, surrounded by a fainter halo about twice the size of the bright shell (Schwarz et al. 1992). In the KSPEC imaging channel, however, the PN was seen to be double-lobed, with the lobes on the minor axis of the bright elliptical region. Spectra were obtained at two positions, one centered on the E lobe, and the other position 5 arcseconds NW in the halo region. The lobe spectrum shows bright H I and He I lines, with a stellar continuum contribution out to about 1.5 μm. There is also unidentified line emission at 2.286 μm. The halo spectrum is quite different, with weak Paβ and continuum emission, and is probably reflected star and nebular emission.

3.1.10. NGC 6826

This elliptical PN is morphologically similar to NGC 3242, with a bright elliptical inner ionized ring, ansae along the major axis, and a fainter halo that envelopes the system (Balick 1987). The I-band image in Paper I shows evidence for a shell between the inner bright ring and the outer halo, at the same diameter as the ansae.

The spectra are shown in Figure 7. The bright core is dominated by stellar continuum emission. The other positions are dominated by the H I lines. The spectrum labeled SW Lobe was taken on the inner

bright ring directly SW of the central star. The SW Halo position was taken in the halo midway between the bright ring and the outer edge of the PN. The lobe and halo emission is similar, except for relatively brighter lines of He I at 1.7002 μm in the lobe. There is also some continuum emission at the short wavelength end of the nebular positions, which is probably scattered light from the central star.

3.1.11. NGC 7009

NGC 7009 (the "Saturn" nebula) is an elliptical with an interesting twisted symmetry in its shell and in the various filaments and knots of emission. Balick et al. (1998) recently published HST images that show the "microstructures" in this PN. The images show that the inner knots are actually groups of FLIERs, and jets in [N II] are seen that terminate at the tips of the nebula.

Two positions were sampled, one in the E halo region on the edge of the PN, and one in the N part of the nebula. Both positions show a contribution from stellar continuum emission from the central star. The halo emission is similar to the spectrum taken on the north edge of the PN.

3.1.12. IC 351

This compact PN has a double-lobed structure with a round halo (Hua & Grundseth 1986; Aaquist & Kwok 1990; Manchado et al. 1996). Feibelman, Hyung, & Aller (1996) obtained UV and optical spectra of IC 351 that show it to be a high excitation nebula, but without the presence of the usual silicon lines, and suggest that the silicon atoms could be locked up in grains.

This spectrum suffers from an incomplete subtraction of OH lines, due to the sky frames not being taken properly for the on-source images. The OH lines show up in emission mainly in the H and K-band portions of the spectrum. However, the major features of H I and He I emission lines can be seen.

3.1.13. IC 418

The spectrum of this well-studied young, low-excitation PN was previously shown to be dominated in the near-IR by lines of H I and He I, with a hot dust continuum (Willner et al. 1979; Zhang & Kwok 1992; Hodapp et al. 1994). Hora et al. (1993) and Paper I showed broad- and narrow-band near-IR images of the PN, showing the elliptical, double-lobed structure in the IR.

Three positions in the nebula were observed to determine the spectral variations across the object. The positions observed were on the central star, the peak of the E lobe, and in the halo region outside of the bright ring (Figure 9). In the central position, stellar continuum is visible, rising towards shorter wavelengths. The nebular lines are similar in the central and lobe positions. The halo emission is almost devoid of lines; there is some faint Paβ present as well as Brγ, this is possibly reflected from the bright lobes. The main component of the halo emission is a weak continuum that rises towards longer wavelengths.

3.1.14. IC 2149

This peculiar PN has a bright core and a roughly bipolar nebula extending roughly E-W, but does not show the usual H_2 signature of bipolar PN. The two spectra shown in Figure 10 were taken centered on the bright core, and on the E lobe. The core spectrum shows strong stellar continuum, with the nebular lines superimposed. The E lobe emission is primarily from H I and He I lines, in addition to weak continuum emission which is probably reflected from the central star.

3.1.15. IC 3568

This round PN consists of spherical shells, an inner bright one and a outer halo. Balick et al. (1987) showed that the structure was consistent with simple hydrodynamic models of PN that are shaped by interior stellar winds. The spectrum taken on the N edge of the round PN IC 3568 is shown in Figure 11. The predominant features are H I and He I emission lines, and low level continuum emission which is probably reflected from the central star.

3.1.16. IC 4593

Bohigas & Olguin (1996) obtained spectroscopy and imaging of this PN which has two inner shells surrounded by an outer highly excited halo. IC 4593 is unusual in that the condensations outside of the inner region are located asymmetrically in the SW region.

Two spectra were taken on this PN, one positioned on the central star, and the other at a position 3″ E (Figure 11). The core shows bright stellar continuum, with nebular lines superimposed, and Paβ absorption.

The E spectrum has the typical H I and He I emission lines. The sky subtraction was not of high quality for this spectrum, which resulted in OH airglow lines showing up in emission in the H and K spectral regions.

3.1.17. J 320

Images of J 320 (Balick 1987) show it to have a central region that is elongated roughly E-W, but the low level flux has a N-S elongation indicating a shell or streamer extending in this direction. Three spectra for J 320 are shown in Figure 12, centered on the core (C), offset 1″ N (P1), and offset 1.″5 N (P15). The core has a stronger contribution from stellar continuum, but otherwise the spectra are similar. We therefore see no spectral differences in the N extension of the nebula.

3.1.18. M 4-18

This young, low-excitation PN was recently imaged with HST by Dayal et al. (1997) and shows a toroidal shell surrounding the central star. There is strong mid-IR emission from warm ($\sim$ 200K) dust that has a similar morphology but the position angle of the dust emission maxima is orthogonal to those shown in Hα emission. The spectrum of the core of this PN shown in Figure 13 has strong stellar continuum, as well as H I and He I line emission. The slit was positioned N-S across the compact ring of the PN, so the ionized regions of the nebula are included in this spectrum.

3.2. H I - line and H_2 emission

The emission lines present in the spectra of this PNe group contain those mentioned in the previous section plus lines from molecular hydrogen. The H_2 lines are strongest in the K band, although in some objects there are lines visible in the H and J bands as well. In the objects where more than one slit position was measured, there is often a large change of the relative line strength of H I versus H_2 emission, indicating that the emission is being produced in different regions of the nebula. In general, the H_2 emission is more likely to be in the outer regions of the PNe, whereas the H I emission more closely traces the ionized regions and has similar morphology to the optical appearance. The PNe in this group all have some bipolar symmetry in their shape, most being of the "butterfly" morphology characterized by narrow equatorial regions and large bipolar lobes (e.g., M 2-9, Hb 12), although some are classified as elliptical based on the shape of the brightest components. Tables 5 and 6 list the line identifications and extracted fluxes for the PNe in this section.

3.2.1. H_2 excitation in PNe

A near-infrared emission line spectrum from molecular hydrogen can occur through slow electric quadrupole vibration-rotation transitions in the ground electronic state. Because $T_{ex} \gtrsim 1000$ K is required to produce a detectable near-IR spectrum from H_2, special excitation conditions must exist when the near-IR spectrum is present. In Paper I we discussed mechanisms of H_2 excitation in PNe; see also Kastner et al. (1996). If detected in sufficient number, the observed H_2 line ratios are an excellent diagnostic for determining the relative importance of shocks and UV photons in a photodissociation region (PDR) for the excitation of the H_2 emission. Even if excitation cannot be determined, the presence of H_2 emission is important to understanding the conditions in PNe and how they evolve through wind interactions and photodissociation. An analysis of the H_2 emission can determine the ortho-to-para (O/P) ratio, the rotational excitation temperature $T_{ex}(J)$, and the vibrational excitation temperature $T_{ex}(v)$ of the molecules. If the rotational and vibrational excitation temperatures differ, then UV excitation is indicated. This is most readily determined by comparing the column densities in the upper state vibration-rotation levels with the upper state energy (in temperature units; see Hora & Latter 1994, 1996 for a full discussion; see also Black & van Dishoeck 1987; Sternberg & Dalgarno 1989). When many H_2 lines are detected, especially those from highly excited levels that fall in the J band, a much stronger case can be made for the importance of UV excitation than does the traditional $v = 2 \rightarrow 1$ S(0) to $v = 1 \rightarrow 0$ S(1) line ratio (e.g. Hora & Latter 1994, 1996). The comparision of the column densities to the upper state energy levels has been done for the PNe with detected H_2 emission and the results are summarized in Table 8. We list only the rotational excitation temperature. For collisionally (shock) excited spectra, the rotational and vibrational excitation temperatures are coupled and the same. For UV excited spectra, the vibrational temperature is the result of a cascade through levels and not a thermal process. The rotational levels are easily thermalized by collisions. The O/P ratio is in general rather un-

certain, especially if only v = 1 lines are detected. We did not attempt to determine the O/P ratio for objects without sufficient line detections. A lower than thermal O/P ratio indicates that the H_2 emission is not thermally excited. A subthermal O/P ratio is not caused by the UV excitation process itself, but is a function of chemistry and density in the PDR (e.g., Hora & Latter 1996; Black & van Dishoeck 1987). We show selected excitation diagrams for several objects that are discussed below (Figure 32).

3.2.2. NGC 40

This is the first reported detection of H_2 in NGC 40. The spectrum was taken centered on the W lobe, and the H_2 lines are relatively weak compared to the H I and He I lines from the ionized gas in this region. The H_2 emission was not detected in the narrowband imaging surveys of Paper I or Kastner et al. (1996), so the molecular emission must be confined to a region near the bright ionized gas that dominates the spectrum.

The morphological classification of NGC 40 is middle elliptical (Balick 1987), so this goes against the previously observed strong correlation between bipolar morphology and H_2 detection. However, if one examines the low-level emission in the N and S regions of this PN (see Paper I), one can see material that has broken through and expanded beyond the elliptical shell defined by the E and W bright lobes. Mellema (1995) has found the morphology consistent with models of "barrel"-shaped PNe, which have roughly cylindrical emission regions slightly bowed outwards at the equatorial plane, and less dense polar regions. Higher resolution and more sensitive optical imaging has recently been carried out by Meaburn et al. (1996) show gas escaping from the polar regions of the PN, with other filamentary structure in the outer halo. The data suggest that the H_2 is shock excited. But, insufficient line detections make this result less than firm.

3.2.3. NGC 2440

NGC 2440 is a bipolar PN with complex morphological and spectral structure. In the optical, the nebula is bipolar with the major axis in roughly the E-W direction for the large outer lobes (Balick 1987; Schwartz 1992). However, there are two bright lobes near the core that are positioned along an axis roughly perpendicular to the major axis of the outer lobes. There are two fainter knots that are also along a roughly E-W axis, but not aligned with the outer lobes. There are filaments and knots throughout the lobes. Lopez et al. (1998) finds up to three outflowing bipolar structures in the lobes, and find from their kinematic study that the inner bright lobes (their lobes "A" and "B") are the emission maxima from a radially-expanding toroid viewed nearly in the plane of the sky.

In the near-IR, the inner pairs of lobes are also prominent, but the large E-W lobes are not visible (see Paper I). Instead, there is a circular outer halo visible in H_2 that is not quite centered on the inner lobe structure. Also visible are faint H_2 "spikes" that extend from the center to the circular outer halo, roughly in the equatorial plane of the large optical E-W lobes (Latter & Hora 1998).

The spectra shown in Figure 15 were taken at two different positions in the PN: on the N lobe, and on the fainter E small knot. The N lobe exhibits H I and He I lines from the ionized gas in this region, but also has significant H_2 emission. There is also strong [Fe II] emission at 1.64 and 1.257 μm. In contrast, the E knot is predominantly H_2 emission, with the only H I lines detected being Paβ and Brγ. There is strong [Fe II] emission at 1.64 and 1.257 μm in this region as well. We did an excitation analysis for the three positions observed. UV excitation dominates, except for the NE position, for which there is insufficient data. The low value of the O/P ratio is suggestive of the H_2 emission arrising from a PDR at this location as well.

Since the inner region of NGC 2440 is morphologically complex and any line of sight through the PN is likely to intersect several distinct regions, it is probably the case that the ionized and molecular zones are not mixed as the spectra might seem to indicate, but that the slit simply includes several nebular components, or is looking through a PDR and is sampling both the molecular and the recently ionized gas.

3.2.4. NGC 6720

NGC 6720 (the "Ring Nebula") is probably the best-known PN, and is the archetype for the ring or elliptical morphology that characterizes the brightest part of the nebula. The emission is not consistent with a uniform prolate shell, however, since the ratio of flux between the edge and center of the ring is higher than expected from a limb-brightened shell

(Lame & Pogge 1994). Balick et al. (1992) has suggested that NGC 6720 is actually a bipolar PN viewed along the polar axis, based on narrow-band imaging and high-resolution spectroscopic observations. This view is supported by the presence of H_2 in the nebula and halo, which correlates strongly with bipolar morphology. Guerrero, Manchado, & Chu (1997) draw different conclusions, however, based on their chemical abundance and kinematic study of the nebula. They argue that the Ring has a prolate ellipsoid structure, with a halo of remnant red giant wind.

Our spectra of the Ring (Figure 16) were obtained at two positions, one on the bright ring directly N of the central star, and the second position several arcseconds further north, off the bright ring but on a moderately bright (in H_2) position in the halo. Both positions show bright H_2 emission, with the lobe position also showing contributions from emission lines of H I and He I from the ionized gas, as one would expect based on the visible wavelength and IR images showing the distribution of the line emission. The ring spectrum is strongly UV excited, indicating it is the PDR interface to the outer molecular shell.

3.2.5. NGC 7026

The late elliptical PN NGC 7026 has two bright lobes on either side (E-W) of the central star, with fainter bipolar emission extending roughly N-S from the core. Cuesta, Phillips, & Mampaso (1996) obtained optical spectra and imaging of this object and found kinematically complex structure, with several separate outflows at the outer edge of an inner spherical shell, and suggested that the primary shell may be undergoing breakup in transition to a more typical bipolar outflow structure.

Two positions were sampled in NGC 7026, shown in Figure 17, centered on the E and W bright lobes near the central star. The lobe spectra are nearly identical, as one might expect from the symmetry in this PN. The H_2 emission in this PN is fairly weak at these positions. This might be due to the H_2 being concentrated in other regions of the PN, and not in the bright ionized lobes that were sampled by the spectra presented here. We are unable to determine the excitation.

3.2.6. NGC 7027

NGC 7027 is one of the most highly studied PN at all wavelengths, particularly in the infrared because of its brightness and wealth of spectral features. Treffers et al. (1976) obtained a spectrum for $\lambda = 0.9-2.7$ μm with a beam that included the entire nebula. They identified the major near-IR spectral components, including the first detection of H_2 lines in a PN, and the first detection of the unidentified line at 2.29 μm. Since then, several near-IR spectra have been published, including Scrimger et al. (1978), Smith, Larson, & Fink (1981), and Rudy et al. (1992).

Narrowband imaging has shown that the H I and He I emission is primarily in the bright inner ring of the nebula, and the H_2 emission is in what appears to be bipolar lobes outside of this shell (Graham et al. 1993; Paper I; Latter et al. 1998). It has been argued before based on morphology that the H_2 is in a PDR (Graham et al. 1993). Our data clearly demonstrate this to be the case, with the H_2 showing a strongly UV excited spectrum in a relatively high density medium (see Figure 32b).

3.2.7. BD+30° 3639

The young PN BD+30°3639 is well-studied in the infrared, notable because of its large IR emission excess. It has many similarities to NGC 7027, including its IR morphology and the presence of H_2 in the near-IR and features from polycyclic aromatic hydrocarbons (PAHs; sometimes called UIR features) in the mid-IR. Rudy et al. (1991) obtained a $\lambda = 0.46 - 1.3$ μm spectrum of BD+30°3639; high-resolution visible and near-IR images were recently obtained by Harrington et al. (1997) and Latter et al. (1998), and ground-based near- and mid-IR images have been presented by Hora et al. (1993), Paper I, and Shupe et al. (1998).

Three positions in BD+30°3639 were sampled in the spectra presented in Figure 19; the emission peak on the N lobe of the ring, the E side of the ring, and on the H_2 emission region located approximately 3″ E of the ring. These spectra show a steady progression of decreasing emission from the ionized gas and increasing molecular emission as one moves east. As for NGC 7027, the H_2 emission is UV excited (Figure 32a) and defines the PDR (see also Shupe et al. 1998).

3.2.8. Hubble 12

Hubble 12 (Hb 12) has been notable primarily because it represents one of the clearest cases known of UV excited near-IR fluorescent H_2 emission (Dinerstein et al. 1988; Ramsay et al. 1993). Our Hb 12

results from this survey and our imaging survey were presented in a previous paper (Hora & Latter 1996); the spectra are reproduced here for comparison with the rest of the survey.

Dinerstein et al. had mapped the inner structure and found it to be elliptical surrounding the central star; our deep H_2 images showed the emission to be tracing the edges of a cylindrical shell around the star, with faint bipolar lobes extending N-S. We also detected [Fe II] at 1.64 μm in a position along the edge of the shell, indicating a transition between the inner region around the central star and the outer nebula. The line ratios observed were in excellent agreement with predictions by theoretical H_2 fluorescence calculations, and we found no significant differences between the excitation in the two positions of the nebula that were sampled (see also Luhman & Rieke 1996).

3.2.9. IC 2003

IC 2003 is a round, high-excitation PN that has a ring of emission, with a bright knot on the S edge (Manchado et al. 1996; Zhang & Kwok 1998). Feibelman (1997) obtained IUE spectra of this PN that shows a wealth of nebular and stellar lines. The IR spectra presented in Figure 21 shows that there is little continuum from the nebula; the emission is primarily from H I lines in the J, H, and K bands. There is strong UIR emission at 2.29 μm but none detected at 2.19 μm. H_2 emission is tentatively detected in the K-band in the $v = 1 \rightarrow 0$ S(1), $v = 3 \rightarrow 2$ S(1), and $v = 1 \rightarrow 0$ Q(1) lines. Each of the lines are detected at roughly a 2σ level. The line fluxes are not reliable or numerous enough to allow fitting of the line ratios.

3.2.10. IRAS 21282+5050

The young, carbon-rich PN IRAS 21282+5050 (I21282 hereafter) has been identified as having an 07(f)-[WC11] nucleus (Cohen & Jones 1987) with possibly a binary at its center. Strong ^{12}CO has been detected in a clumpy expanding shell (Likkel et al. 1988) with elongated emission N-S. Shibata et al. (1989) believe the elongated emission suggests the presence of a dust torus in the E-W direction; however, Meixner et al. (1993) see evidence for a clumpy, expanding elliptical envelope. The elongated structure is also seen in the visible (Kwok et al. 1993). Weak continuum flux at 2 and 6 cm suggests a young PN just beginning to be ionized (Likkel et al. 1994; Meixner et al. 1993). Kwok et al. (1993) believe there has been a recent sharp drop in luminosity based on the measured CO/FIR ratio. Weak HCO^+ and ^{13}CO are present (Likkel et al. 1988).

Two positions were sampled on I21282, centered on the bright core, and offset approximately 3″ N and 3″ W. The core is dominated by continuum emission from the central star. Also present are both emission lines from the ionized gas, and H_2 features in the K-band. I21282 is compact, about 4″ in diameter at K (Paper I). The slit therefore samples a slice through the entire nebula, and as a result this spectrum does not necessarily imply that the molecular and ionized gas is mixed. The Lobe spectrum shows primarily lines of H_2 (with the OH night sky lines showing up in absorption because of imperfect sky subtraction in this spectrum). The lack of emission lines due to H I and He I in the Lobe spectrum indicates that the H_2 emission is predominantly in the outer regions of the PN. The data are suggestive of shock excitation, but this should be considered tentative.

3.2.11. M 1-16

M 1-16 is a PN with a near-IR bright central region and bipolar lobes with fast winds extending at least 35″ from the core (Schwartz et al. 1992; Aspin et al. 1993; Sahai et al. 1994). Several spectra were obtained in this PN scanning across the central region; the two positions shown in Figure 22 are on the core position and 1″ S of the core. Both positions show H_2 emission; the S position is slightly brighter in both H_2 and the ionized nebular lines. Our data reveal that the H_2 is UV excited in both regions observed. This had be suggested earlier by Aspin et al. (1993). The core shows a slight rise towards long wavelengths indicating emission from warm dust continuum.

3.2.12. M 1-92

M 1-92 ("Minkowski's Footprint") is a biplor protoplanetary nebula similar in near-IR appearance to AFGL 618, and has evidence of highly collimated outflows along the bipolar axis (Paper I; Trammell & Goodrich 1996 and reference therein). Two positions were sampled in M 1-92, one in the core and one on the NW bipolar lobe. There are problems with the sky background subtraction in both spectra, which are most prominent in the $\lambda = 1.9 - 2.1$ μm region of the spectrum, but also contribute to a lower signal to noise ratio (S/N) over the whole dataset. Nevertheless, the primary characteristics are apparent. The

core region is dominated by strong warm dust continuum emission. There is also weak Brγ and Paβ emission, but the other most other H I and He I lines are too weak to be detected. The lobe position shows weak H_2 emission. The emission appears to be shock excited, but the low excitation suggested by our data is suggestive of UV excitation. Data of higher S/N are required to discern the dominant excitation mechanism. There might also be H_2 emission near the core that is being masked by the strong continuum emission. In both positions, there also seems to be CO bandhead emission at $\lambda = 2.3 - 2.5$ μm although the S/N is not high in these regions.

3.2.13. M 2-9

M 2-9 (the "Butterfly") is a highly symmetric bipolar nebula, with lobes extending from opposite sides of a bright central core, nearly in the plane of the sky. Bright knots of emission are visible in the lobes at the N and S ends. Our results for M 2-9 from this survey were previously presented in Hora & Latter (1994). High-resolution imaging in several near-IR lines indicated that the lobes had a double-shell structure, with the inner shell dominated by H I and He I line emission from ionized gas and continuum emission scattered from the central source, and the outer shell of the lobes showing strong H_2 emission which exhibit a spectrum consistent with UV excitation in a PDR. The core region shows a strong dust continuum component, as well as emission lines from H I, He I, Fe II, [Fe II] and O I. The N knot has strong [Fe II] emission, with relatively weaker H I, He I, and H_2 emission.

3.2.14. Vy 2-2

Vy 2-2 is a compact PN, so very little is known about its morphology. The spectrum obtained in this survey was taken centered on the bright core and the slit sampled most or all of the emission from this object. The spectrum contains stellar continuum, lines of H I and He I emission from the nebula, and weak H_2 emission. This detection confirms the indication of H_2 emission as reported by Dinerstein et al. (1986). The spectrum shown in Figure 25 is similar to others in this category, such as BD+30°3639 and NGC 2440, where several nebular components are superimposed because of the position and size of the slit. As for those objects, the H_2 spectrum is also UV excited.

3.3. H_2 dominated

The PNe in this group have spectra that primarily contain emission lines of H_2. These objects all have bipolar morphology, and most are young or proto-PNe (PPNe). The PPNe also have warm continuum dust emission or stellar continuum that is strongest in the core. Table 7 lists the line identifications and fluxes for the PNe in this section.

3.3.1. NGC 2346

NGC 2346 is a PN with faint bipolar lobes. The brightest part of the nebula is in the "equatorial" region near the central star where the bipolar lobes meet. Walsh, Meaburn, & Whitehead (1991) performed deep imaging and spectroscopy that showed the full extent of the lobes, and they model the PN as two ellipsoidal shells that are joined near the central star. The distribution of the H_2 emission is similar to the optical (Zuckerman & Gatley 1988; Kastner et al. 1994; Paper I).

The near-IR spectrum of NGC 2346 in Figure 26 is dominated by UV-excited H_2 emission, as shown in Figure 32d. The spectrum was obtained with the slit positioned on the bright condensation to the W of the central star. There is also weak Paβ and Brγ emission seen, which is possibly reflected from near the central star.

3.3.2. J 900

The PN J 900 is a bipolar nebula with an unusual "jet"-like structure and an outer shell structure that is seen primarily in H_2 emission (Shupe et al. 1995; Paper I). The spectrum of J 900 shown in Figure 26 was obtained at a position N of the brighter lobe just NW of the central star, centered on the "jet" of emission. Problems with sky-subtraction caused the J and H-band portions of the spectrum continuum to be slightly negative. There is no detected continuum in any part of the spectrum. The H_2 spectrum is shock excited in a moderate velocity wind (Figure 32e).

3.3.3. AFGL 618

AFGL 618 is a carbon-rich, bipolar reflection nebula with a relatively hot central star ($\approx 30,000$ K), similar spectra in the two lobes, and the eastern lobe is significantly brighter than the other. In this as in other ways, the object bears a great resemblance to AFGL 2688 (see below), despite the fact that their

central star temperatures differ by about a factor of 5. The visible spectrum shows many emission lines characteristic of ionized gas (Westbrook et al. 1975), with a small H II region surrounding the central object (Carsenty & Solf 1982). The near-IR spectrum of AFGL 618 is also dominated by rotation-vibration lines of H_2 (Thronson 1981; Thronson 1983; Latter et al. 1992; Paper I).

AFGL 618 exhibits a rich spectrum of molecular line emission (Lo and Bechis 1976; Knapp et al. 1982; Cernicharo et al. 1989; Kahane et al. 1992; Martin-Pintado & Bachiller 1992; Bachiller et al. 1997; Young 1997). The lines detected include ^{12}CO, ^{13}CO, $C^{17}O$, $C^{18}O$, CS, NH_3, HCN, HCO^+, CN, and C I.

Two of the positions sampled are presented here in Figure 27 – the core spectrum and one taken 2.″4 E of the core. Both spectra show strong H_2 emission, along with [Fe II] and weak Paβ and Brγ. In addition, the core has a warm dust continuum that is apparent throughout the spectrum, and clear CO bandhead features in the 2.3 – 2.4 μm region. The CO features are also present but at lower levels in the 2.″4 E spectrum position. Our analysis of the H_2 spectrum confirms the earlier results by Latter et al. (1992) – the spectrum is dominated by a shock heated component, but a UV excited component is clearly present as well (Figure 32c).

3.3.4. AFGL 2688

AFGL 2688 (the "Egg Nebula") is a bipolar reflection nebula (Ney et al. 1975) at visible and near-infrared wavelengths. It has a central star that exhibits the spectrum of a carbon-rich supergiant (Crampton et al. 1975; Lo & Bechis 1976). Similar in visible appearance to AFGL 915, each lobe shows two "jets" or "horns" extending away from the central region (Crampton et al. 1975; Latter et al. 1993; Sahai et al. 1998a). The lobes have identical spectra at visible wavelengths, but their brightness differs significantly (Cohen & Kuhi 1977). The near-IR spectrum is dominated by H_2 rotation-vibration lines (Thronson 1982; Beckwith 1984; Latter et al. 1993). A central source is seen in the mid-IR and longer wavelengths, with fainter extended emission along the axis of the nebula (Hora et al. 1996). There is an enigmatic equatorial region seen in H_2 emission and might be traced by other molecular species, such as HCN (Latter et al. 1993; Bieging & Ngyuen-Quang-Rieu 1996; Sahai et al. 1998b).

Similar to AFGL 618, this object also has a rich molecular content. SiC_2 is seen in absorption (Cohen & Kuhi 1977); this feature is usually found in stars of the highest carbon abundance. Strong absorption features of C_3 and emission in C_2 (Crampton et al. 1975) are present, while C_2 is also seen in absorption in reflected light from the lobes (Bakker et al. 1997). The CO $J = 1 \rightarrow 0$ line shows three distinct velocity structures (Kawabe et al. 1987; Young et al. 1992).

Our results for this object from this survey were previously presented in Hora & Latter (1994, 1995) and our narrowband imaging in Latter et al. (1993). The spectra are reproduced here for comparison with the rest of the survey. Spectra were obtained at several positions in the nebula, including positions along the N lobe, and in the equatorial region (see Hora & Latter 1994 for details). The emission is segregated; the core is dominated by continuum emission, there are emission lines from C_2 and CN further from the core along the lobes, and the H_2 emission is confined to the ends of the lobes and in the equatorial region in what appears to be a ring or toroidal structure (Latter et al. 1993; Sahai et al. 1998b). Our analysis of the H_2 line ratios showed that the emission is collisionally excited in shocks, with no discernible difference between the emission in the lobes and the equatorial region.

3.4. Continuum - dominated

These are young PNe or PPNe that have strong warm dust continuum and little line emission. The strongest component is in general the core, with most of the emission from an unresolved point source. In some of the nebulae, emission structure extends a few arcseconds from the core region. Also, in objects such as AFGL 915, they are associated with larger optical nebulae that extend arcminutes from the core. In this survey we have sampled only the regions near the core.

3.4.1. AFGL 915

AFGL 915 (the "Red Rectangle") is a carbon-rich biconical reflection nebula with a metal-depleted spectroscopic binary at its center (Cohen et al. 1975). The nebula appears axially symmetric and shows spikes running tangent to the edge of the bicone. Surrounding the post-AGB star at its center is a circumbinary disk viewed edge-on (Jura, Balm, & Kahane 1995) which could be oxygen-rich (Waters et al.

1998).

C_2 and CN are not detected near the binary, though C_2 is present in emission in the reflection lobes. CH^+ (0,0) and (1,0) are detected in emission (Bakker et al. 1997; Balm & Jura 1992). CO is underabundant, with relatively weak emission and broad wings detected (Dayal & Bieging 1996; Greaves & Holland 1997; Loup et al. 1993; Bujarrabal et al. 1992). Glinski et al. (1997) found CO and C I. in the UV in both absorption and emission. They expect strong CO overtone emission in the IR based on their observations of hot CO emission and absorption in the UV. The object shows ERE (extended red emission) from about λ = 5400 to 7200 Å and a set of emission bands around 5800 Å (Schmidt, Cohen, & Margon 1980) whose carriers might be the same material as the carriers of the DIBs (diffuse interstellar bands). This object also shows strong emission in the PAH bands at 3.3, 7.7, and 11.2 μm (Cohen et al. 1975), which are located predominantly in the lobes and spikes of emission (Bregman et al. 1993; Hora et al. 1996).

Spectra taken at two different positions are shown, one centered on the core, and the other at 4″ S of the core. Both show strong warm dust continuum, and the core also has strong CO bandhead emission features in the $\lambda = 2.3 - 2.4$ μm range.

3.4.2. IRC+10°420

IRC+10°420 is a highly evolved, OH/IR star that is thought to be in a post-red supergiant phase (Jones et al. 1993). There is some evidence (Oudmaijer 1995; Oudmaijer et al. 1996) that the star's spectral type and photospheric temperature are changing rapidly. Recent HST imaging by Humphreys et al. (1997) shows that the circumstellar environment around this star is extremely complex, with spherical outer shells that extend to a diameter of 6 arcseconds, and several inner condensations. In the near- and mid-infrared, bipolar lobes are visible that extend $\sim$ 2 arcseconds from the core.

The spectrum of IRC+10°420 shown in Figure 30 was taken centered on the object. The slit length includes the inner few arcseconds of the object, although it is dominated by the bright core. The observed spectrum shows a bright and relatively featureless continuum.

3.4.3. M 2-56

The PPN M 2-56 is a bipolar nebula with a bright central core. It is similar in morphology to AFGL 618, although it seems to be at an earlier evolutionary stage since it does not appear to have an H II. region (Trammell, Dinerstein, & Goodrich 1993; Goodrich 1991). The spectrum of M 2-56 shown in Figure 30 was taken centered on the core of this PPN. The dominant feature is a hot dust continuum that is most prominent in the K band region of the spectrum. There are some residual features in the spectrum from imperfect sky subtraction, mostly in the K band.

4. Discussion and Summary

4.1. Spectral Categories

The PNe spectra presented in this paper were grouped according to spectral characteristics as described above. The groups are an efficient way to present the data, but also can be seen to correlate strongly with other characteristics of the PN.

4.1.1. Morphology

The group of H I - line dominated PNe is composed of primarily elliptical or round PNe, along with the peculiar or irregular nebulae of the sample. In general these PNe are well-known from optical studies, identified either by their morphology or their optical spectra. Many of the PNe in this group of the sample, however, do have IR "excess" continuum emission from warm dust, which in some cases prompted their inclusion in this sample.

The spectral groups with molecular and/or dust continuum emission are primarily bipolar. This classification includes objects such as NGC 6720 which have a ring morphology but are thought to be bipolar viewed pole-on, Hb 12 which is brightest in H_2 in the equatorial region and along the outer edges of the lobes, M 2-9 which is brightest in H_2 at the edges of the lobes with no equatorial emission other than at the core, and AFGL 2688 which is brightest along the axis of the bipolar lobes, with H_2 emission in the equatorial plane. Clearly this is a heterogeneous group with a wide range of emission and morphological differences that imply a range of evolutionary tracks and states.

4.1.2. The Carbon-to-Oxygen Ratio

Carbon stars, although a small fraction of all AGB stars, return about half of the total mass injected into the ISM by all AGB stars, since they have on average much higher mass loss rates ($> 10^{-4} M_{\odot}\ yr^{-1}$) than do O-rich objects. The carbon-to-oxygen (C/O) abundance ratio in PNe has previously been shown to correlate with morphology (Zuckerman & Aller 1986), with bipolar PNe tending to be carbon-rich. It is therefore expected that the C/O ratio also correlates with the spectral classifications presented here. This is in general the case, with the H I - line dominated PNe having C/O ratios less than or about 1, whereas the remaining categories which are dominated by the bipolar PNe have C/O ratios >1, as reported by Zuckerman & Aller (1986) and Rola & Stasińska (1994). Rola & Stasińska discuss problems with previous determinations of the C/O ratio, and use different criteria that result in a slightly lower percentage of carbon-rich PNe (35%) than others. We use their ratios in the discussion below.

The morphology of PN also has been shown to depend on the progenitor mass (see Corradi & Schwarz 1995), with the bipolar PN being more massive than other morphological types. This relationship, along with the link between carbon abundance and morphology, suggests that carbon stars are the projenitors of bipolar PN and those with a large amount of molecular material. The mechanisms that cause massive carbon-rich stars to preferentially form bipolar PN are still not understood.

There are some exceptions to the correlation of morphological type to C/O ratio; in particular, NGC 6543 has a much higher value (9.55) than the others in the class. In the other extreme, NGC 2346 stands out as having a low C/O ratio (0.35) compared to other bipolar PNe in the H_2 - dominated group. This object is a much more evolved object than the others in its group (e.g., AFGL 2688), and exhibits weak Paβ emission, showing that the ionized gas is present although weak relative to the molecular emission in the nebula.

4.2. Summary of Molecular Hydrogen Emission in PNe

A long standing problem in the interpretation of H_2 emission from interstellar and circumstellar environments is understanding the excitation mechanism. Three fundamental mechanisms are possible. One is excitation of a near-infrared fluorescence spectrum resulting from a rotational-vibrational cascade in the ground electronic state following electronic excitation by the absorption a UV photon in the Lyman and Werner bands (Black & van Dishoeck 1987). The second excitation mechanism is collisional excitation in a warm gas ($T_K \gtrsim 1600$ K). While UV excitation in a low density gas produces an easily identifiable spectrum, the level populations can be driven to produce thermal line ratios when the UV flux is large and densities begin to exceed $\approx 10^4$ cm^{-3} (Sternberg & Dalgarno 1989). Detailed spectral and morphological analysis are often required to determine an origin of the near-IR spectrum. The third excitation mechanism is formation of H_2 on the surfaces of dust grains and in the gas phase. While potentially important in isolated regions of certain objects, we do not consider this to be generally important in PNe and PPNe relative to the other two processes. This is because molecular formation in PNe is relatively slow compared to dissociation rates.

In PNe and PPNe, the situation can be complicated by both dominant excitation mechanisms being present simultaneously, and in different forms. Several ways of exciting near-IR emission from H_2 have been identified as possible: direct thermal excitation in warm gas created behind moderate velocity shockwaves, direct excitation by UV photons from the hot central star, somewhat indirectly by collisional excitation in warm gas created by rapid grain streaming (e.g. Jura & Kroto 1990), and excitation through absorption of Lyα photons (by an accidental resonances with the $B^1\Sigma_u^+ - X^1\Sigma_g^+$ $v = 1 - 2$ P(5) and R(6) transitions of H_2) which can be generated in a nearby strong shock (e.g., Black & van Dishoeck 1987).

The first two mechanisms have been clearly identified in several PNe, such as thermal excitation in AFGL 2688 (e.g., Hora & Latter 1994; Sahai et al. 1998a), pure UV excitation in a low density gas around Hb 12 (e.g., Dinerstein et al. 1988; Hora & Latter 1996; Luhman & Rieke 1996), and UV excitation in a high density gas in M 2-9 (Hora & Latter 1994) and NGC 7027 (Graham et al. 1993b; this paper). A combined spectrum was found from a detailed analysis of AFGL 618 (Latter et al. 1992; this paper). While the form of the excitation might be clear for these and other objects, it is not always evident what is the source of the warm gas or UV photons. Winds are present in AFGL 2688 which could directly shock heat the gas, but considerable grain streaming is likely

taking place as well (see Jura & Kroto 1990).

Very fast winds and dissociating shocks are present in AFGL 618, M 2-9 (e.g., Kelly, Latter, & Hora 1998), and M 1-16 (Sahai et al. 1994; Schwarz 1992) and all show clear evidence of UV excitation. In addition, the photon path to the H_2 emitting regions is not clearly in a direct line-of-sight to the central star, which for photons coming from the central star suggests scattering in what is a fairly low density medium. Alternatively, we are seeing in each of these objects excitation of H_2 at the bipolar lobe walls by UV photons generated within strong shocks produced by the fast winds. This hypothesis was explored through detailed modeling by Latter et al. (1992) of AFGL 618, but the high relative intensity of the thermally excited emission and poor spatial resolution limited this analysis. The presence of very fast winds in the lobes of each of these objects, and the presence of UV excited H_2 emission at the lobe walls strongly suggests that indirect excitation of the H_2 is occurring by interactions with photons generated by wind produced shockwaves. Detailed modeling of sensitive, high spatial resolution spectra is required. It is also evident, in general, that without detailed spectra, H_2 is a rather poor diagnostic of overall conditions in PNe and PPNe.

If we conclude that all of the ways to excite H_2 in PNe and PPNe listed above are present and important, what does this imply for our understanding of these objects and the utility of H_2 as a diagnostic? It is now well understood that the presence of molecular emission from PNe and PPNe is tied to the morphology of the objects such that if molecular emission is present, the object has a bipolar morphology (e.g., Zuckerman & Gatley 1988; Latter et al. 1996; Kastner et al. 1996, and references therein). Does this suggest that H_2 can be more easily excited in a bipolar nebula? We have argued that H_2 emission is excited in multiple ways in PNe and PPNe. While special conditions are required for H_2 emission to be seen in near-IR spectra, the conditions that drive the excitation are common in all PNe and PPNe and are not clearly dependent on morphological type. A conclusion that can be drawn from this argument alone is that molecular material is present in nebulae with a bipolar morphology and a significant amount of molecular material is *not* present in other morphological types. Therefore, objects that have a bipolar morphology must have a dense, high mass envelope in which the molecular material can be shielded and survive dissociation for relatively long times – suggesting a high mass loss rate and a high mass progenitor star. A correlation between bipolar morphology and high mass progenitor stars has been found by others (e.g., Corradi & Schwarz 1995). It seems clear that the presence of H_2 emission in a PN is not tied to directly to the morphology, but that the bipolar morphology is intimately related to the density and mass of the circumstellar envelope, and therefore the mass of the progenitor star. Why high mass, high mass loss rate asymptotic giant branch stars shed material in an axisymmetric, not spherical, way remains a mystery.

4.3. Spectral Sampling of Morphological Features

This survey has differed from many previous investigations in that a short, narrow slit was used to obtain the data, rather than a large beam that could include most or all of the nebula. Because of this, one cannot easily use the spectra presented here to model the PNe in a global sense, if that requires a measurement of the total flux from the object. Also, if a complete census of emission lines were required, some might be missed if there were variations of emission characteristics across the nebula and certain regions were not sampled.

The spatial selectivity that prevents viewing the entire PN at once, however, has proven to be an advantage when trying to examine various aspects of the PN, including variations across the nebula, as a function of distance from the central star, or in examining certain morphological features. For example, in M 2-9 and NGC 2440, the emission of the lobe walls and emission knots were separately sampled, which showed the large spectral differences in these regions. This information is important for modeling the structure and formation of the PN. Another reason why the small aperture is useful is that if the emission from a group of lines such as H_2 is to be modeled, it is important to compare the emission from a clump of material where the conditions do not vary greatly over its size. For example, the emission from H_2 present very close to the central star in a strong UV field could be quite different from H_2 emission from the outer parts of the halo. Also, the small slit has aided in detecting weak H_2 emission from several PNe such as NGC 40, where detection would have been difficult if the central star and the rest of the nebula could not be excluded from the measurement.

We thank Xander Tielens and David Hollenbach for useful discussions and encouragement. We acknowledge support from NASA grant 399-20-61 from the Long Term Space Astrophysics Program. WBL was supported during part of this study by a National Research Council Research Associateship.

REFERENCES

Aaquist, O. B., & Kwok, S. 1990, A&AS, 84, 229

Acker, A., Marcout, J., Ochsenbein, F., Scholn, C., Stenholm, B., & Tylenda, R. 1992, The Strasbourg-ESO Catalogue of Galactic Planetary Nebulae (München: ESO)

Aspin, C. et al. 1993, A&A, 278, 255

Bachiller, R., Fuente, A., Bujarrabal, V., Colomer, F., Loup, C., Omont, A., & de Jong, T. 1997, A&A, 319, 235

Bakker, E.J., van Dishoeck, E.F., Waters, L.B.F.M., & Shoenmaker, T. 1997, A&A, 323, 469

Balick, B. 1987, AJ, 94, 671

Balick, B., Bignell, C. R., Hjellming, R. M., & Owen, R. 1987, AJ, 94, 948

Balick, B., Gonzalez, G., Frank, A., & Jacoby, G. 1992, ApJ, 392, 582

Balick, B., Alexander, J., Hajian, A. R., Terzian, Y., Perinotto, M., & Patriarchi, P. 1998, AJ, 116, 360

Barker, T. 1991, ApJ, 371, 217

Beckwith, S., Beck, S.C., & Gatley, I. 1984, ApJ, 280, 648

Bieging, J. H. & Ngyuen-Quang-Rieu 1996, AJ, 112, 706

Black, J. H., & van Dishoeck, E. F. 1987, ApJ, 322, 412

Bohigas, J., & Olguin, L. 1996, RMxAA, 32, 47

Bowers, C. W., Blair, W. P., Long, K. S., & Davidsen, A. F. 1995, ApJ, 444, 748

Bregman, J. D., Rank, D., Temi, P., Hudgins, D., & Kay, L. 1993, ApJ, 411, 794

Bryce, M., Balick, B., & Meaburn, J. 1994, MNRAS, 266, 721

Bujarrabal, V., Alcolea, J., & Planesas, P. 1992, A&A, 257, 701

Carsenty, U., & Solf, J. 1982, A&A, 106, 307

Cernicharo, J., Guelin, M., Martin-Pintado, J., Denalver, J.,& Maversberger, R. 1989, A&A, 222, L1

Cohen, M., & Barlow, M. J. 1974, ApJ, 193, 401

Cohen, M. & Jones, B. F. 1987, ApJ, 321, L151

Cohen, M. & Kuhi, L.V. 1977, ApJ, 213, 79

Cohen, M., et al. 1975, Ap.J. 196, 179

Corradi, R. L. M., & Schwarz, H. E. 1995, A&A, 293, 871

Crampton, D., Cowley, A.P., & Humphreys, R.M. 1975, ApJ, 198, L135.

Cuesta, L., Phillips, J. P., & Mampaso, A. 1996, A&A, 313, 243

Dayal, A. & Bieging, J.H. 1996, Ap.J. 472, 703

Dayal, A., Sahai, R., Trauger, J., Hora, J. L., Fazio, G. G., Hoffmann, W. F., Bieging, J. H., Deutsch, L. K., & Latter, W. B. 1997, BAAS, 191, 1509

Dinerstein, H. L., Carr, J. S., Harvey, P. M., & Lester, D. F. 1986, in Summer School on Interstellar Processes (Abstract book), p. 43

Dinerstein, H. L., Lester, D. F., Carr, J. S., & Harvey, P. M. 1988, ApJ, 327, L27

Dinerstein, H. L., & Crawford, J. 1998, in Proc. IAU Symp. 180, in press

Feibelman, W. A., Hyung, S., & Aller, L. H. 1996, MNRAS, 278, 625

Feibelman, W. A. 1997, ApJS, 109, 481

Garcia-Lario, P., Manchado, A., Suso, S. R., Pottasch, S. R., & Olling, R. 1990, A&AS, 82, 497

Geballe, T. R., Burton, M. G., & Isaacman, I. 1991, MNRAS, 253, 75

Gillett, F. C., Merrill, K. M., & Stein, W. A. 1972, ApJ, 172, 367

Glinski, R.J., Lauroesch, J.T., Reese, M.D., & Sitko, M.L. 1997, Ap.J. 490, 826

Goodrich, R. W. 1991, ApJ, 376, 654

Graham, J. R., Serabyn, E., Herbst, T. M., Matthews, K., Neugebauer, G., Soifer, B. T., Wilson, T. D., & Beckwith, S. 1993, AJ, 105, 250

Graham, J. R., Herbst, T. M., Matthews, K., Neugebauer, G., Soifer, T., Serabyn, E., & Beckwith, S. 1993b, ApJ, 408, L105

Greaves, J.S. & Holland, W.S. 1997, A&A, 327, 342

Guerrero, M. A., Manchado, A., & Chu, Y.-H. 1997, ApJ, 487, 328

Harrington, J. P., & Borkowski, K. J. 1994, BAAS, 26, 1469

Harrington, J. P., Lame, N. J., White, S. M., & Borkowski, K. J. 1997, AJ, 113, 2147

Hodapp, K.-W., Hora, J. L., Irwin, E., & Young, T. 1994, PASP, 106, 87

Hora, J. L., Deutsch, L. K., Hoffmann, W. F., Fazio, G. G., & Shivanandan, K. 1993, ApJ, 413, 304

Hora, J. L., & Latter, W. B. 1994, ApJ, 437, 281

Hora, J. L., & Latter, W. B. 1995, ApJ, 449, 397

Hora, J. L., Deutsch, L. K., Hoffmann, W. F., & Fazio, G. G. 1996, AJ, 112, 2064

Hrivnak, Kwok, S., & Geballe, T. R. 1993, ApJ, 420, 783

Hua, C. T., & Grundseth, B. 1986, AJ, 92, 853

Humphreys, R. M., et al. 1997, AJ, 114, 2778

Hyung, S., Aller, L. H., & Feibelman, W. A. 1994, MNRAS, 269, 975

Jones, T. J., et al. 1993, ApJ, 411, 323

Jura, M., Balm, S.P., & Kahane, C. 1995, Ap.J. 453, 721

Kahane, C., Cernicharo, J., Gomez-Gonzalez, J., & Guelin, M. 1992, A&A, 256, 235

Kastner, J. H., Weintraub, D. A., Gatley, I., Merrill, K. M., & Probst, R. 1996, ApJ, 462, 777

Kawabe, R., Ishiguro, M., Kasuga, T., Morita, K.I., Ukita, N., Kobayashi, H., Okumura, S., Fomalont, E., & Kaifu, N. 1987, ApJ, 314, 322

Kelly, D. M., & Latter, W. B. 1995, AJ, 109, 1320

Kelly, D. M., Latter, W. B., & Hora 1998, in preparation

Knapp, G.R., Phillips, T.G., Leighton, R.B., Lo, K.Y., Wannier, P.G., & Wooten, H.A. 1982, ApJ, 252, 616

Kwok, S., Hrivnak, B. J., & Langill, P. P. 1993, ApJ, 408, 586

Lame, N. J., & Pogge, R. W. 1994, AJ, 108, 1860

Latter, W. B., Hora, J. L., Kelly, D. M., Deutsch, L. K., & Maloney, P. R. 1993, AJ, 106, 260

Latter, W.B., Kelly, D. M., Hora, J. L., & Deutsch, L. K. 1995, ApJS, 100, 159 (Paper I)

Latter, W. B., Maloney, P. R., Kelly, D. M., Black, J. H., Rieke, G. H., & Rieke, M. J. 1992, ApJ, 389, 347

Latter, W. B., Hora, J. L., Kelly, D. M., Dayal, A., Bieging, J. H., Tielens, A. G. G. M., & Trammell, S., 1998, BAAS, 191, 1510

Latter, W. B., & Hora, J. L 1997, in IAU Symp. 180, *Planetary Nebulae*, eds. H. J. Habing & H. J. G. L. M. Lamers, 254

Likkel, L., Forveille, T., Omont, A., & Morris, M. 1988, A&A, 198, L1

Likkel, L., Morris, M., Kastner, J. H., & Forveille, T. 1994, A&A, 282, 190.

Lo, K.Y. & Bechis, K.P. 1976, ApJ, 205, L21

Lopez, J. A., Meaburn, J., Bryce, M., & Holloway, A. J. 1998, ApJ, 493, 803

Loup, C., Forveille, T., Omont, A., & Paul, J.F. 1993, A&AS, 99, 291.

Luhman, K., & Rieke, G. H. 1996, ApJ, 461, 298

Luhman, M. L., Luhman, K. L., Benedict, T., Jaffe, D. T., & Fischer, J. 1997, ApJ, 480, L133

Manchado, A., Guerrero, M. A., Stanghellini, L., & Serra- Ricart, M. 1996, The IAC Morphological Catalog of Northern Galactic Planetary Nebulae (Tenerife: Instituto de Astrofisica de Canarias).

Martin-Pintado, J. & Bachiller, R. 1992, ApJ, 391, L93

Meaburn, J., Lopez, J. A., Bryce, M., & Mellema, G. 1996, A&A, 307, 579

Meixner, M., Skinner, C. J., Temi, P., Rank, D., Bregman, J., Ball, J. R., Keto, E., Arens, J.F., & Jernigan, J.G. 1993, ApJ, 411, 266

Mellema, G. 1995, MNRAS, 277, 173

Ney, E. P., Merrill, K. M., Becklin, E. E., Neugebauer, G., & Wynn-Williams, C. G. 1975, ApJ, 198, L129

O'Dell, C. R., Weiner, L. D., & Chu, Y.-H. 1990, ApJ, 362, 226

Oudmaijer, R. D. 1995, Doctoral Dissertation, Groningen

Oudmaijer, R. D., Groenewegen, M., Matthews, N., Blommaert, J., & Sahu, K. 1996, MNRAS, 280, 1062

Pottasch, S. R. 1986, Proc, 131

Persi, P., Preite Martinez, A., Ferrari-Toniolo, M., & Spinoglio, L. 1987, in Planetary and protoplanetary nebulae: From IRAS to ISO (Dordrecht, D. Reidel), 221

Phillips, J. P., & Cuesta, L. 1996, AJ, 111, 1227

Ramsay, S. K., Chrysostomou, A., Geballe, T. R., Brand, P. W. J. L., & Mountain, M. 1993, MNRAS, 263, 695

Rao, K. N., Humphreys, C. J., & Rank, D. H. 1966, Vacuum Wavelengths in the Infrared (New York: Academic Press, Inc.)

Reay, N. K., Atherton, P. D., & Taylor, K. 1983, MNRAS, 203, 1087

Rieke, G. H., & Lebofsky, M. J. 1985, ApJ, 288, 618

Rola, C., & Stasińska, G. 1994, A&A, 282, 199

Rudy, R. J., Rossano, G. S., Erwin, P. & Puetter, R. C. 1991, ApJ, 368, 468

Rudy, R. J., Erwin, P., Rossano, G. S., & Puetter, R. C. 1992, ApJ, 384, 536

Sahai, R., Wootten, A., Schwarz, H. E., & Wild, W. 1994, ApJ, 428, 237

Sahai, R., et al. 1998a, ApJ, 493, 301

Sahai, R., et al. 1998b, ApJ, 492, 163

Schmidt, G. D., Cohen, M., & Margon, B. 1980, Ap.J. 239, L133

Schwarz, H. E., Corradi, R. L. M., & Melnick, J. 1992, A&AS, 96, 23

Scrimger, M. J., Lowe, R. P., Moorhead, J. M., & Wehlau, W. H. 1978, PASP, 90, 257

Shibata, K. M., Tamura, S., Deguchi, S., Hirano, N., Kameya, O., & Kasuga, T. 1989, ApJ, 345, L55

Shupe, D. L., Armus, L., Matthews, K., & Soifer, B. T. 1995, ApJ, 109, 1173

Shupe, D. L., Larkin, J. E., Knop, R. A., Armus, L., Matthews, K, & Soifer, B. T. 1998, ApJ, 498, 267

Smith, H. A., Larson, H. P., & Fink, U. 1981, ApJ, 244, 835

Sternberg, A., & Dalgarno, A. 1989, ApJ, 338, 197

Thronson, H.A. 1981, ApJ; 248, 984

Thronson, H.A. 1982, AJ, 87, 1207

Thronson, H.A. 1983, ApJ, 264, 599

Trammell, S. R., Dinerstein, H. L., & Goodrich, R. W. 1993, ApJ, 402, 249

Treffers, R. R., Fink, U., Larson, H. P., & Gautier III, T. N. 1976, ApJ, 209, 793

Walsh, J. R., Meaburn, J., & Whitehead, M. J. 1991, A&A, 248, 613

Waters, L.B.F.M., et al. 1998, Nature 391, 868

Wiese, W. L., Smith, M. W., & Miles, B. M. 1969, Nat. Stand. Ref. Data Ser., Nat. Bur. Stand. (US), 22, 189

Willner, S. P., Jones, B., Puetter, R. C., Russell, R. W., & Soifer, B. T. 1979, ApJ, 234, 496

Westbrook, W. E., Becklin, E. E., Merrill, K. M., Neugebauer, G., Schmidt, M., Willner, S. P., & Wynn-Williams, C. G. 1975, ApJ, 202, 407

Whitelock, P. A. 1985, MNRAS, 213, 59

Young, K., Serabyn, G., Phillips, T.G., Knapp, G.R., Gusten, R., & Schultz, A. 1992, ApJ, 385, 265

Young K. 1997, ApJ, 488, L157

Zhang, C. Y., & Kwok, S. 1992, ApJ, 385, 255

Zhang, C. Y., & Kwok, S. 1998, ApJS, 117, 341

Zuckerman, B., & Gatley, I. 1988, ApJ, 324, 501

This 2-column preprint was prepared with the AAS LaTeX macros v4.0.

Fig. 1.— Spectra of NGC 1535, NGC 2022, and NGC 2392. The spectra have been offset and scaled by the constants shown in the plot labels. At the bottom, some of the prominent lines have been labeled with small vertical lines. The first row are H I, the second row He I, and below the rows individual lines have been indicated. The positions in the nebula where these spectra were taken is given in Table 1.

Fig. 2.— NGC 3242 (see caption to Figure 1).

Fig. 3.— NGC 6210 (see caption to Figure 1).

Fig. 4.— NGC 6790 and NGC 6543 (see caption to Figure 1).

Fig. 5.— NGC 6572 (see caption to Figure 1).

Fig. 6.— NGC 6803 (see caption to Figure 1).

Fig. 7.— NGC 6826 (see caption to Figure 1).

Fig. 8.— NGC 7662 and IC 351 (see caption to Figure 1).

Fig. 9.— IC 418 (see caption to Figure 1).

Fig. 10.— IC 2149 (see caption to Figure 1).

Fig. 11.— IC 3568 and IC 4593 (see caption to Figure 1).

Fig. 12.— J320 (see caption to Figure 1).

Fig. 13.— M 4-18 (see caption to Figure 1).

Fig. 14.— Spectra of NGC 40 and NGC 2440. The spectra have been offset and scaled by the constants shown in the plot labels. At the bottom, some of the prominent lines have been labeled with small vertical lines. The first row are H I, the second row He I, and the third row H_2. Below the rows individual lines have been indicated. The positions in the nebula where these spectra were taken is given in Table 1.

Fig. 15.— NGC 2440 (see caption to Figure 14).

Fig. 16.— NGC 6720 (see caption to Figure 14).

Fig. 17.— NGC 7026 (see caption to Figure 14).

Fig. 18.— NGC 7027 (see caption to Figure 14).

Fig. 19.— BD+30°3639 (see caption to Figure 14).

Fig. 20.— Hubble 12 (see caption to Figure 14).

Fig. 21.— IC 2003 and IRAS 21282+5050 (see caption to Figure 14).

Fig. 22.— M 1-16 (see caption to Figure 14).

Fig. 23.— M 1-92 (see caption to Figure 14).

Fig. 24.— M 2-9 (see caption to Figure 14).

Fig. 25.— M 2-9 and Vy 2-2 (see caption to Figure 14).

Fig. 26.— J 900 and NGC 2346 (see caption to Figure 14).

Fig. 27.— AFGL 618 (see caption to Figure 14).

Fig. 28.— AFGL 2688 (see caption to Figure 14).

Fig. 29.— AFGL 915 (see caption to Figure 14).

Fig. 30.— M 2-56 and IRC+10°420 (see caption to Figure 14).

Fig. 31.— M 1-78 and K 4-45 (see caption to Figure 14).

Fig. 32.— Excitation diagram for several of the PNe detected in H_2. Shown are the upper state vibration-rotation level populations relative to that in the $v = 1$, $J = 3$ level plotted against the energy of the upper state in Kelvin. The statistical weight, g_J, for odd J levels includes the ortho-to-para ratio as determined from the data (Table 8), or if not determined the thermal value of 3 was used. The data are labeled by the upper state vibration level. Linear fits to the different vibrational levels determines the rotational excitation temperature. The lines shown are characteristic for this value of $T_{ex}(J)$. Line ratios not used in the analysis because of blending are not plotted. Dereddening of the H_2 spectrum has been done using the attenuation values shown in Table 8 (or not at all). **a)** BD+30°3639 at the "H2" slit position shows strong UV excitation (see also Shupe et al. (1998). **b)** NGC 7027 at the "T" slit position also shows strong UV excitation at relatively high density (see also Graham et al. (1993). **c)** AFGL 618 at 2.″4 E of the core shows a combined UV and shock excited spectrum (see also Latter et al. 1992). The arrow is connected to the $v = 1$ (square) point and indicates an upper limit. The dotted line is a linear fit to the $v = 1$ and $v = 2$ data points. **d)** NGC 2346 is also dominated by UV excitation. The solid line is a linear fit ($T_{ex} = 2500$ K) to all the data points and is offset for clarity. The dashed lines are representative of $T_{ex}(J) = 1260$ K. **e)** J 900 shows only shock excitation of the H_2. For another example of a shock (collisional) excitation diagram, see AFGL 2688 in Hora & Latter (1994).

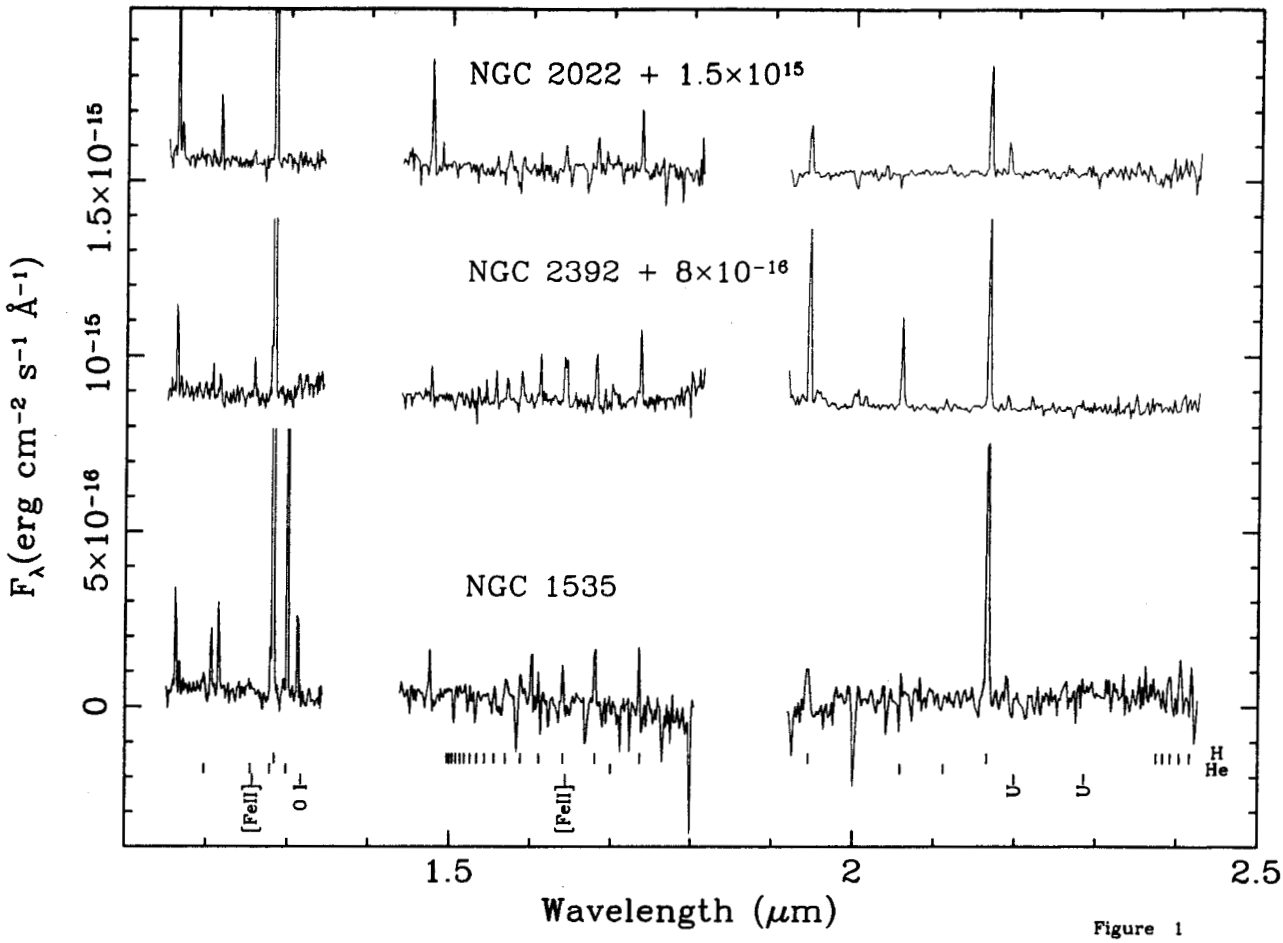

Figure 1

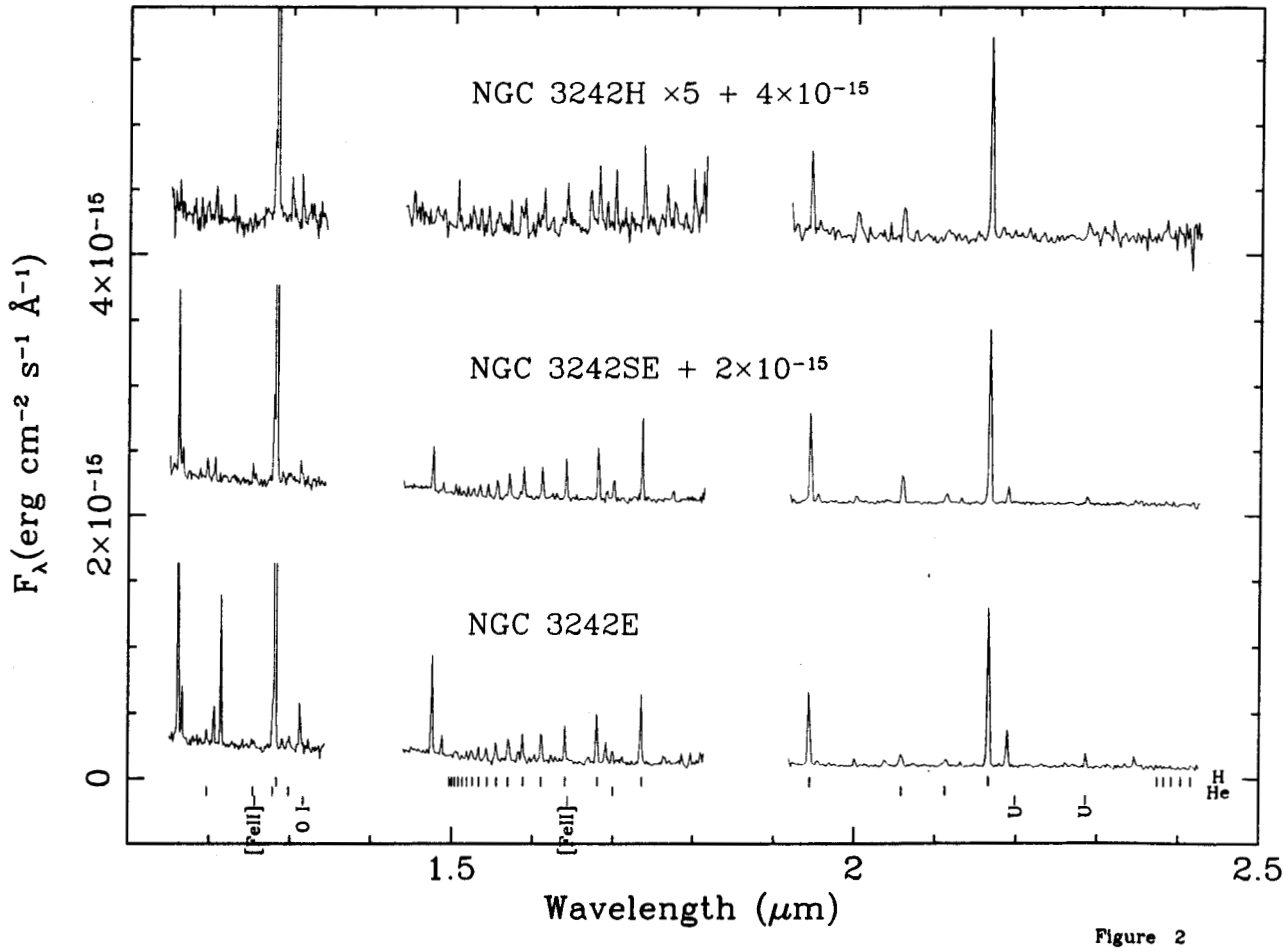

Figure 2

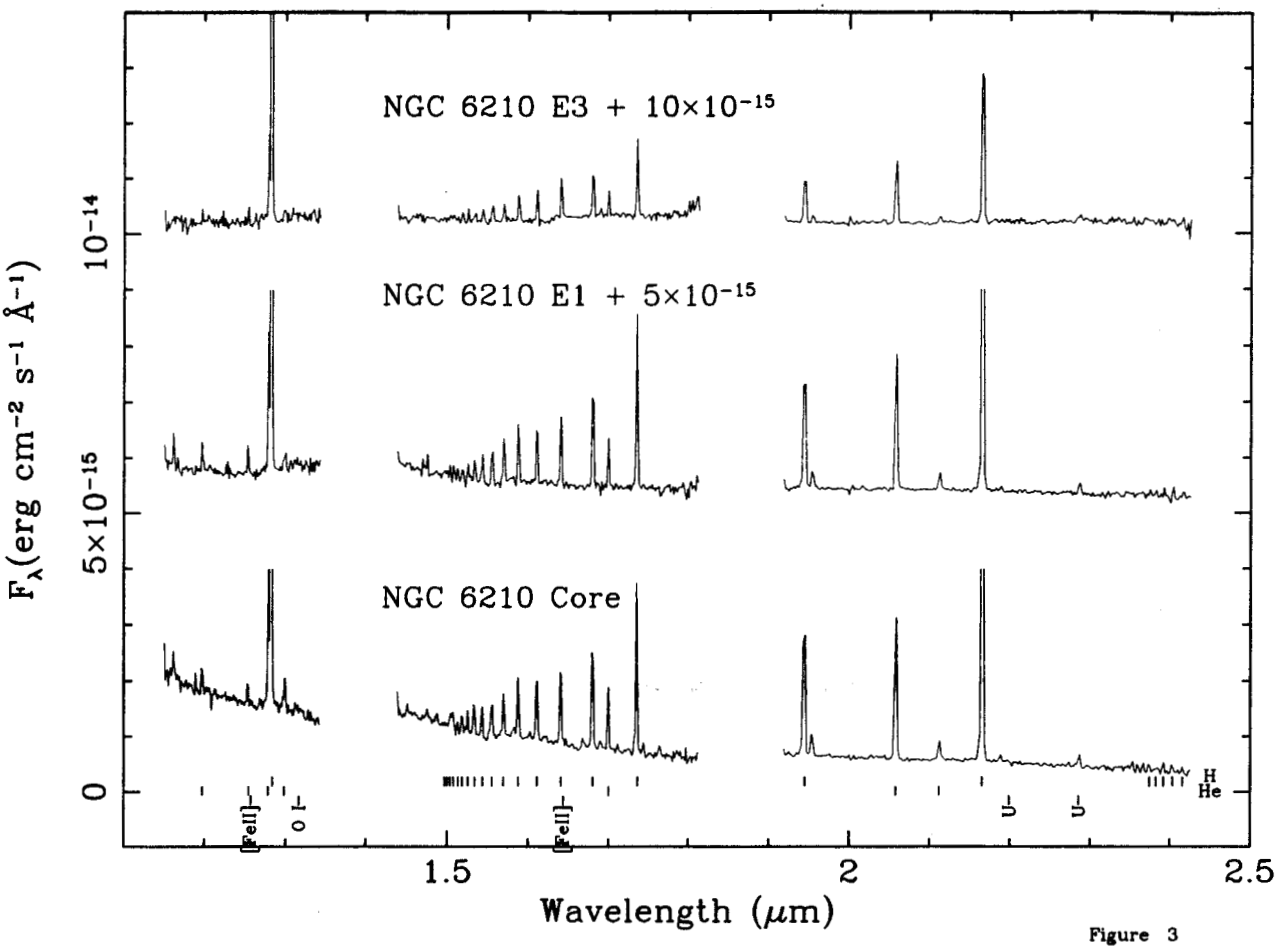

Figure 3

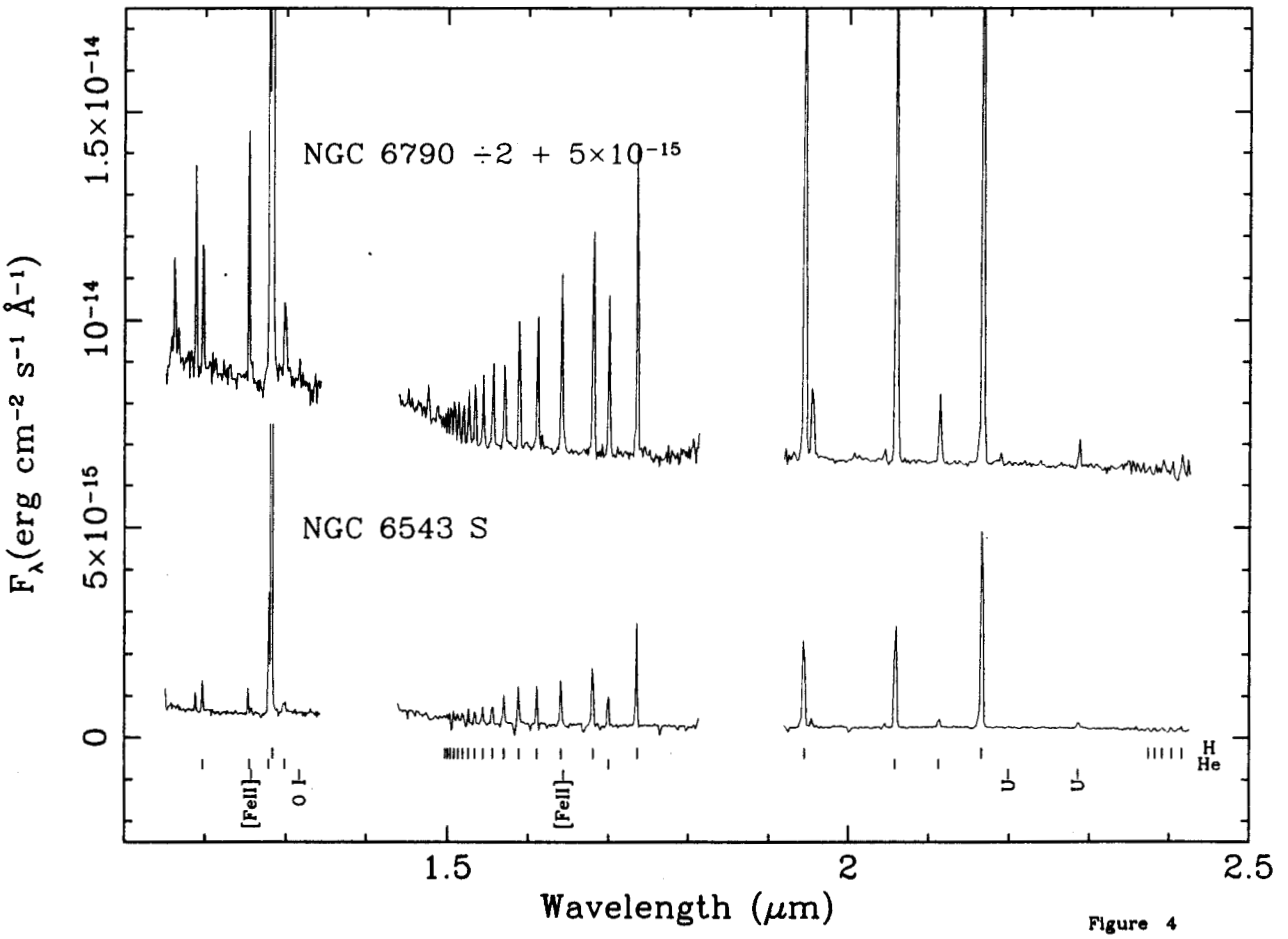

Figure 4

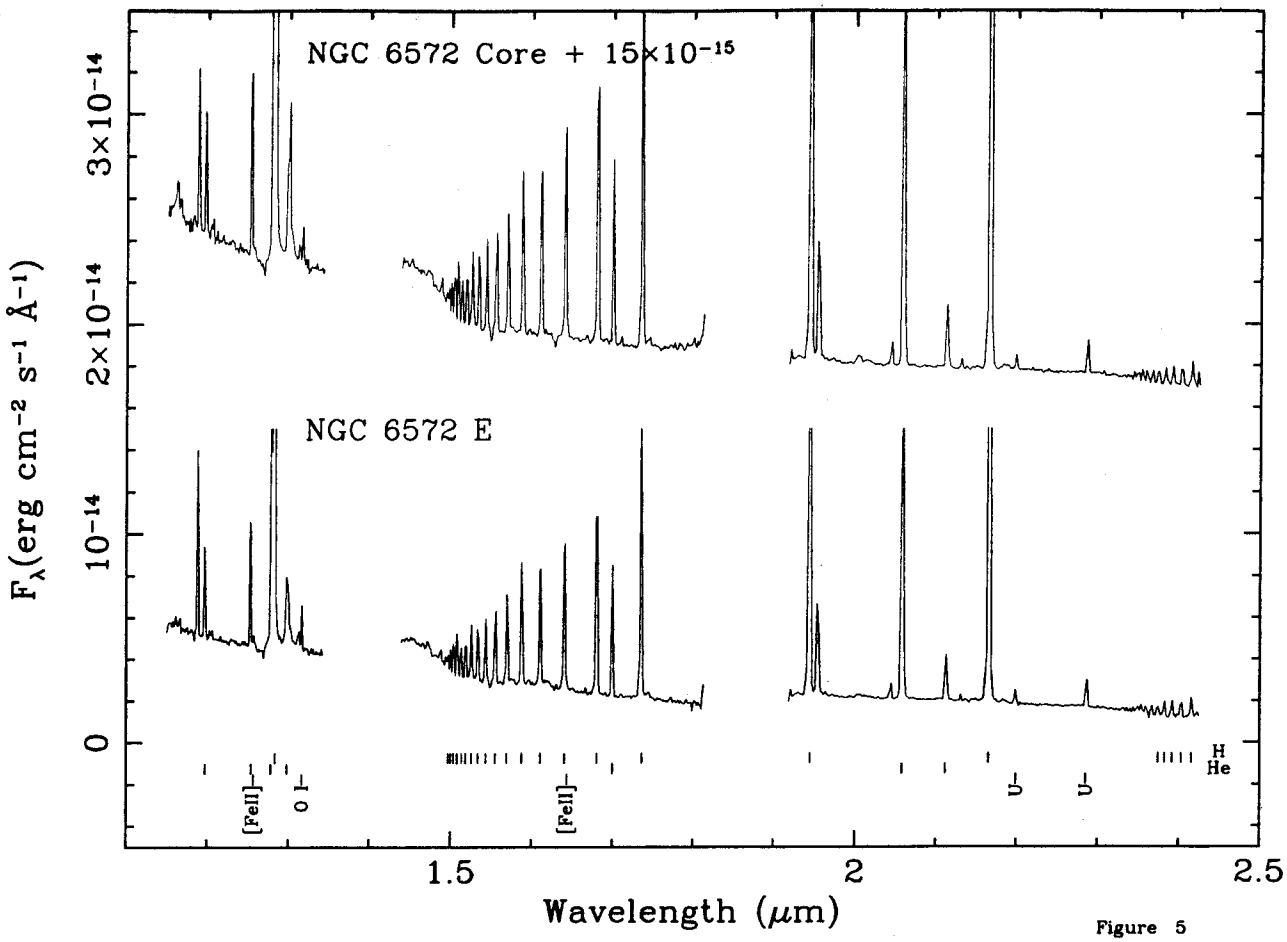

Figure 5

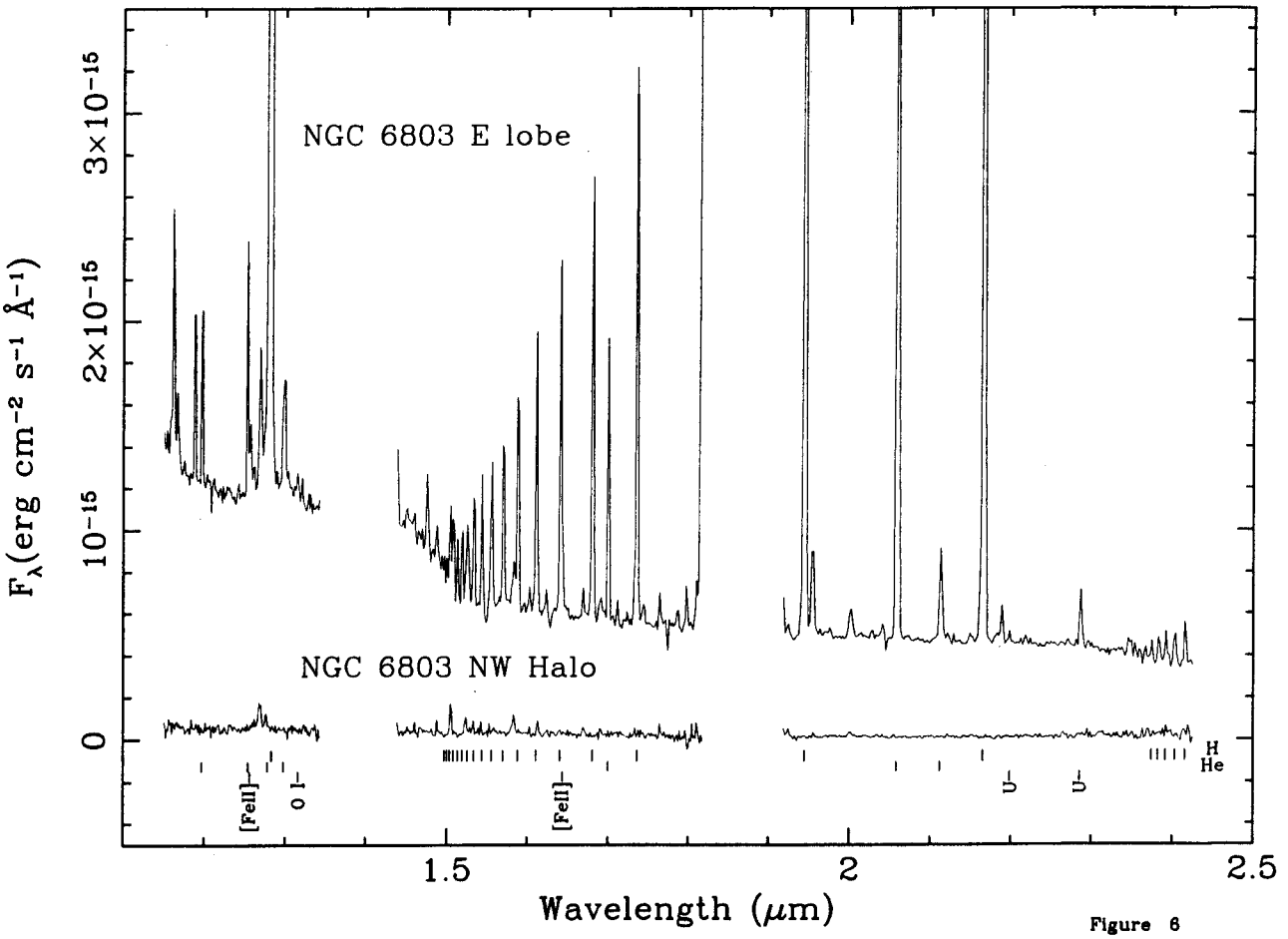

Figure 6

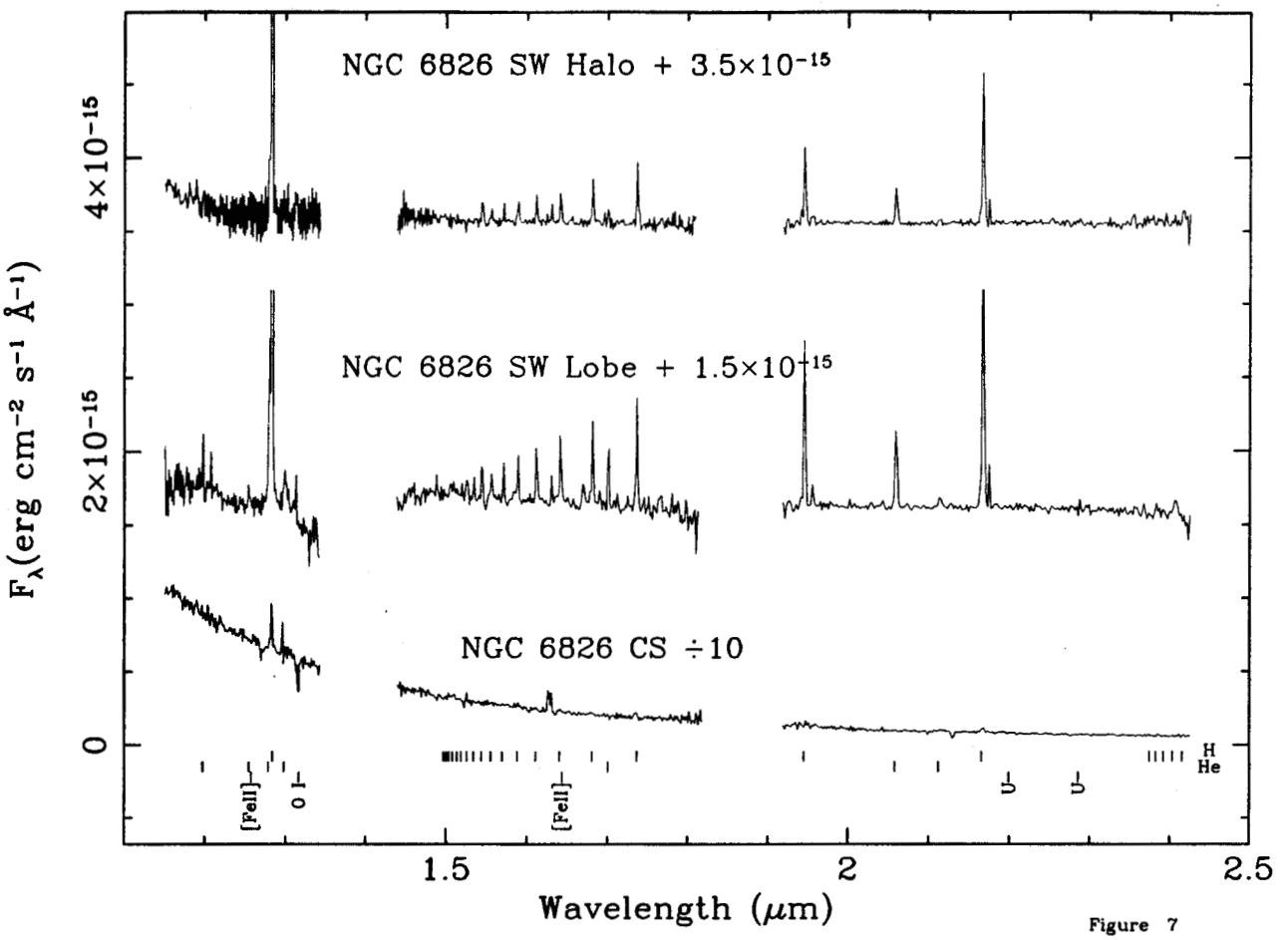

Figure 7

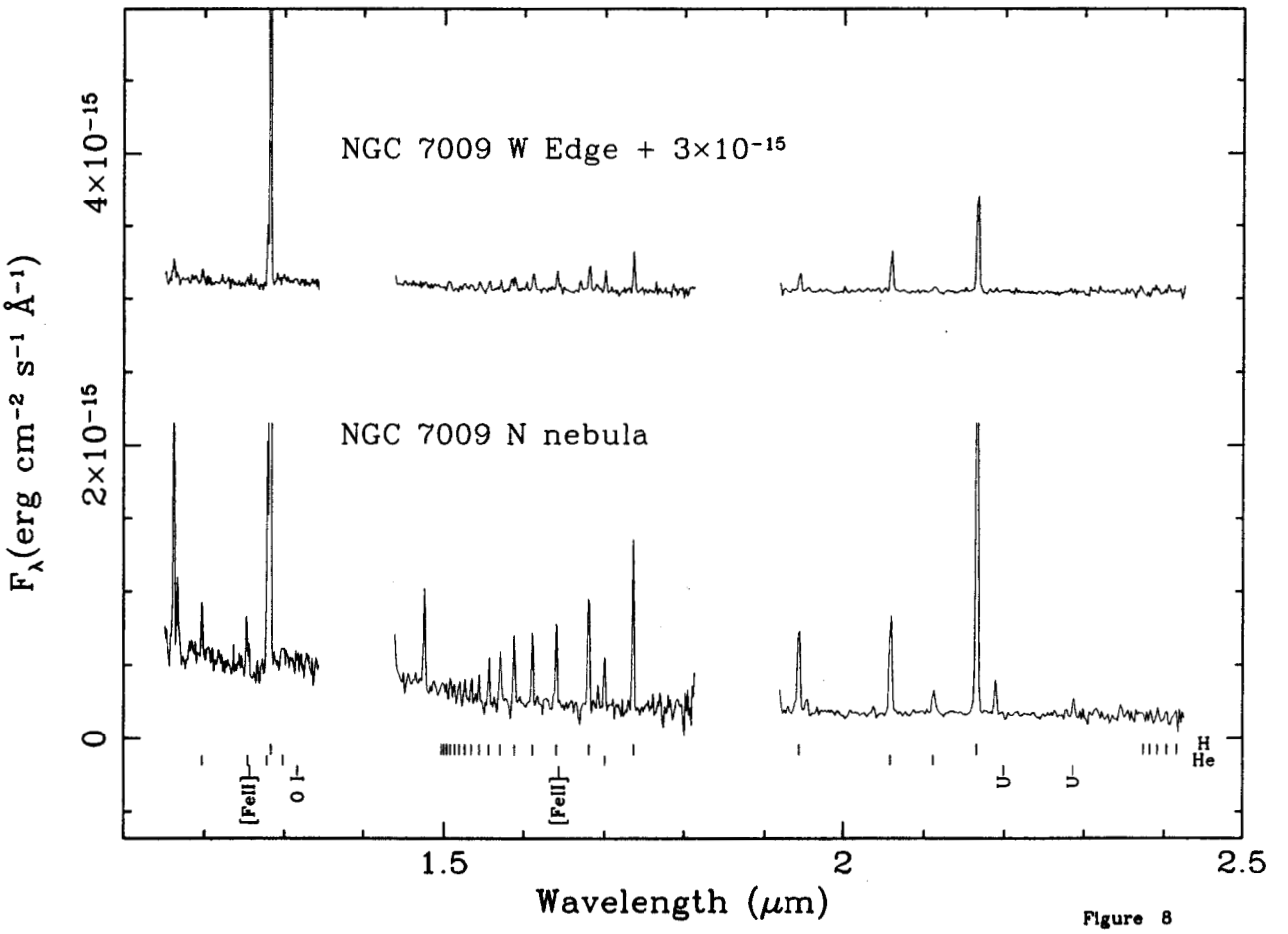

Figure 8

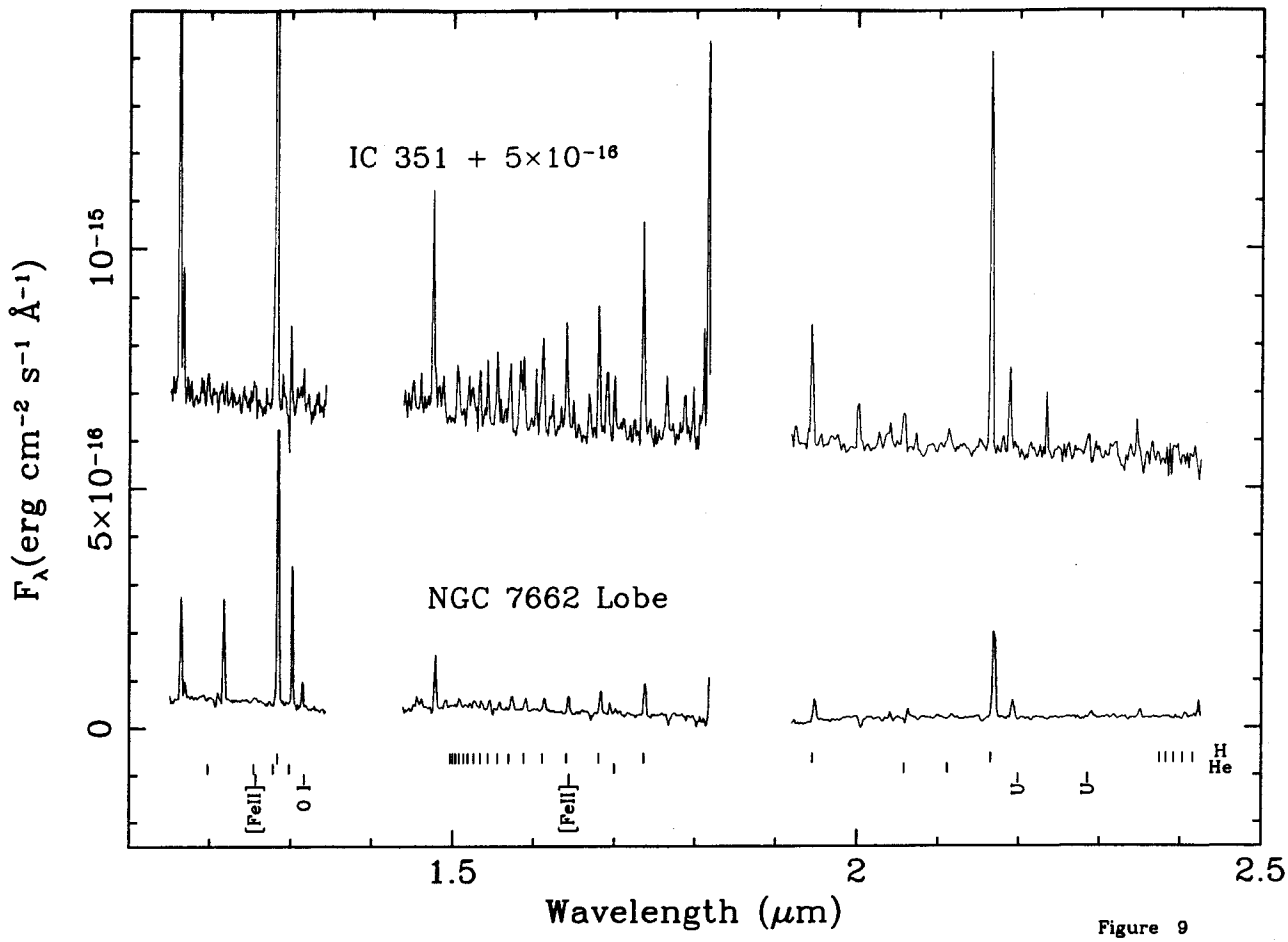

Figure 9

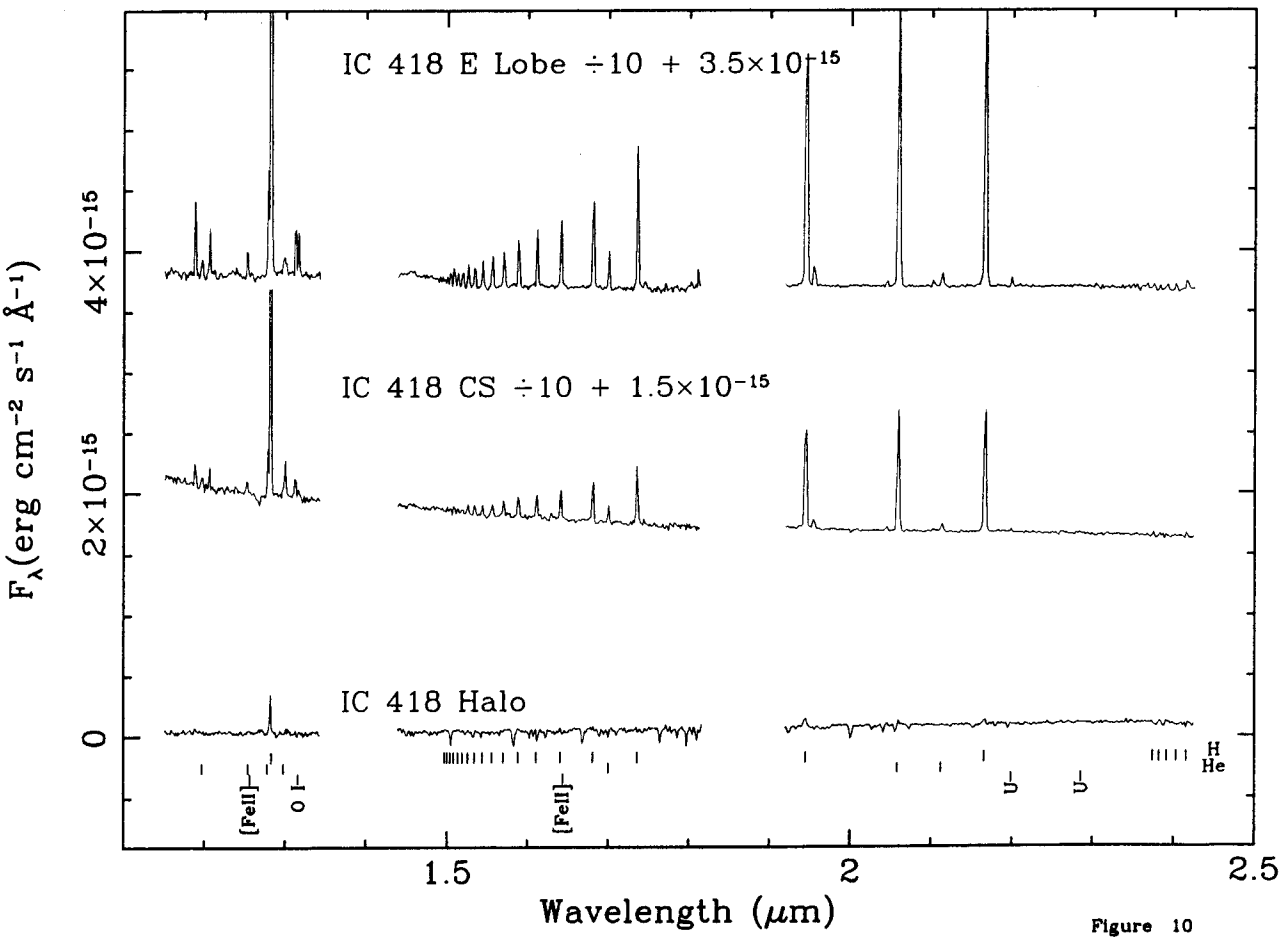

Figure 10

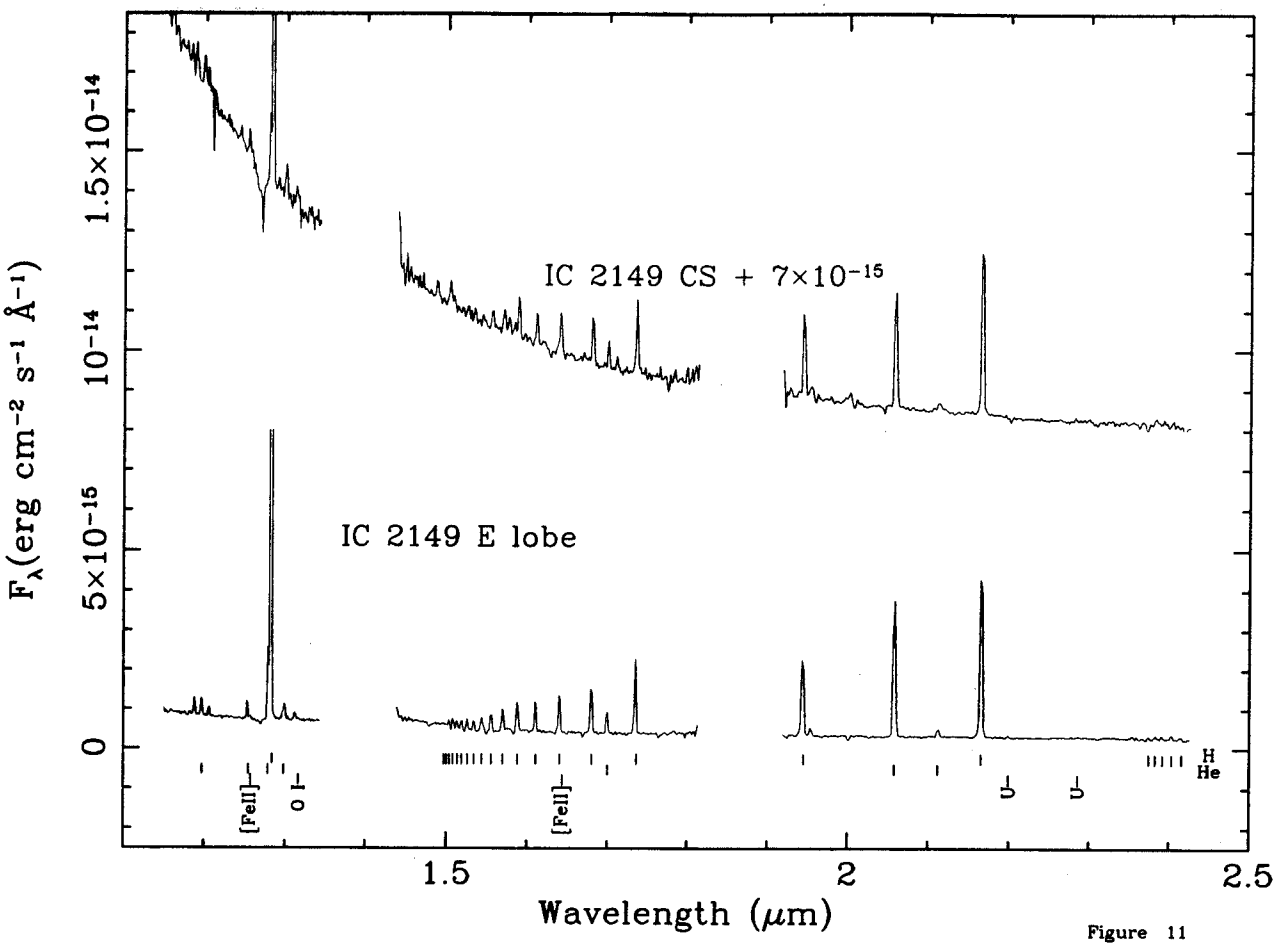

Figure 11

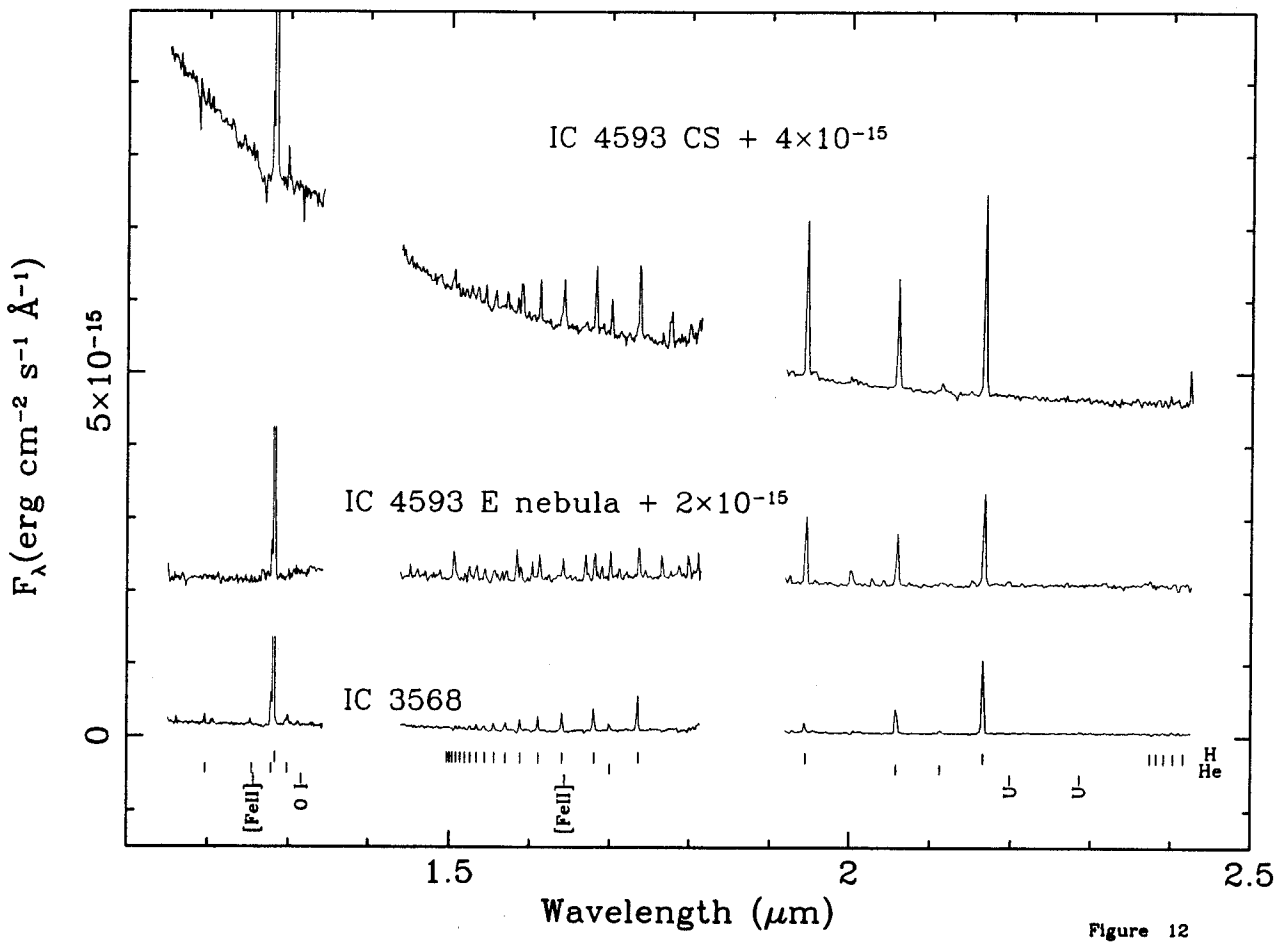

Figure 12

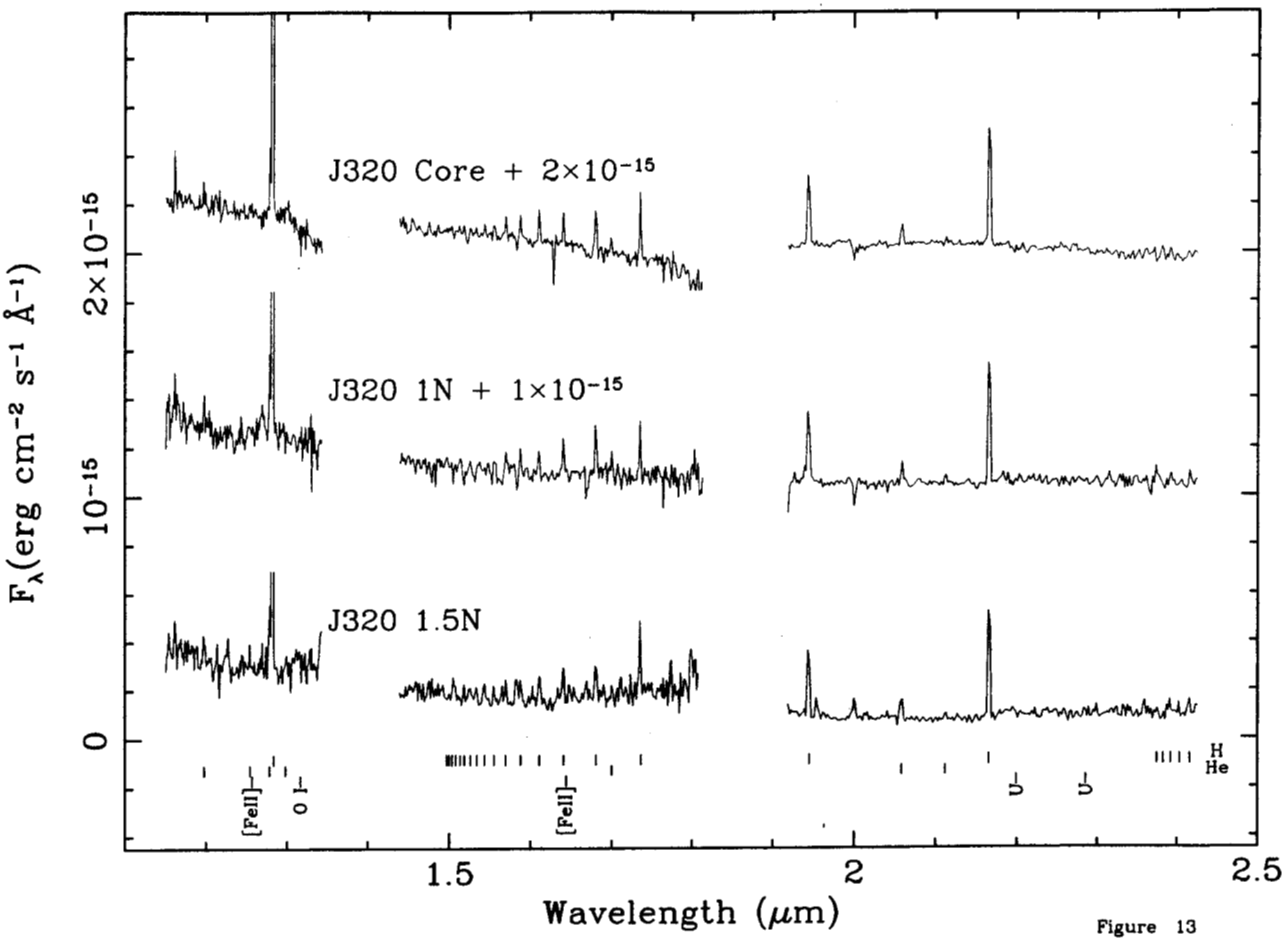

Figure 13

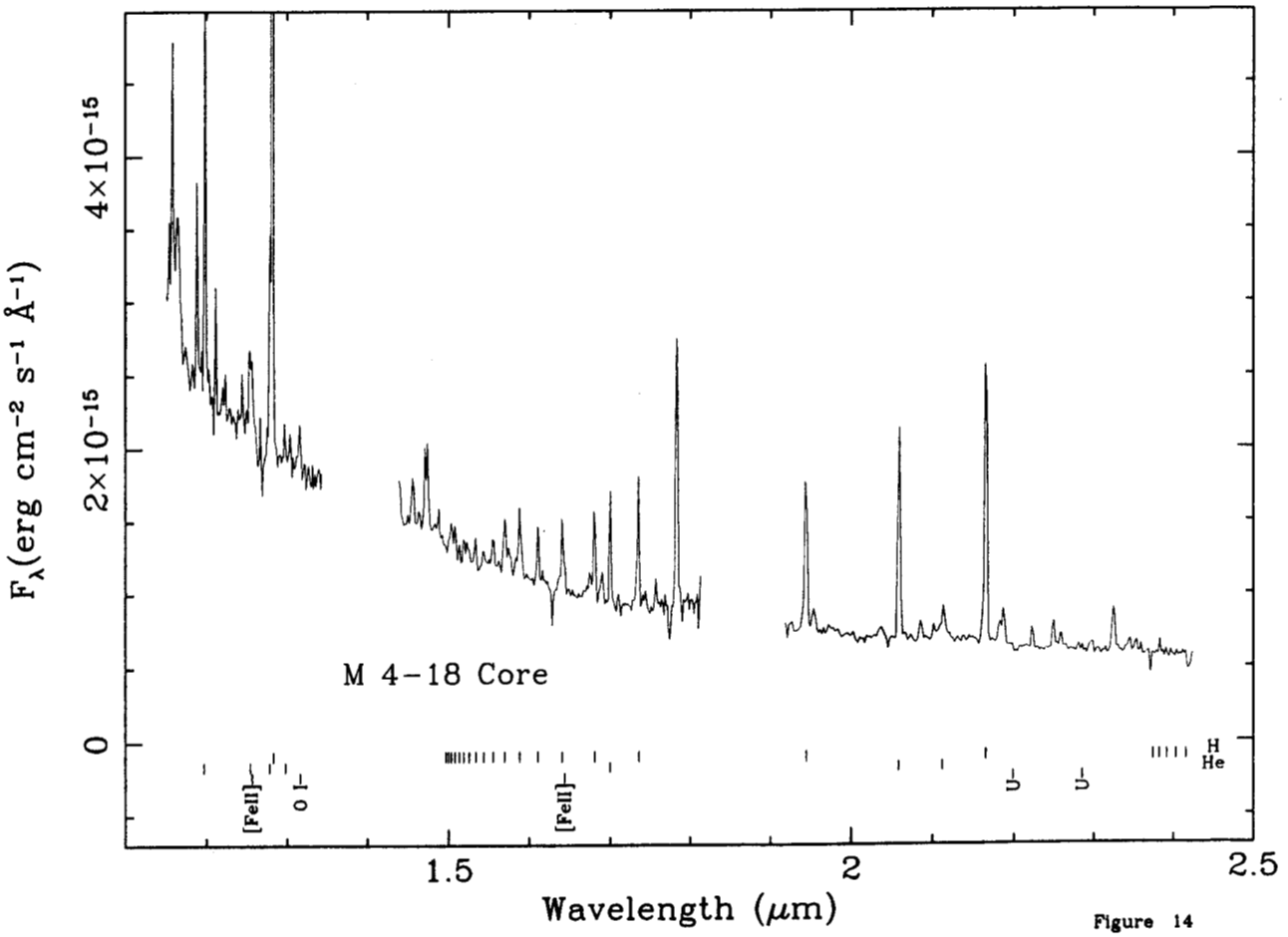

Figure 14

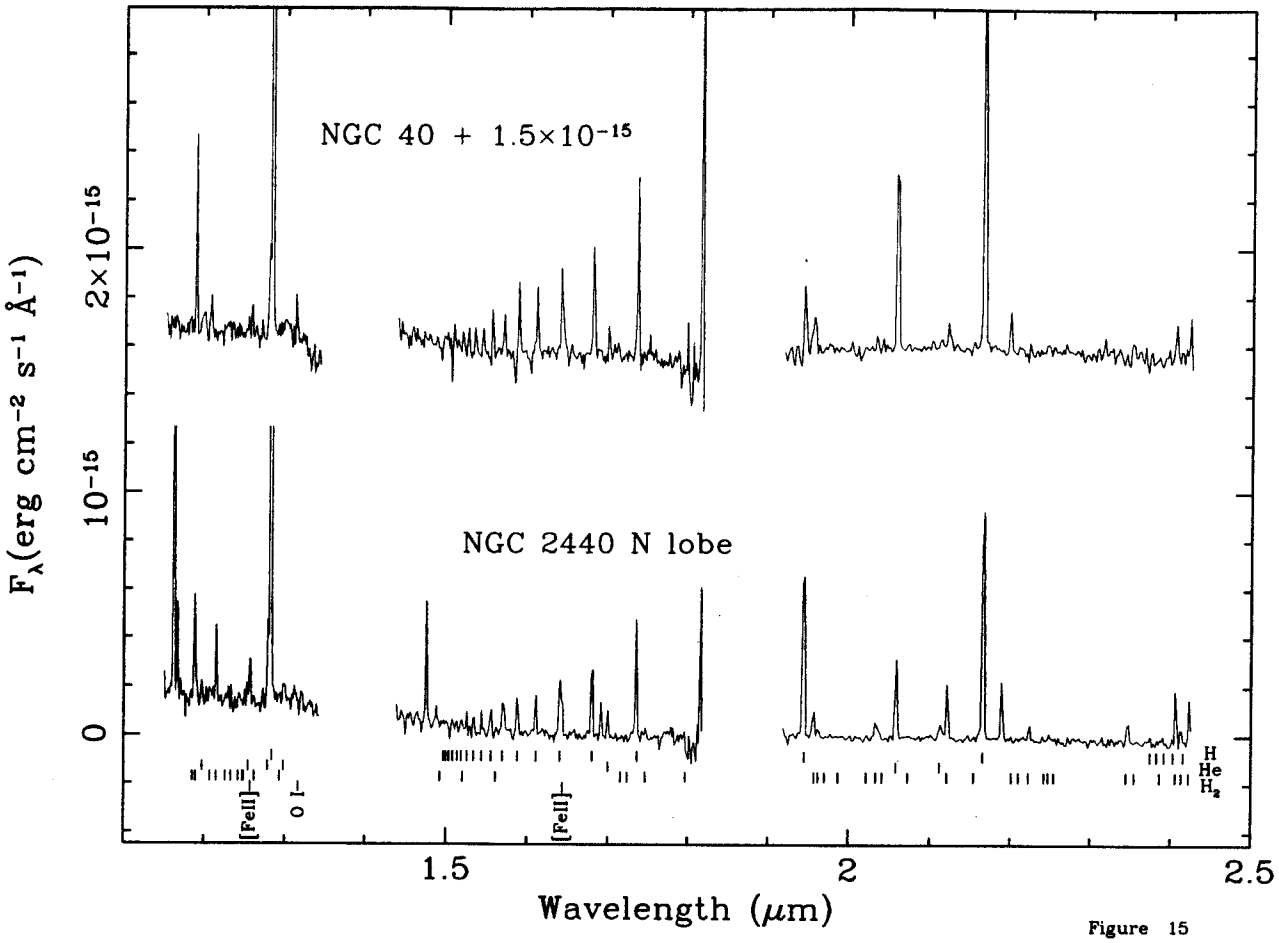

Figure 15

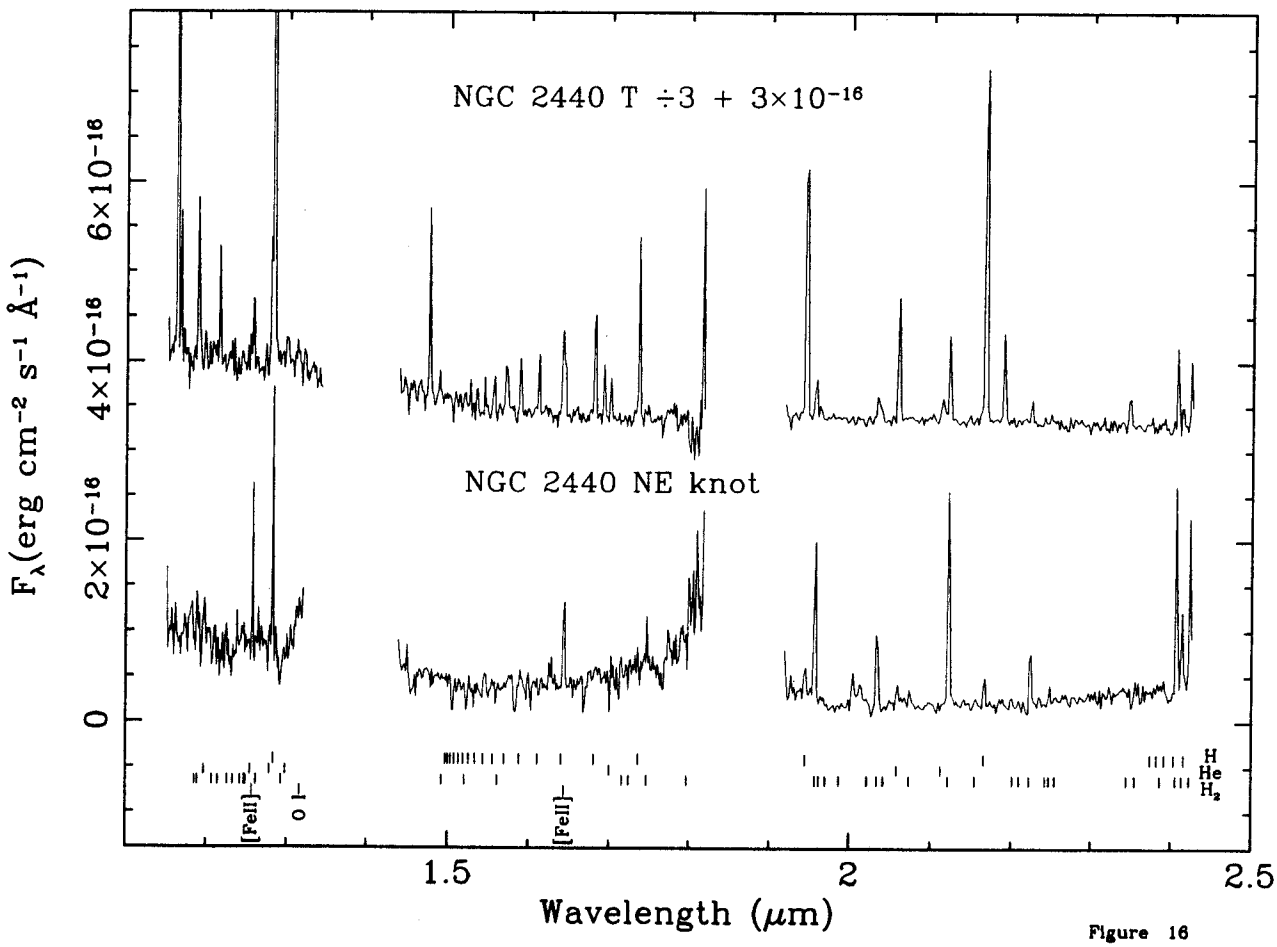

Figure 16

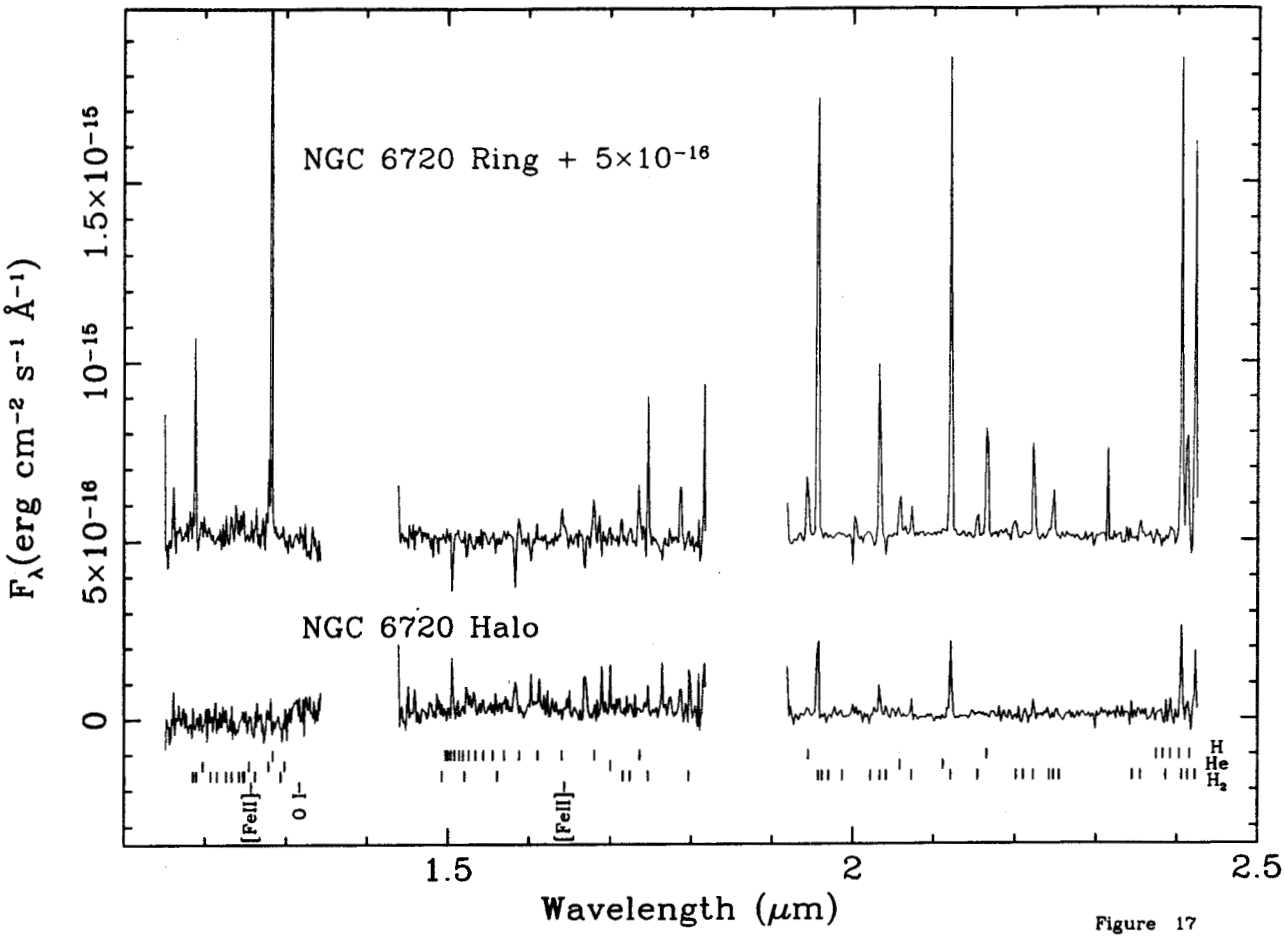

Figure 17

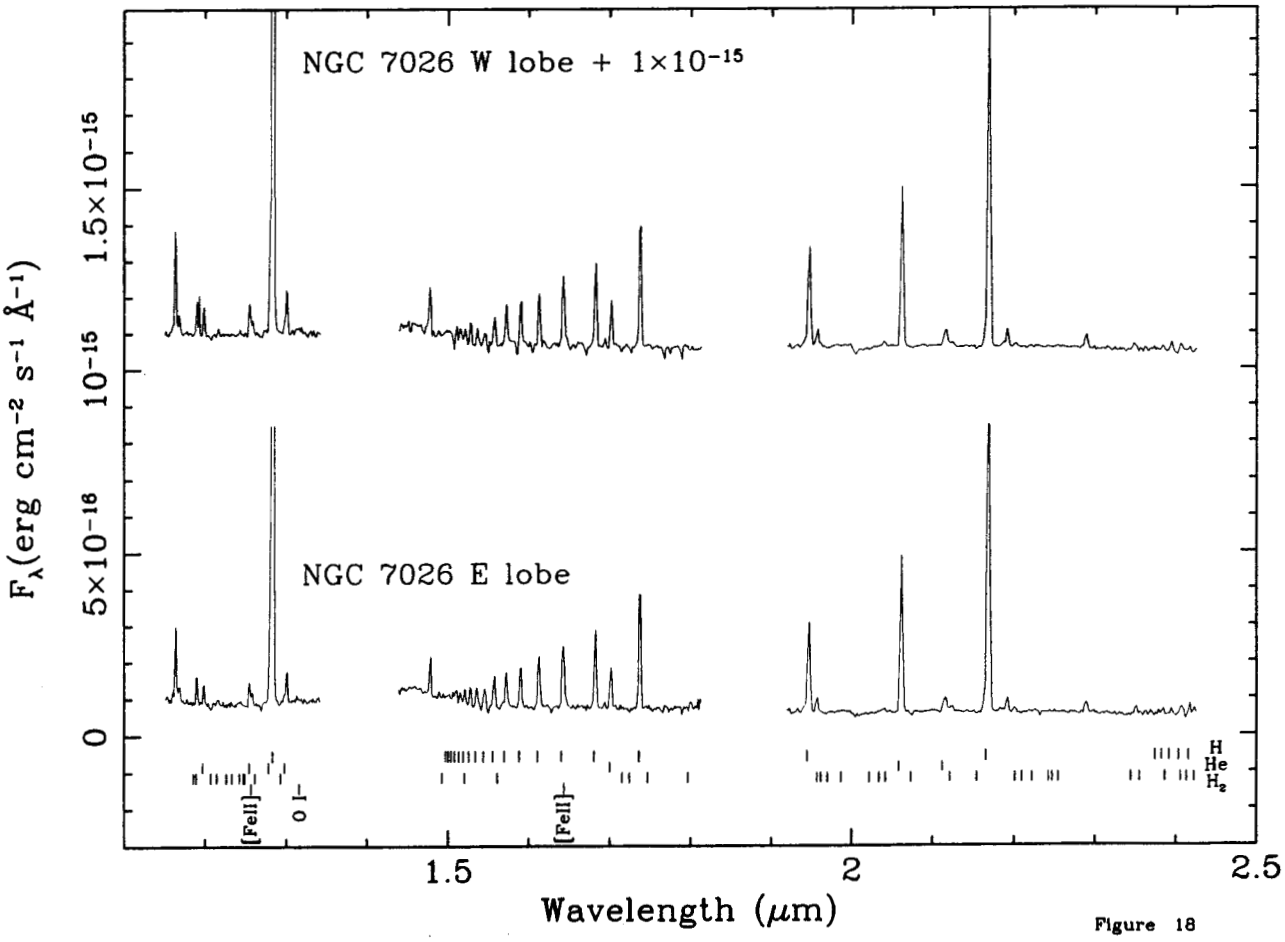

Figure 18

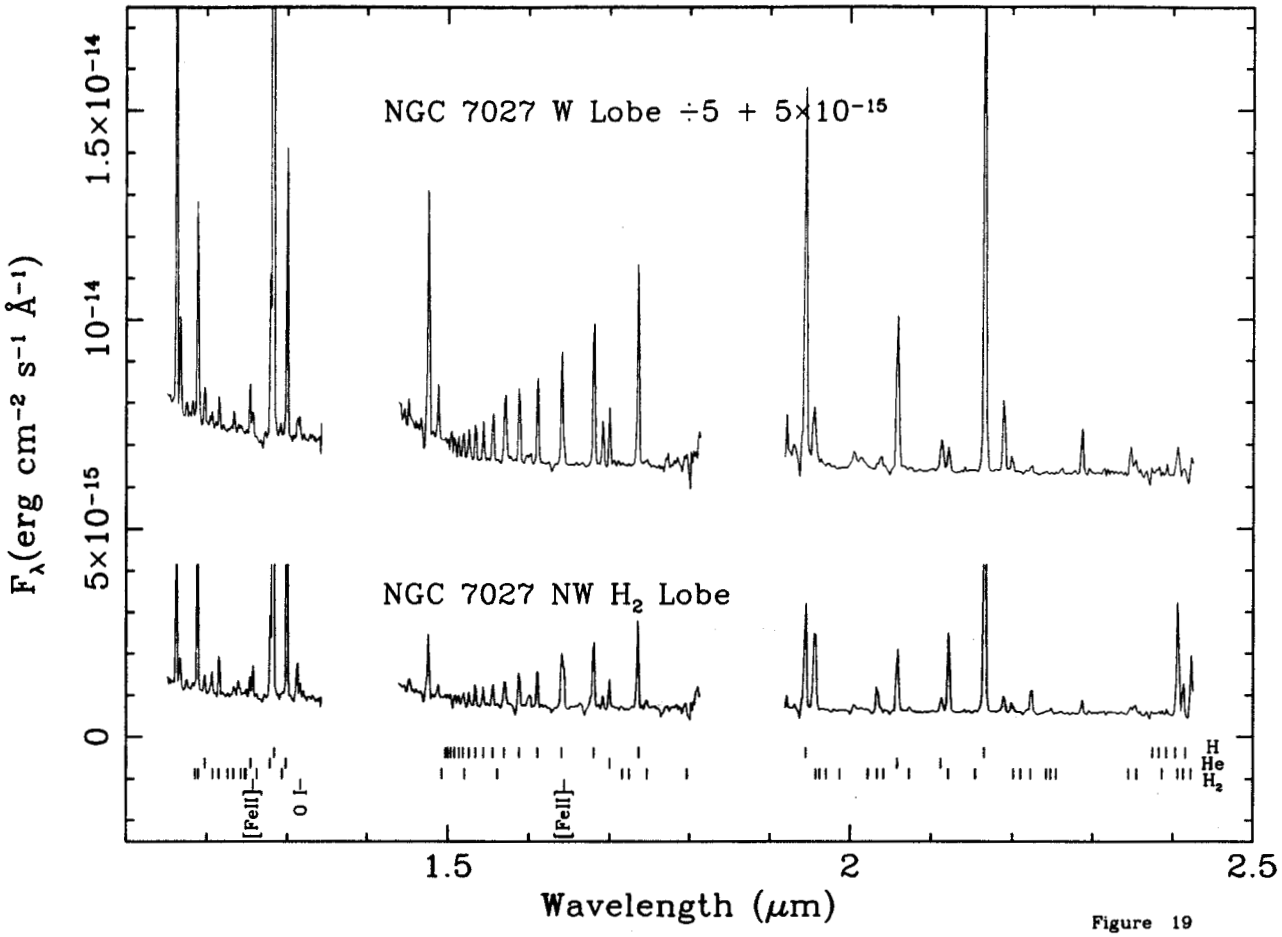

Figure 19

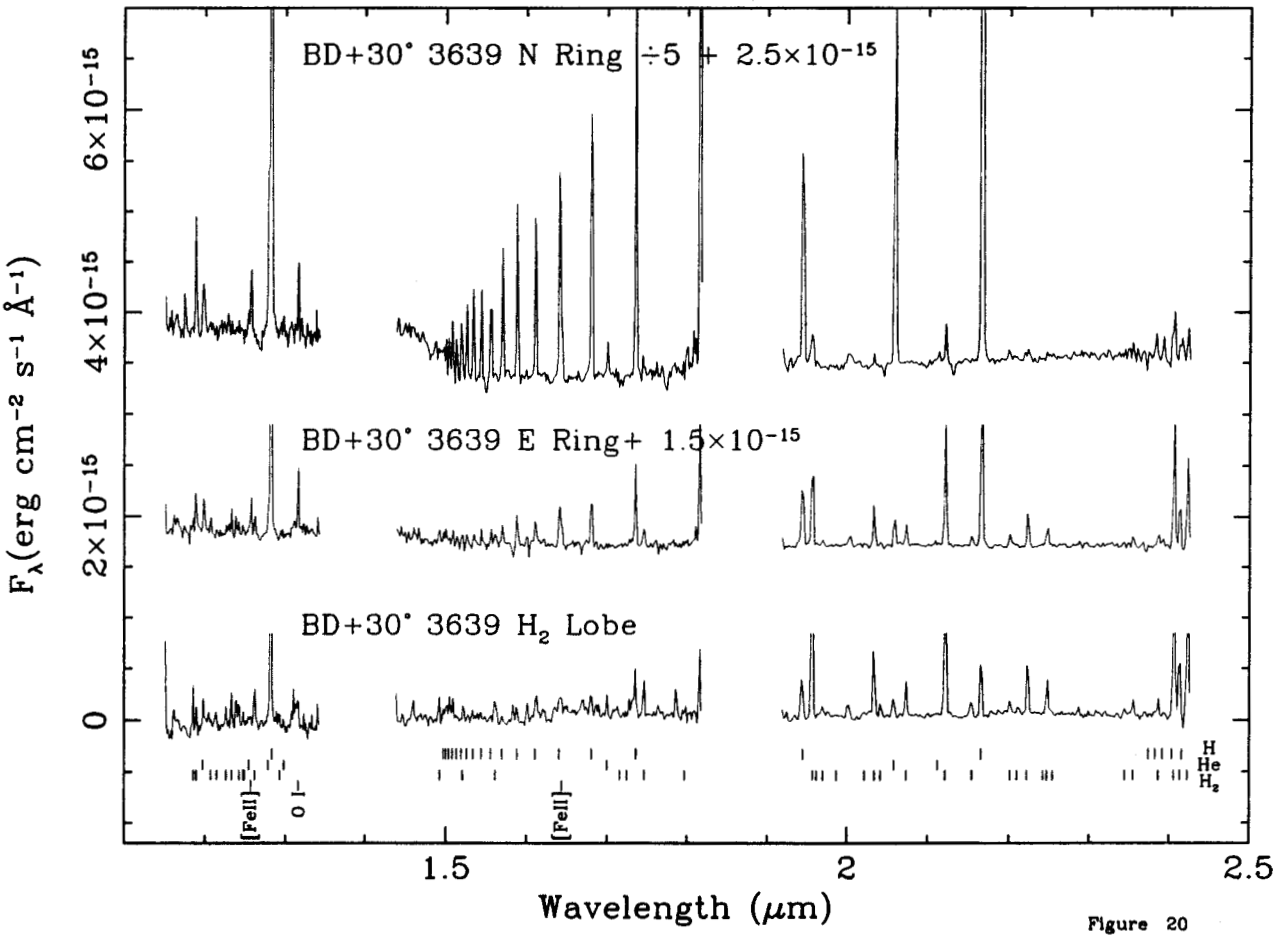

Figure 20

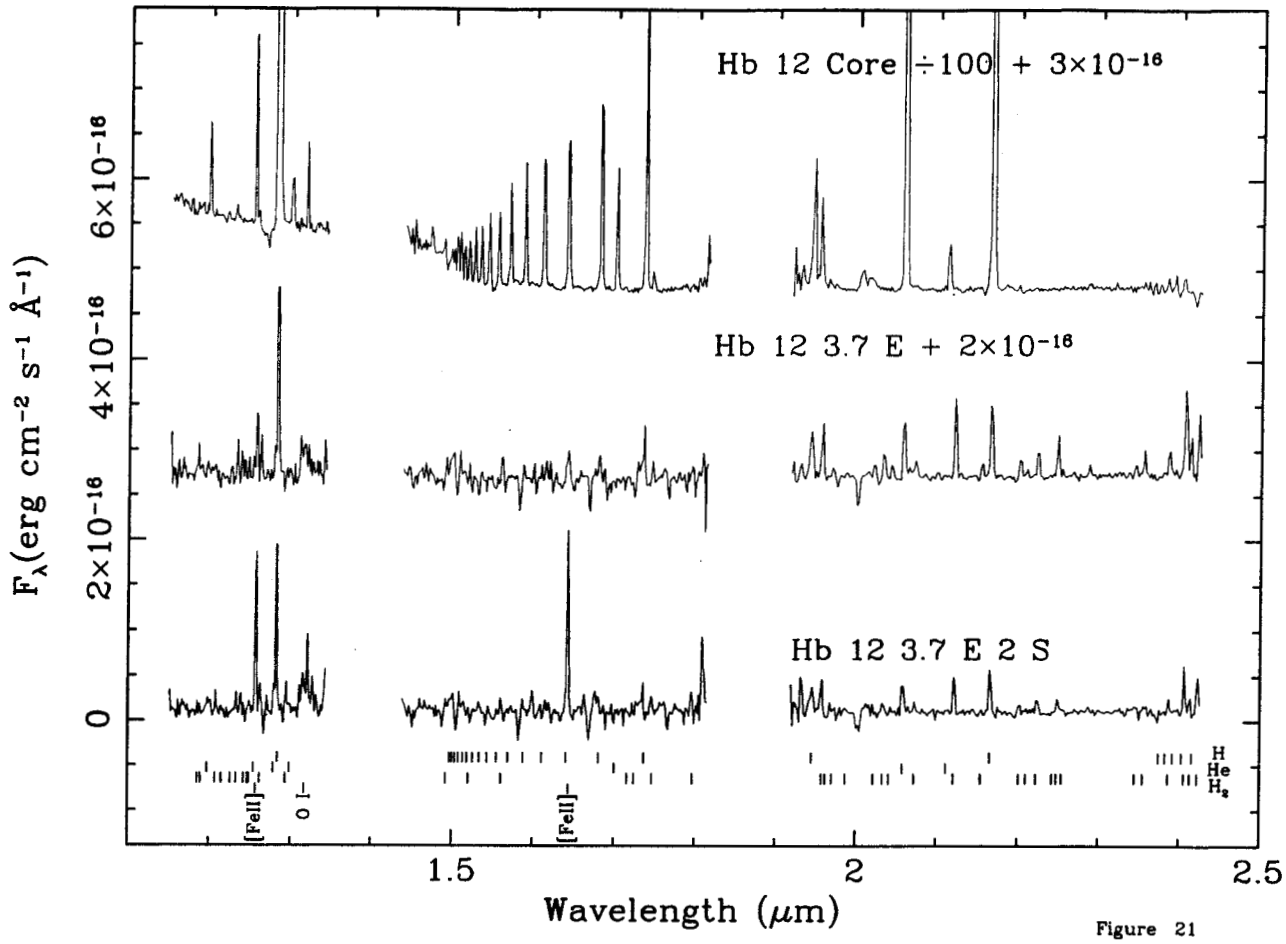

Figure 21

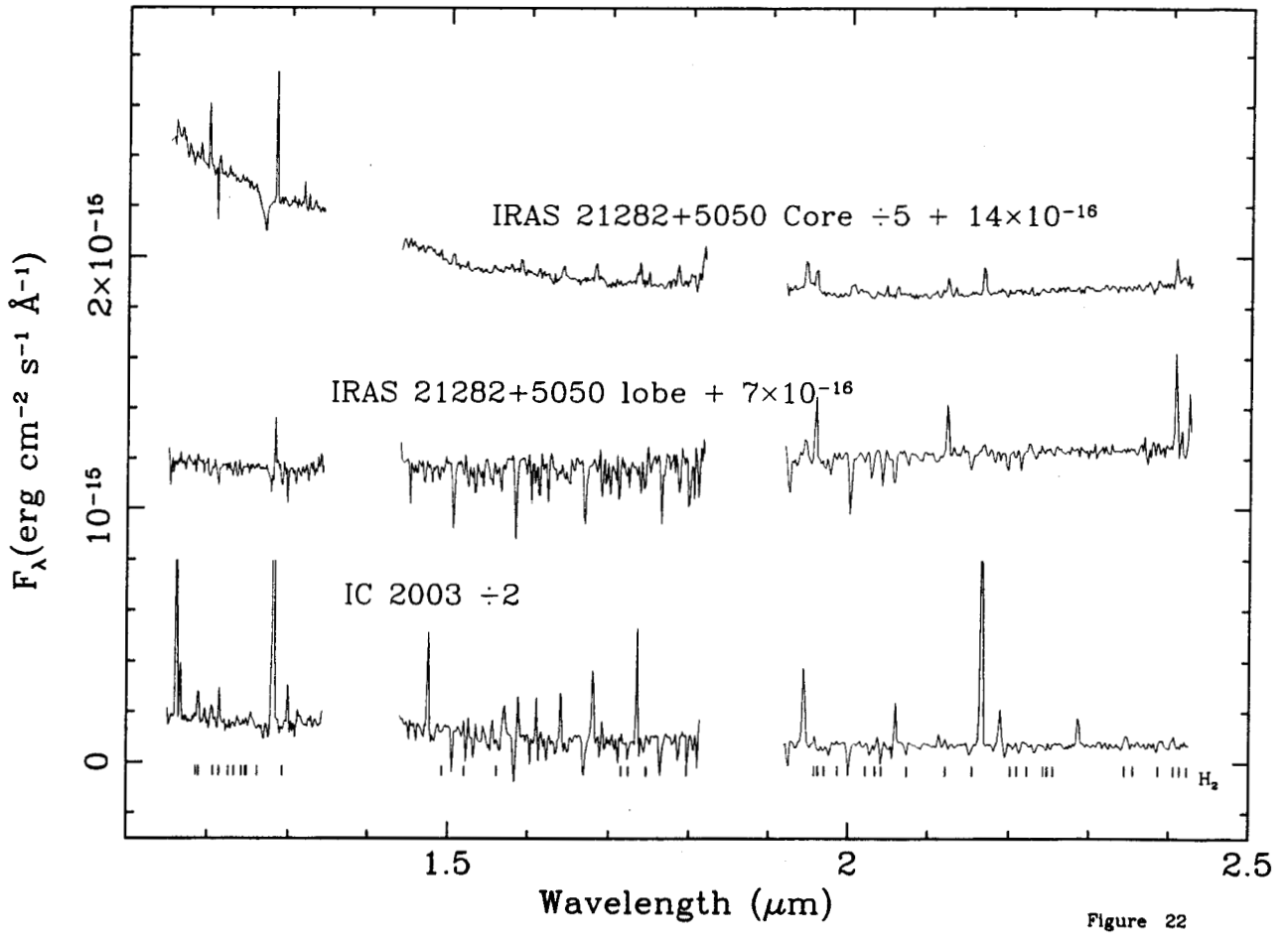

Figure 22

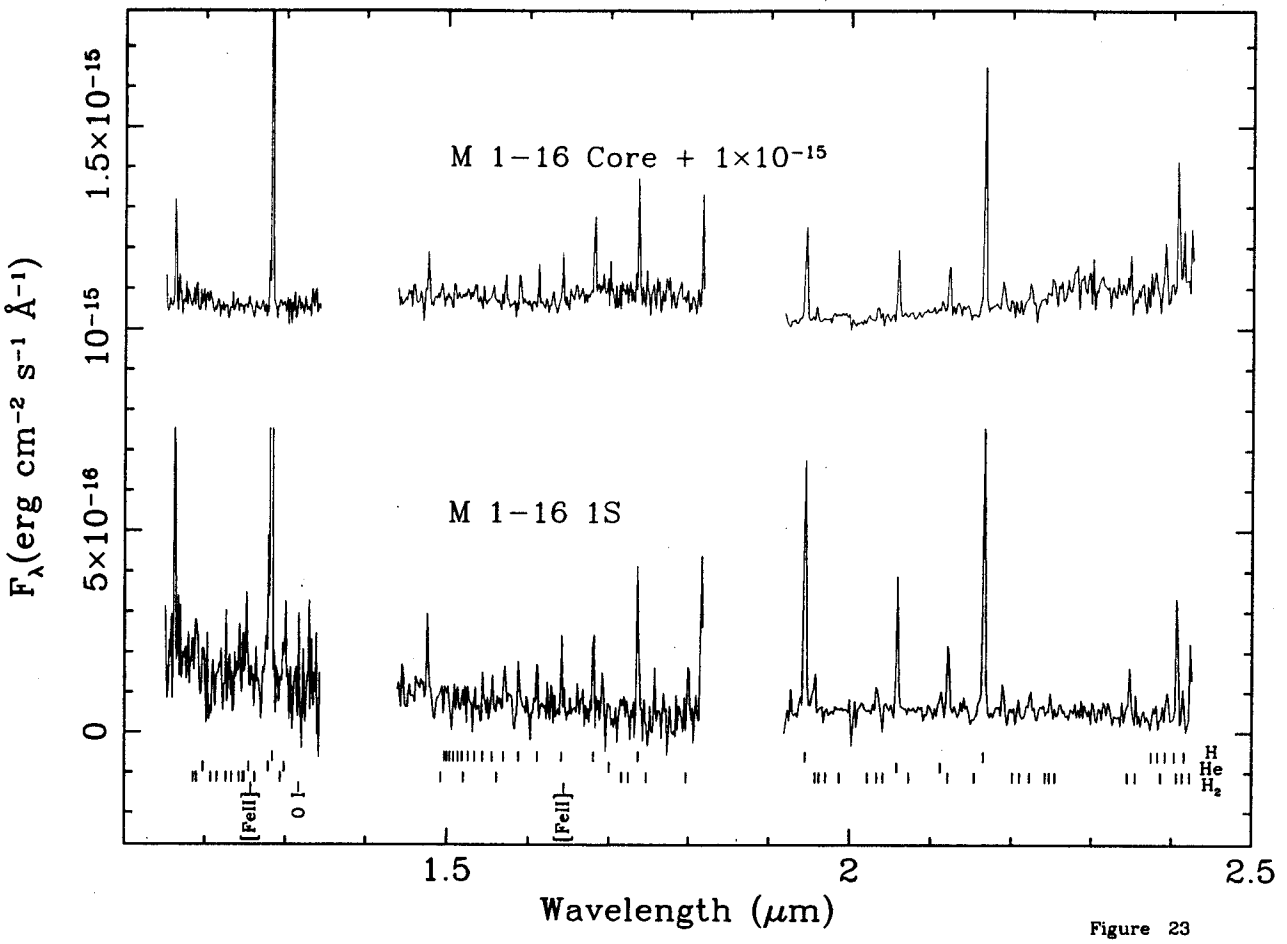

Figure 23

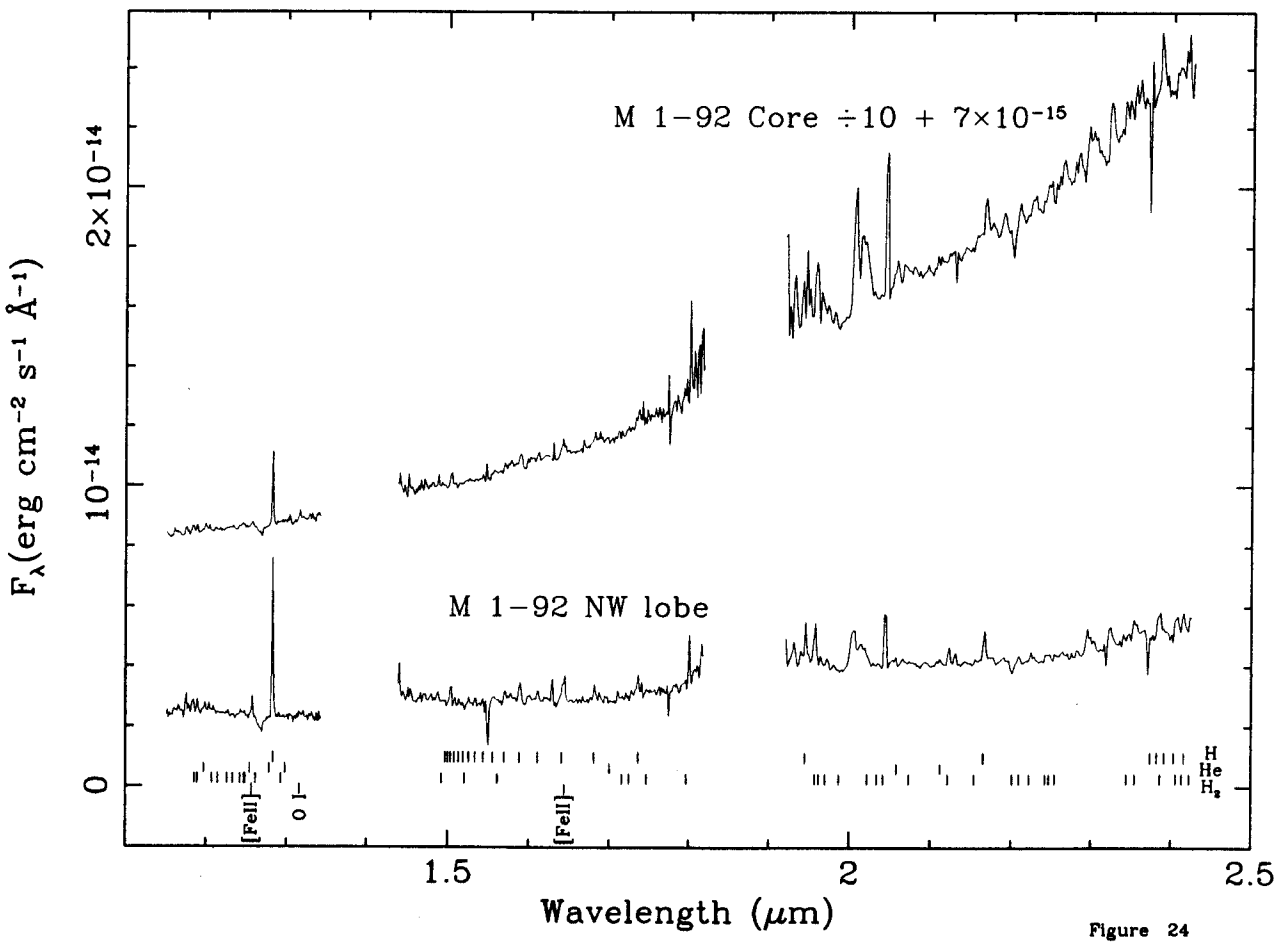

Figure 24

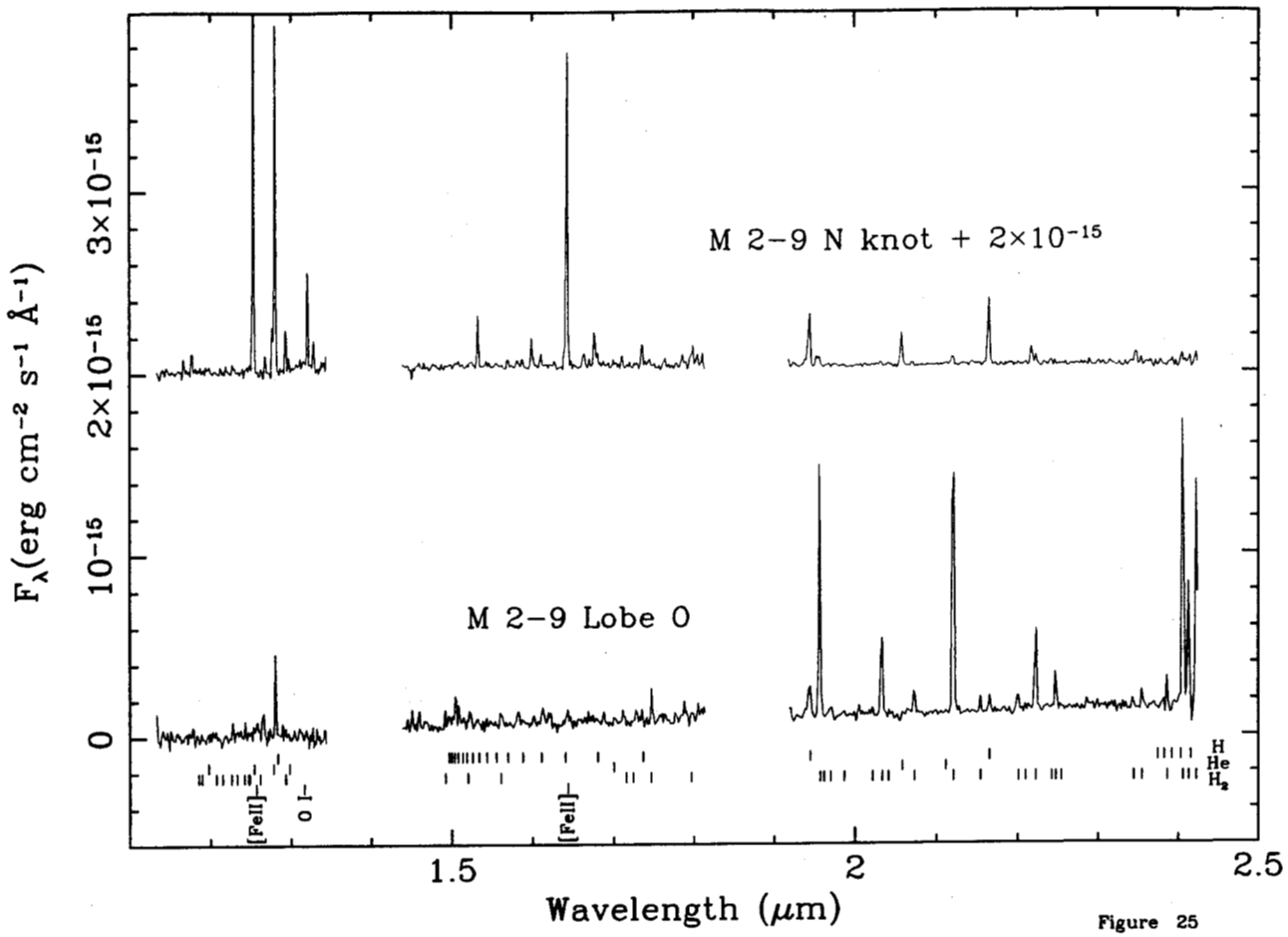

Figure 25

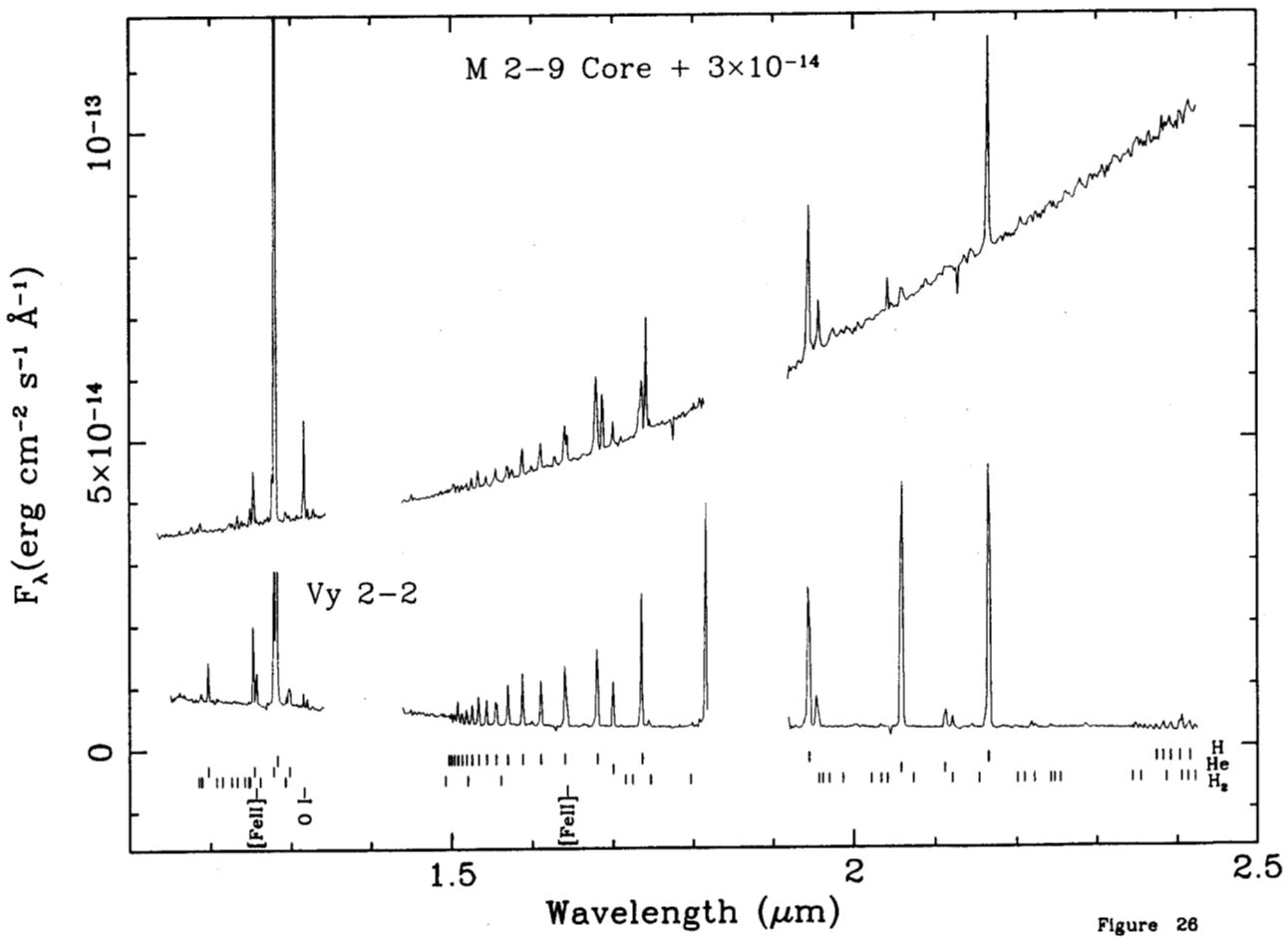

Figure 26

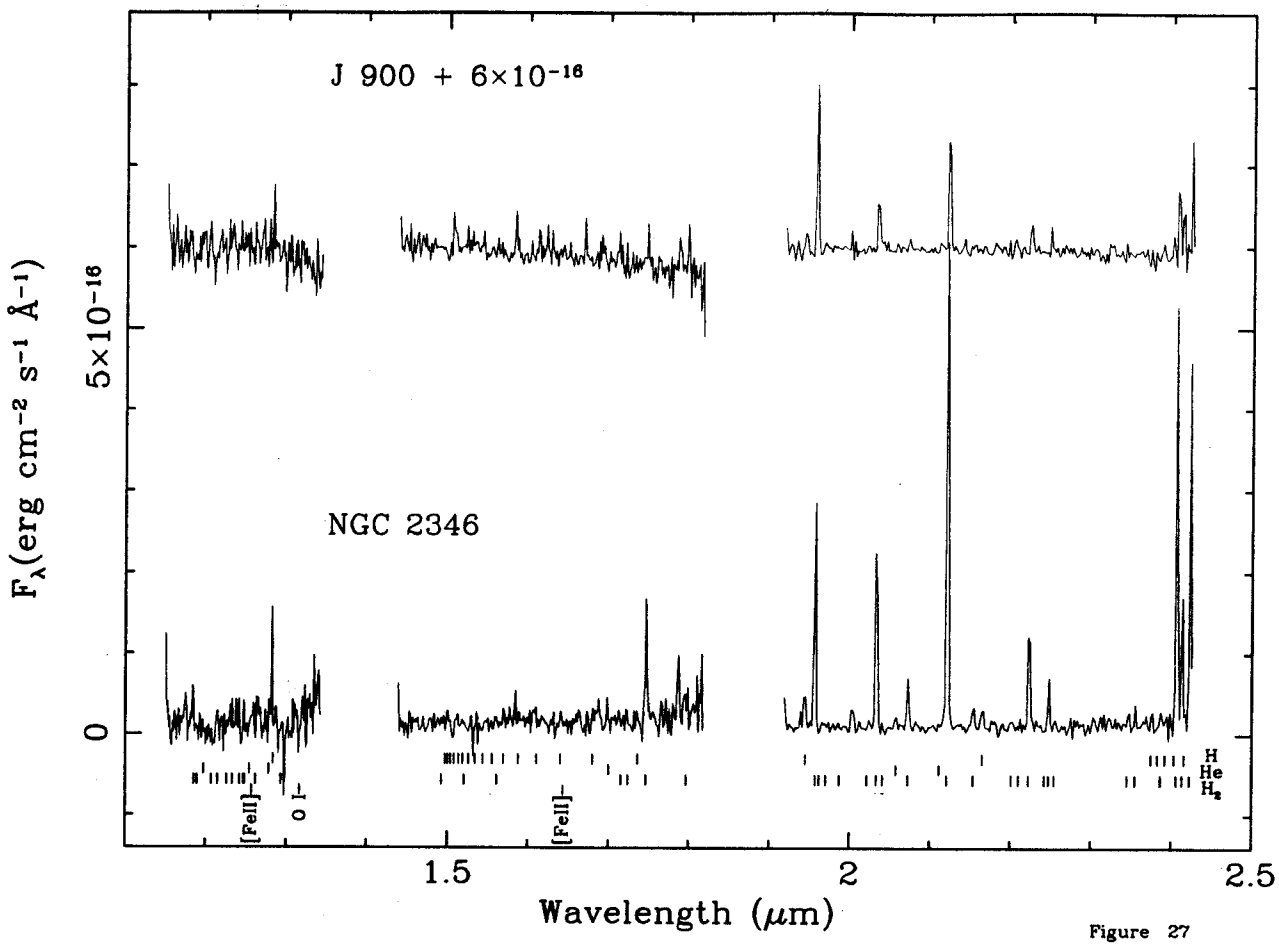

Figure 27

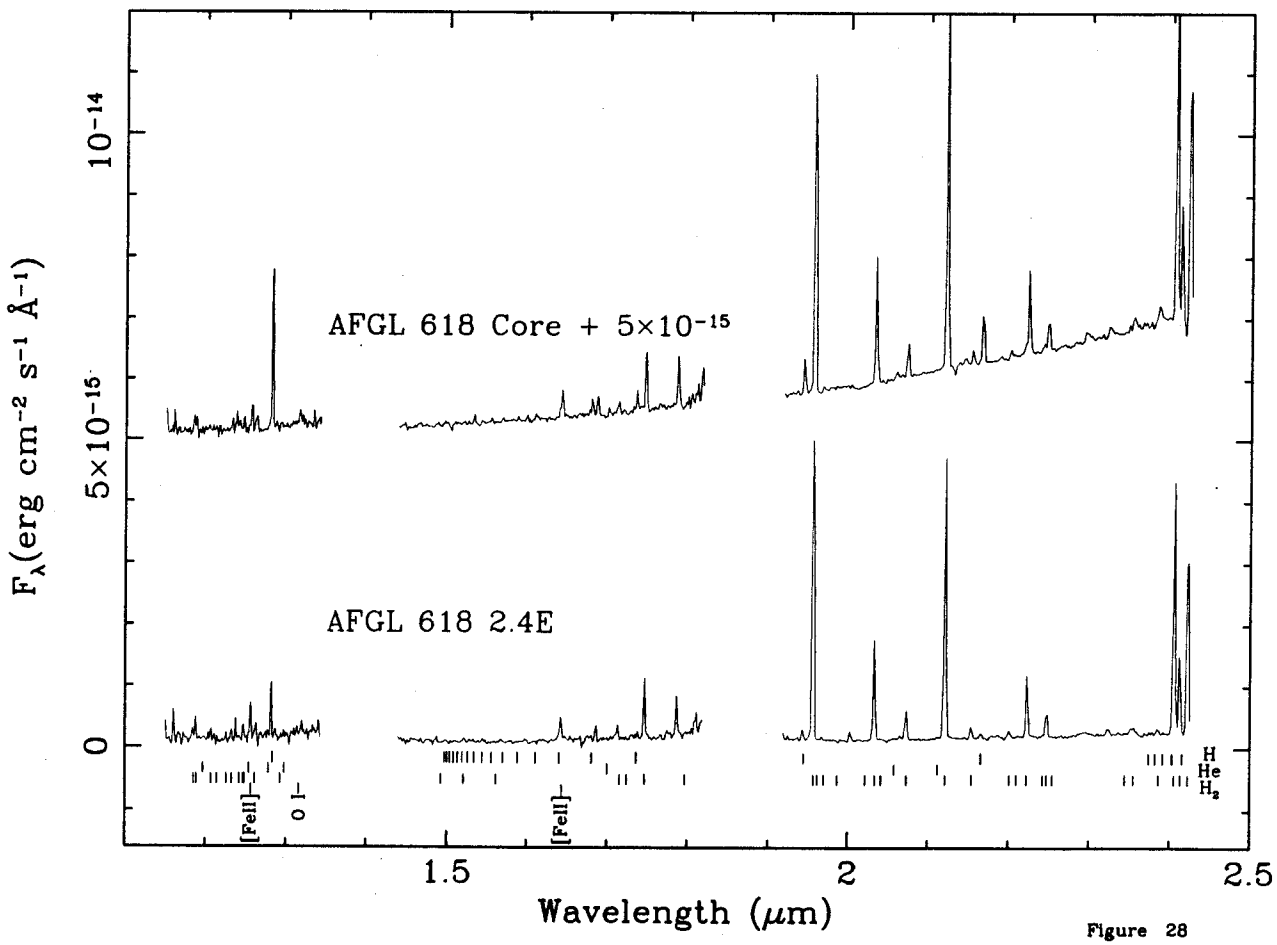

Figure 28

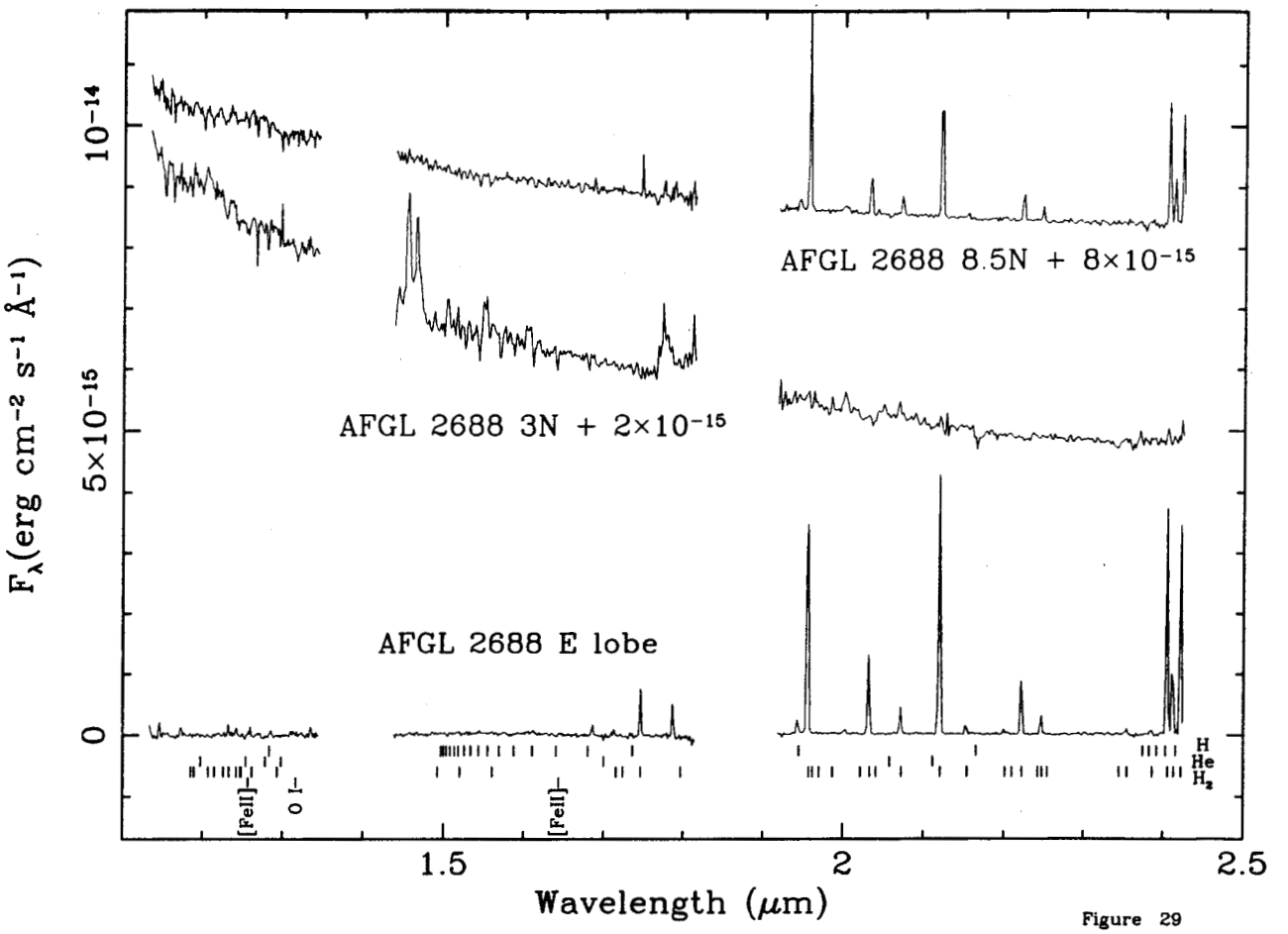

Figure 29

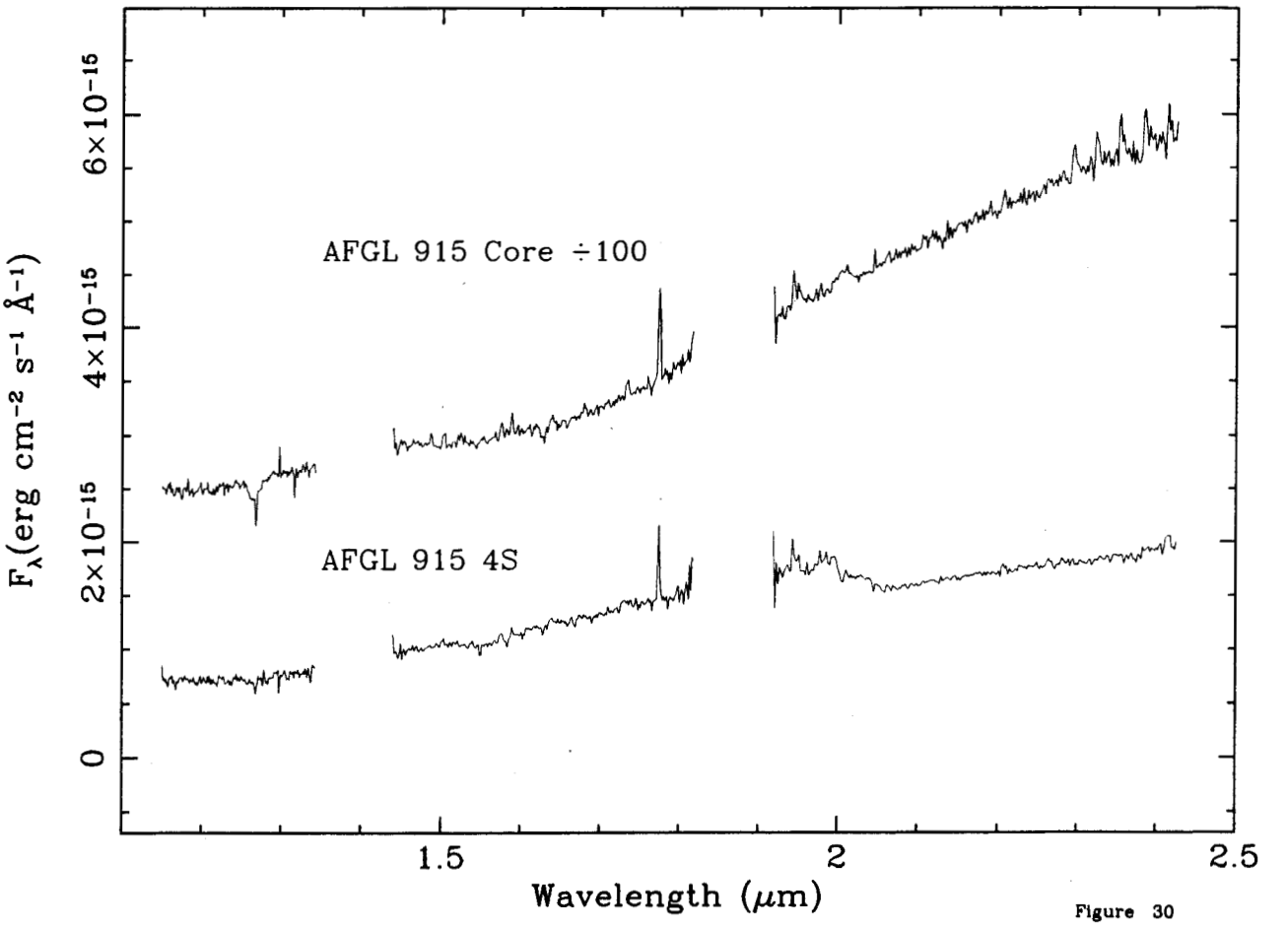

Figure 30

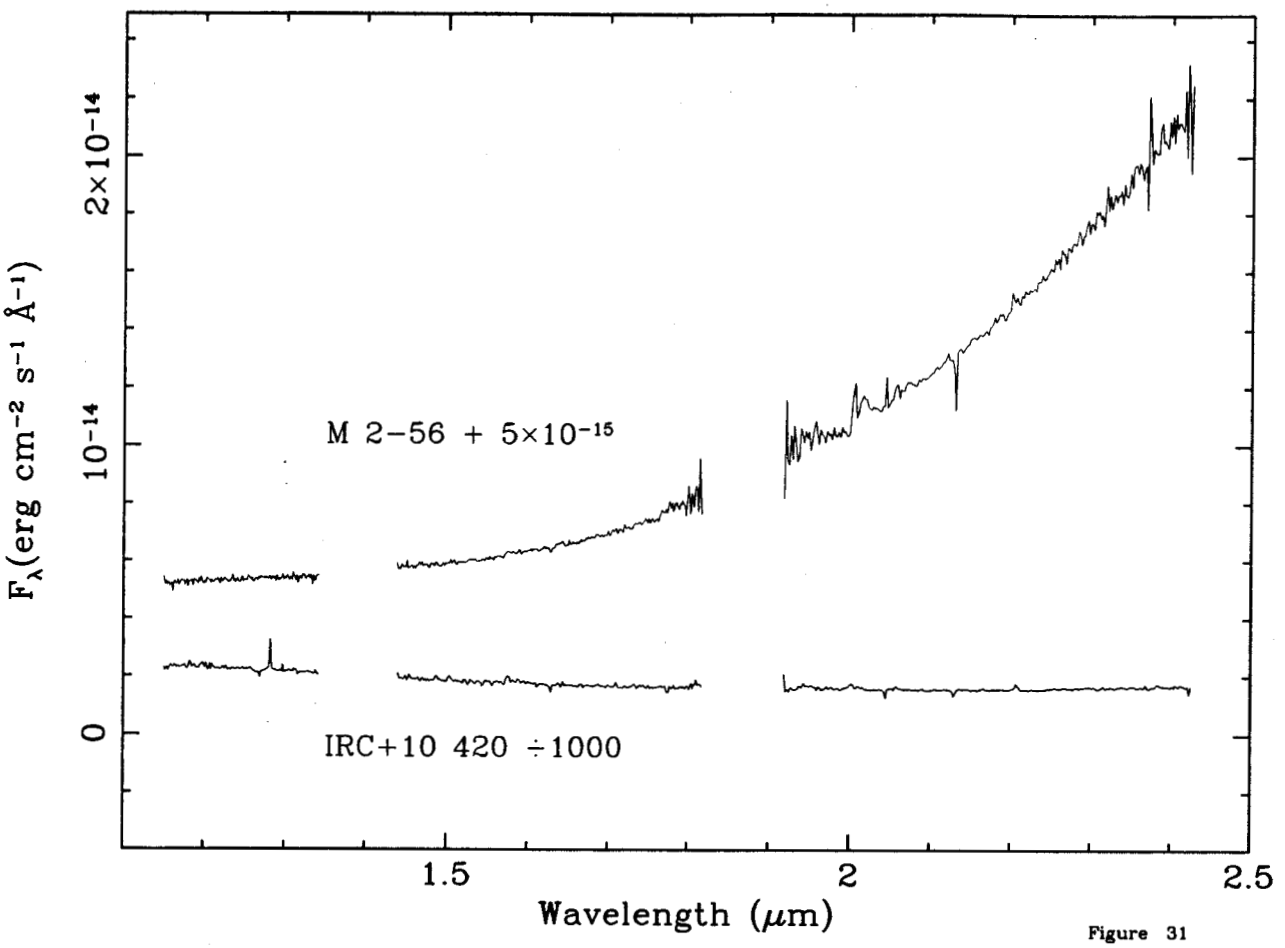

Figure 31

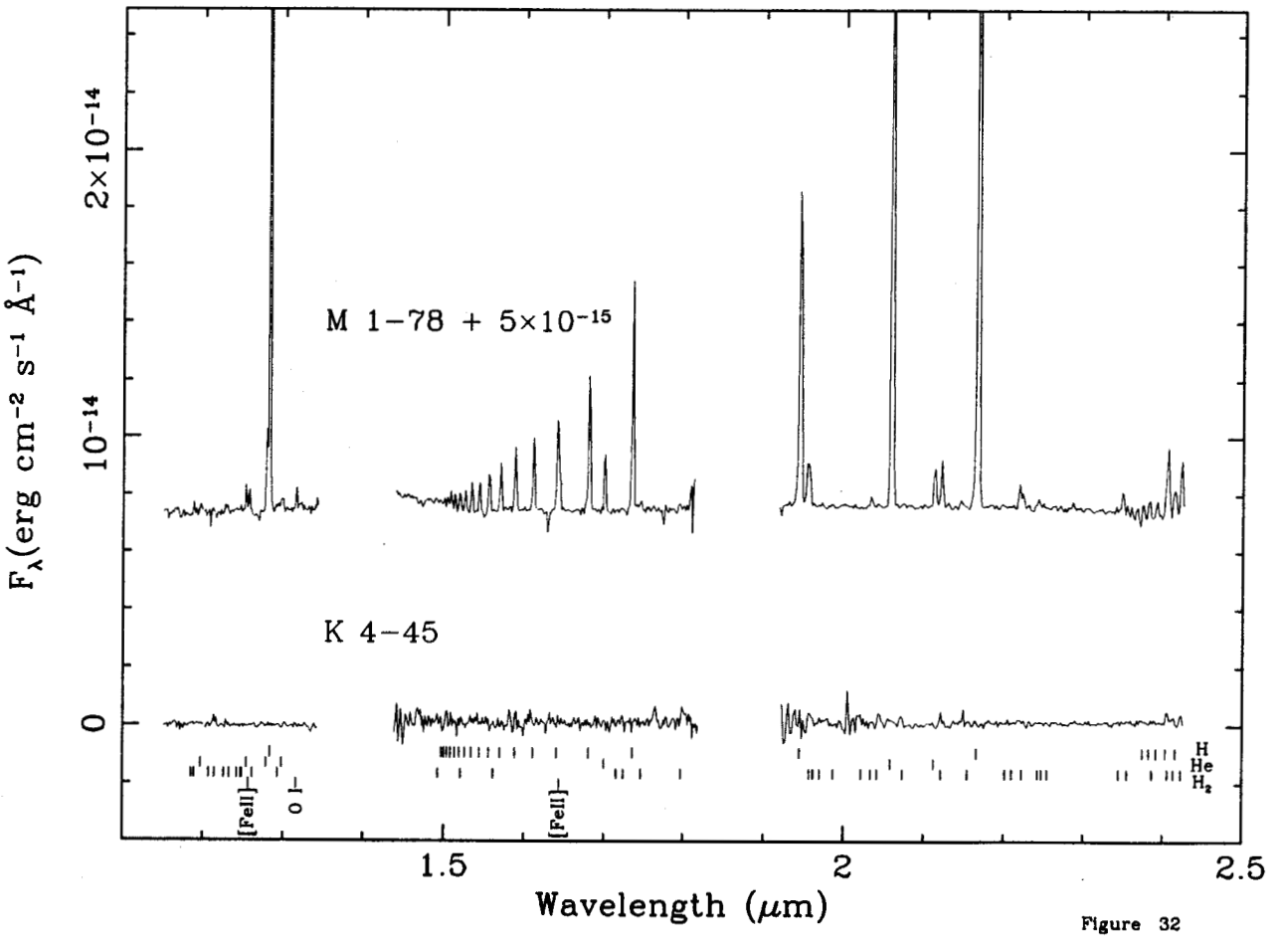

Figure 32

Figure 33a

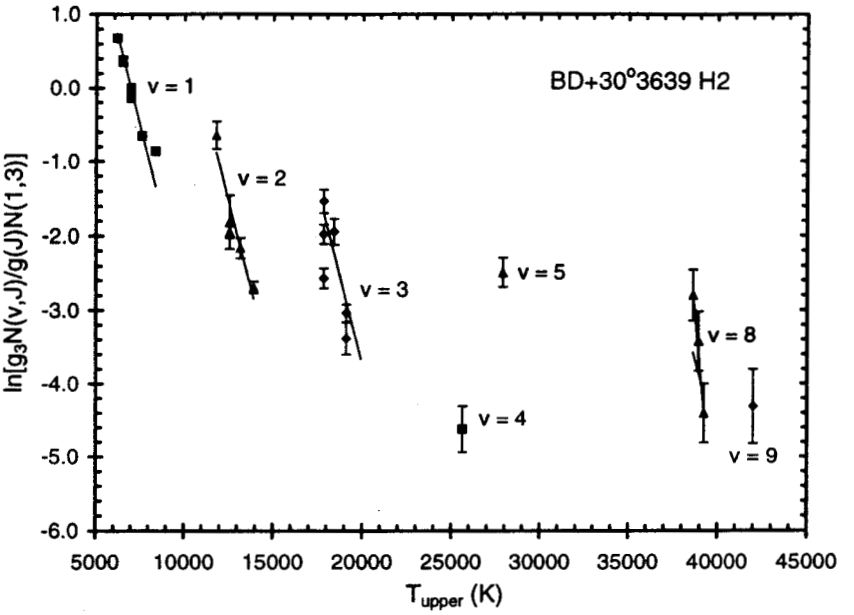

Figure 33b

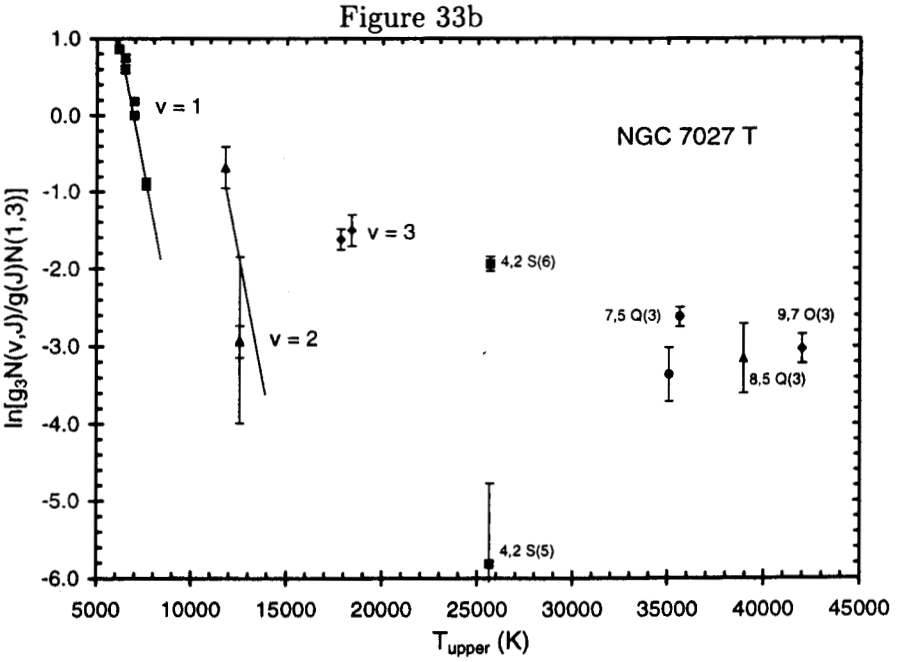

Figure 33c

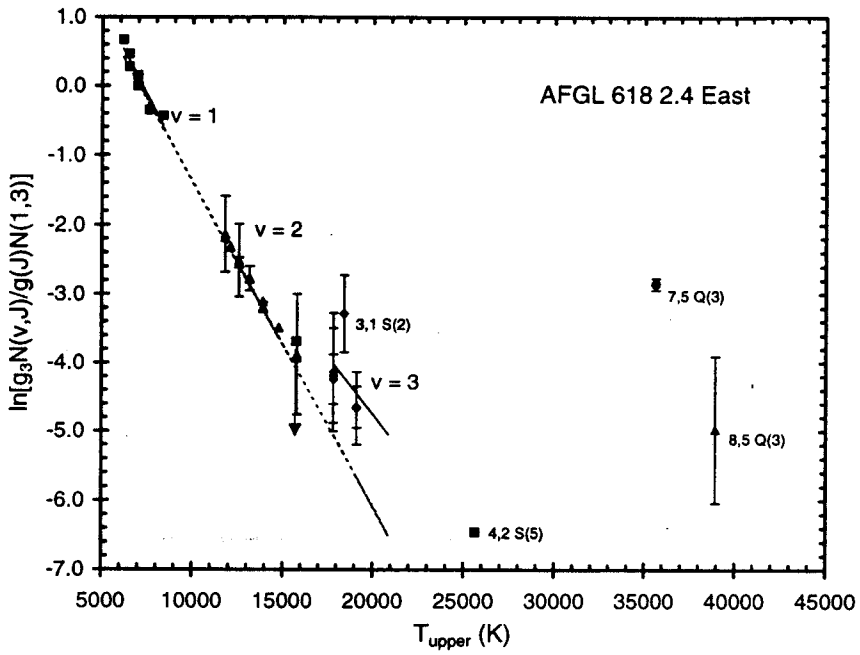

Figure 33d

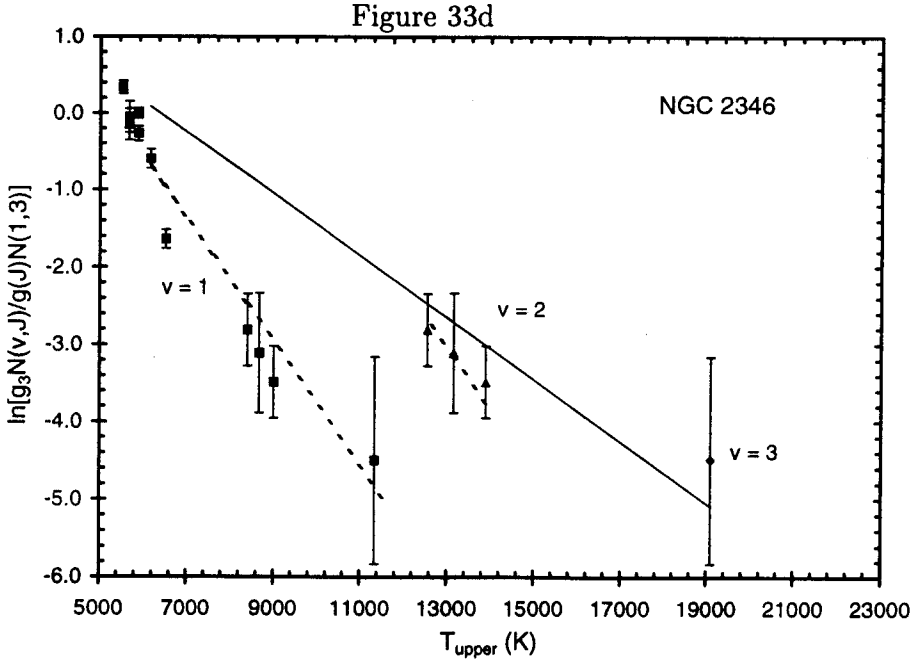

Figure 33e

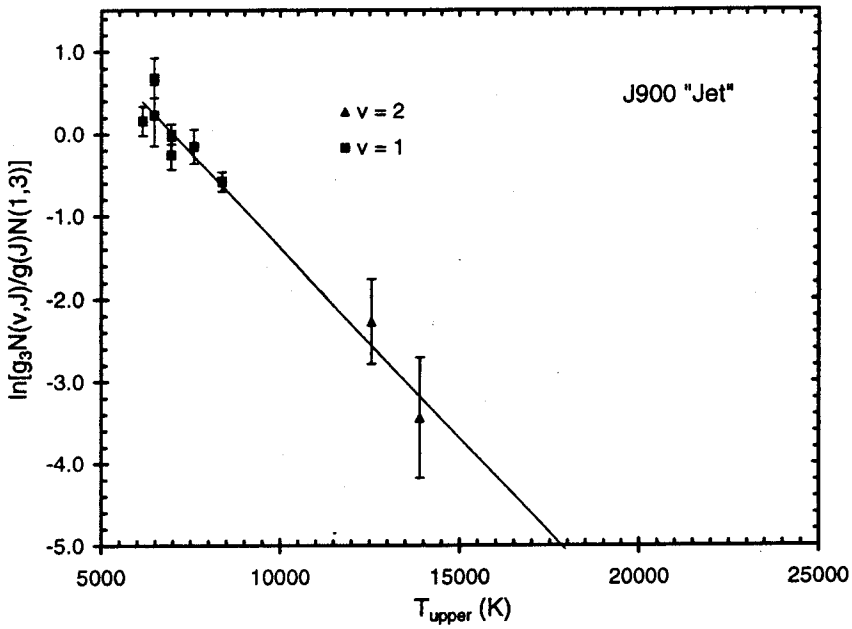
J900 "Jet"
▲ v = 2
■ v = 1
1.0
0.0
-1.0
-2.0
-3.0
-4.0
-5.0
5000
10000
15000
20000
25000
ln[g3N(v,J)/g(J)N(1,3)]
Tupper (K)

TABLE 1

PN SURVEY SUMMARY

No.	Object	PN G #[a]	Observation Dates (UT)	Slit Orient	Positions[b]	Spectral Components[c]	Classical Morphology[d]
Hydrogen recomb. line dominated							
1	NGC 1535	206.4-40.5	9/25/94	NS	W lobe	Hl	eR
2	NGC 2022	196.6-10.9	9/27/94	EW	E ring	Hl	eE
3	NGC 2392	197.8+17.3	2/01/94	NS	E lobe	Hl	eRo
4	NGC 3242	261.0+32.0	1/31-2/01/94	NS	SE knot, E ring, SW halo	Hl	eE
5	NGC 6210	043.1+37.7	7/05/93	NS	Core, 1″E, 3″E	Hl	I
6	NGC 6543	096.4+29.9	7/05/93	NS	S knot	Hl	P
7	NGC 6572	034.6+11.8	7/05/93	NS	Core, E lobe	Hl, Cs, Cw?	lE?
8	NGC 6790	037.8-06.3	7/05/93	NS	Core	Hl, Cw	S
9	NGC 6803	046.4-04.1	9/26/94	NS	E lobe, NW halo	Hl	mE
10	NGC 6826	083.5+12.7	9/01/93	NS	CS, SW lobe, halo	Hl	eE
11	NGC 7009	037.7-34.5	9/26/94	NS	N nebula, W edge	Hl	mE
12	NGC 7662	106.5-17.6	10/16/92	NS	Lobe	Hl, Cs	eE
13	IC 351	159.0-15.1	9/28/94	EW	Center	Hl	...
14	IC 418	215.2-24.2	1/31/94	NS	CS, E Lobe, Halo	Hl, Cw	eE
15	IC 2149	166.1+10.4	9/27/94	NS	CS, E lobe	Hl, Cs	P
16	IC 3568	123.6+34.5	2/02/94	EW	CS, N lobe	Hl	E
17	IC 4593	025.3+40.8	7/05/93	NS	CS, E nebula	Hl, Cs	I
18	J 320	190.3-17.7	2/02/94	EW	Core, 1″N, 1.″5 N	Hl	B
19	M 4-18	...	9/27/94	NS	Core	Hl, Cw, Cs	
Hydrogen recomb. lines + molecular hydrogen							
20	NGC 40[e]	120.0+09.8	2/01/94	NS	W lobe	Hl, H2	mE
21	NGC 2440	234.8+02.4	2/01-02/94	NS,EW	N, NE lobes	Hl, H2, [Fe II]	B
22	NGC 6720	063.1+13.9	7/04/93	EW	N ring, N halo	Hl, H2	mB
23	NGC 7026[e]	089.0+00.3	10/20/92	NS	W, E Lobes	Hl	lE
24	NGC 7027	084.9-03.4	9/25/94	NS	W lobe, NW H_2 Lobe	Hl, H2, Cw	mE
25	BD+30°3639	064.7+05.0	7/04/93	EW	N & E ring, H_2 Lobe	Hl, H2, Cw	eRo
26	Hb 12	111.8-02.8	9/25/94	NS	CS, 3.″7 E, 3.″7 E 2″S	Hl, H2, Cw,[Fe II]	B
27	IC 2003[e]	161.2-14.8	9/28/94	EW	Center	Hl, H2?, Cw?	...
28	I21282+5050	...	9/28/94	EW	Core, Lobe	H2, Hl, Cw	eE
29	M 1-16	226.7+05.6	2/02/94	NS	Core, 1″S	H2, Hl	B
30	M 1-92[e]	...	9/27/94	NS	Core, NW lobe	Hl, H2?, Cw, CO	B
31	M 2-9	010.8+18.0	7/04-05/93	NS,EW	CS, N knot, NE Lobe	Hl, H2, Cw, [Fe II]	B
32	Vy 2-2[e]	045.4-02.7	7/05/93	NS	Core	Hl, H2?, Cw	S
Molecular hydrogen-dominated							
33	NGC 2346	215.6+03.6	2/02/94	EW	W Filament	H2, Paβ	B
34	AFGL 618	166.4-06.5	1/31/94	NS	Core, 2.″4 E	Cw, H2, CO	B
35	AFGL 2688	...	7/04-05/93	NS,EW	3″N, 8.″5 N, E Lobe	H_2, Cw, Cs	B
36	J 900	194.2+02.5	2/02/94	EW	H_2 lobe	H_2	B
Continuum-dominated							
37	AFGL 915	...	2/02/94	NS	Core, 4″S	Cw, CO, Hl	B
38	IRC+10420	...	7/05/93	NS	nebula	Cw, Hl abs?	S
39	M 2-56	...	2/02/94	EW	nebula	Cw	B
HII regions							
40	K4-45	...	9/28/94	EW	Brightest lobe	H2, Hl	B
41	M 1-78	093.5+01.4	9/26/94	NS 1	SW knot	Hl, H2, Cw	B

[a]Strasbourg Planetary Nebulae catalog number (Acker et al. 1992)

[b]Unless otherwise specified, the slit was centered on the brightest part of component specified. CS - Central Star

[c]Hl - hydrogen recombination lines; H2 - molecular hydrogen; Cs - stellar continuum; Cw - warm dust continuum; CO - CO bandhead emission

[d]Classical morphology categories: E - elliptical; B - Bipolar; Ri - ring; Ro - round; S - stellar (i.e., unresolved); P - peculiar; I - irregular. Modifiers in lower case before category: e - early; m - middle; l - late.

[e]New detection of H_2.

TABLE 2

H I PN LINE FLUXES[a]

Wavelength [b] (Å)	NGC 1535	NGC 2022	NGC 2392	NGC 3242E	NGC 3242SE	NGC 3242H	NGC 6210E1	NGC 6210E7	NGC 6543	NGC 6572C	NGC 6572E	Identification
11618	0.645	1.43	0.461	4.16	2.16	···	1.19	···	···	···	···	?
11664	0.167	0.218	···	0.646	0.344	···	···	···	···	···	···	He I
11892	···	···	···	···	···	···	···	···	0.668	15.3	17.9	He I
11970	···	···	···	0.153	···	···	0.909	···	1.25	12.3	9.3	?
11986	0.489	0.495	···	···	···	···	···	···	···	···	···	He I
12038	···	···	···	···	···	···	···	···	···	1.33	···	?
12057	0.381	···	0.0621	0.580	0.272	···	···	···	···	···	···	?
12147	0.495	0.407	0.132	1.68	···	···	···	···	···	···	···	?
12529	···	···	···	···	0.255	···	1.01	···	1.13	21.4	14.5	He I
12566	···	0.0616	0.200	···	0.106	···	···	···	0.306	1.09	1.10	[Fe II]
12784	0.258	···	0.329	0.568	1.19	0.231	4.14	0.158	4.80	49.2	32.9	He I
12817	6.33	3.77	6.27	18.9	24.6	3.47	68.9	2.91	70.3	736	529	Pa5 (Pa Beta) H I
12977	···	···	···	···	···	···	···	···	···	5.81	6.46	He I
12994	2.92	···	···	···	···	0.112	···	···	···	14.3	···	He I
13118	0.538	···	···	0.597	0.282	0.113	···	···	···	1.29	1.10	?
13155	···	···	···	···	···	···	···	···	···	2.95	3.24	O I

TABLE 2—*Continued*

Wavelength [b] (Å)	NGC 1535	NGC 2022	NGC 2392	NGC 3242E	NGC 3242SE	NGC 3242H	NGC 6210E1	NGC 6210E7	NGC 6543	NGC 6572C	NGC 6572E	Identification
14760	0.361	0.865	0.200	1.61	0.672	···	···	···	···	···	···	?
14881	···	0.0804	···	0.294	0.168	···	···	···	···	···	1.30	?
14960	···	···	···	···	···	0.389	···	···	···	···	···	Br25 H I
15000	···	···	···	···	···	···	0.347	···	0.154	3.58	1.37	Br24 H I
15033	···	···	···	0.239	0.206	···	0.472	···	···	6.30	3.54	Br23 H I
15076	···	···	···	0.209	0.146	···	0.589	···	···	7.04	4.70	Br22 H I
15126	···	···	0.0957	2.36	0.118	···	0.579	···	0.381	5.47	3.62	Br21 H I
15184	···	···	0.0866	0.201	0.170	0.0644	0.592	···	0.445	6.84	4.54	Br20 H I
15254	···	···	0.0933	0.264	0.170	0.125	0.672	···	···	8.42	5.12	Br19 H I
15335	···	···	0.144	0.283	0.226	0.119	1.04	···	0.572	9.88	7.13	Br18 H I
15432	···	···	0.148	0.296	0.284	0.121	1.33	···	0.888	10.3	7.42	Br17 H I
15549	···	0.116	0.205	0.378	0.375	0.104	1.66	···	1.25	12.4	9.32	Br16 H I
15693	···	0.227	0.202	0.543	0.457	0.117	2.03	···	1.66	14.0	10.7	Br15 H I
15826	···	···	···	0.226	0.120	0.128	···	···	···	···	···	?
15875	···	0.134	0.238	0.510	0.567	0.153	2.55	···	2.15	19.3	14.6	Br14 H I
16020	0.435	···	···	···	···	0.0826	···	···	···	···	···	?
16102	···	0.0600	0.376	0.646	0.675	0.206	2.89	···	2.38	23.8	17.7	Br13 H I
16401	0.373	0.235	0.353	0.725	0.805	0.221	3.83	···	3.02	29.2	21.1	Br12 H I
16432	···	···	0.348	···	···	···	···	···	···	···	···	[Fe II]
16690	···	···	···	···	···	0.201	···	···	···	···	···	?
16801	0.488	0.291	0.441	0.960	1.02	0.269	4.90	···	3.64	36.3	26.8	Br11 H I
16997	···	···	0.176	0.297	0.448	0.231	1.97	···	1.92	19.8	14.9	He I
17055	···	···	0.118	···	···	···	···	···	···	···	···	?
17111	···	···	···	0.158	···	···	···	···	···	···	···	?
17356	0.447	0.507	0.651	1.27	1.40	0.326	7.49	···	5.30	48.3	34.8	Br10 H I
17640	···	···	···	···	···	0.164	···	···	···	···	···	?
17733	···	···	···	···	···	0.0961	···	···	···	···	···	?
19446	0.833	0.546	1.70	1.75	2.21	0.404	7.97	0.293	8.03	82.7	64.9	Br8 H I
19549	···	···	···	0.123	0.189	···	1.04	···	0.618	20.4	15.6	He I
20006	···	···	0.120	0.149	0.188	0.168	···	0.270	···	···	···	?
20373	···	···	···	0.145	···	···	···	···	···	···	···	?
20443	···	···	···	···	···	···	···	···	0.301	3.3	2.00	He I
20580	···	···	0.745	0.321	0.846	0.202	8.07	0.376	8.74	75.3	53.6	He I
21124	···	0.109	0.0813	0.175	0.258	0.0514	0.969	···	0.683	10.1	7.31	He I

TABLE 2—*Continued*

Wavelength [b] (Å)	NGC 1535	NGC 2022	NGC 2392	NGC 3242E	NGC 3242SE	NGC 3242H	NGC 6210E1	NGC 6210E7	NGC 6543	NGC 6572C	NGC 6572E	Identification
21310	···	···	···	0.0919	0.122	···	···	···	0.094	1.16	0.302	?
21658	3.24	1.15	2.02	3.88	4.51	1.07	24.0	1.30	17.3	153	115	Br7 (Brγ) H I
21892	···	0.336	0.152	0.793	0.391	···	0.314	···	···	···	···	?
21993	···	···	···	···	···	···	···	···	0.0974	1.74	1.83	U[c]
22858	···	···	···	0.299	0.216	0.116	0.846	···	0.542	4.99	4.36	U[c]
23359	···	···	···	···	···	···	···	···	···	0.502	0.604	Pf ?
23395	···	···	···	···	···	···	···	···	···	0.472	0.444	Pf ?
23443	···	···	···	···	···	···	···	···	0.0958	0.974	0.772	Pf ?
23468	···	···	···	0.244	···	···	···	···	···	···	···	?
23489	···	···	···	···	···	···	0.354	···	···	1.24	1.10	Pf ?
23541	···	···	···	···	···	···	0.220	···	0.0998	1.52	1.37	Pf28 H I
23596	···	···	···	···	···	···	0.360	···	0.240	1.39	1.21	Pf27 H I
23665	···	···	···	···	···	···	0.306	···	0.0232	1.52	1.36	Pf26 H I
23739	···	···	···	···	···	···	0.468	···	0.246	1.99	1.65	Pf25 H I
23828	···	···	···	···	···	···	0.434	···	0.233	1.92	2.05	Pf24 H I
23920	0.438	···	···	···	···	···	0.492	···	0.287	2.43	2.54	Pf23 H I
24031	0.502	···	···	···	···	···	0.258	···	0.287	2.90	2.65	Pf22 H I
24160	0.359	···	···	···	···	···	0.443	···	0.352	3.29	2.91	Pf23 H I

[a]These are the measured wavelengths, with a 1 σ error of $\lesssim$ 5Å.
[b]Fluxes are in units of 10^{-14} erg cm^{-2} s^{-1}, and have not been corrected for extinction.
[c]Unidentified lines observed in several other PNe (see text).

TABLE 3

H I PN LINE FLUXES[a]

Wavelength [b] (Å)	NGC 6803E	NGC 6826SW	NGC 6826SWH	NGC 7009N	NGC 7009W	NGC 7662	IC 351	IC 418C	IC 418E	IC 418H	Identification
11451	...	...	...	...	...	...	...	...	...	...	?
11588	.399	...	...	...	0.177	...	...	...	...	...	?
11618	2.79	...	...	5.02	0.361	...	3.30	...	...	...	?
11664	0.716	...	...	1.07	0.139	0.620	0.530	...	...	...	He I
11693	...	...	...	...	...	0.0904	...	...	...	...	?
11892	2.03	...	...	...	...	...	...	4.87	12.3	...	He I
11970	2.09	0.537	...	0.715	...	...	...	...	2.68	...	?
11986	...	...	...	...	...	...	...	...	...	...	He I
12071	...	0.450	...	...	...	...	...	2.34	6.12	...	?
12147	...	...	...	...	...	...	...	...	...	...	?
12172	...	...	...	...	...	0.569	...	...	...	...	?
12529	2.40	...	...	0.810	...	...	...	2.06	5.17	...	He I
12566	0.434	...	...	0.291	...	...	...	...	...	...	?
12692	1.31	...	...	...	...	...	0.0793	...	...	...	?
12784	8.33	2.03	0.715	2.87	0.763	...	0.459	6.59	15.1	...	He I
12817	123	32.0	14.1	51.0	11.8	2.35	13.7	116	310	0.570	Pa5 (Pa Beta) H I
12977	0.718	...	...	...	...	...	...	...	2.93	...	He I
12994	1.13	...	...	...	...	...	0.359	6.36	1.87	...	He I
13015	...	...	...	...	...	0.781	...	...	...	...	?
13121	...	...	...	...	...	...	...	...	8.65	...	?
13155	...	...	...	...	...	0.138	0.191	3.71	6.50	...	O I

TABLE 3—*Continued*

Wavelength [b] (Å)	NGC 6803E	NGC 6826SW	NGC 6826SWH	NGC 7009N	NGC 7009W	NGC 7662	IC 351	IC 418C	IC 418E	IC 418H	Identification
14562	···	···	···	···	···	0.0793	···	···	···	···	?
14616	···	···	···	···	···	0.0621	···	···	···	···	?
14760	1.08	···	···	1.84	···	0.340	1.14	···	···	···	?
14881	0.611	0.316	···	···	···	···	···	···	···	···	?
14910	···	···	···	···	···	···	···	···	1.09	···	Br? H I
14942	···	···	···	···	···	···	···	···	1.06	···	Br? H I
14960	···	···	···	···	···	···	···	···	0.796	···	Br25 H I
15000	···	···	···	···	···	···	···	1.28	1.20	···	Br24 H I
15033	1.05	0.273	···	···	0.183	···	···	1.18	2.53	···	Br23 H I
15076	1.13	0.236	···	0.549	0.154	0.0572	···	1.80	3.55	···	Br22 H I
15126	0.759	0.135	···	0.425	···	···	···	1.32	2.79	···	Br21 H I
15184	1.04	0.198	···	0.463	0.0942	···	0.260	1.20	3.30	···	Br20 H I
15254	1.08	0.331	···	0.444	0.161	0.0583	0.230	2.10	4.03	···	Br19 H I
15335	1.59	0.313	···	0.510	0.140	0.0505	0.308	2.26	4.78	···	Br18 H I
15432	1.60	0.662	0.452	0.517	0.210	0.0605	0.349	2.12	5.31	···	Br17 H I
15549	2.17	0.410	0.177	0.759	0.208	0.0554	0.402	2.47	6.26	···	Br16 H I
15693	2.38	0.550	0.244	1.14	0.232	0.113	0.407	3.52	7.11	···	Br15 H I
15826	0.609	0.196	···	···	0.262	···	0.410	···	···	···	?
15875	3.20	0.681	0.320	1.25	0.264	0.0968	0.400	4.69	10.0	···	Br14 H I
16020	···	···	···	···	0.156	···	···	···	···	···	?
16102	3.90	0.910	0.413	1.39	0.408	0.104	0.634	5.51	12.8	···	Br13 H I
16401	5.03	1.19	0.507	1.71	0.433	0.131	0.661	7.02	15.3	···	Br12 H I
16432	···	···	···	···	···	···	···	···	···	···	[Fe II]
16690	0.29	0.420	···	···	0.218	···	0.297	···	···	···	?
16801	5.90	1.34	0.657	2.28	0.575	0.175	0.860	8.92	19.6	···	Br11 H I
16920	···	···	···	0.395	···	···	···	···	···	···	?
16997	3.37	1.15	0.247	0.930	0.399	0.0401	0.367	3.26	6.79	···	He I
17111	···	···	···	···	···	···	···	···	···	···	?
17356	8.19	1.68	0.918	3.14	0.808	0.242	1.37	12.7	29.8	···	Br10 H I
17640	0.341	···	···	···	···	···	0.391	···	···	···	?
17733	···	···	···	···	···	···	···	···	···	···	?
19446	18.9	3.08	1.43	2.41	0.481	0.238	0.836	31.7	75.0	0.373	Br8 H I
19549	1.82	0.39	0.159	0.359	0.104	···	···	2.48	5.53	···	He I
20006	0.534	···	···	···	0.0856	···	0.356	···	···	···	?

TABLE 3—*Continued*

Wavelength [b] (Å)	NGC 6803E	NGC 6826SW	NGC 6826SWH	NGC 7009N	NGC 7009W	NGC 7662	IC 351	IC 418C	IC 418E	IC 418H	Identification
20373	···	···	···	0.164	···	···	···	···	···	···	?
20443	···	···	···	···	···	···	···	0.920	1.12	···	?
20580	17.6	1.86	0.832	2.66	0.950	0.0650	0.300	30.8	81.3	0.108	He I
21015	···	···	···	···	···	···	···	···	1.38	···	?
21124	1.84	0.408	···	0.545	0.124	···	0.135	1.90	3.35	···	He I
21216	···	···	···	···	···	···	···	···	···	···	H_2
21514	···	···	···	···	0.0875	···	···	···	···	···	?
21658	27.2	6.21	3.08	10.3	2.76	0.835	3.20	35.7	87.3	0.158	Br7 (Brγ) H I
21892	0.654	···	···	0.757	0.0801	0.169	0.582	···	···	···	?
21993	0.170	···	···	···	···	···	···	0.543	1.81	···	U[c]
22343	···	···	···	···	···	···	0.348	···	···	···	?
22858	1.01	···	···	0.562	···	0.0536	···	···	···	···	U[c]
23359	···	···	···	···	···	···	···	···	···	···	Pf ?
23395	···	···	···	···	···	···	···	···	···	···	Pf ?
23443	0.235	···	···	···	···	···	···	···	···	···	Pf ?
23489	0.241	···	···	···	···	···	···	···	···	···	Pf ?
23505	···	···	···	···	···	0.0715	···	···	···	···	?
23541	0.203	···	···	···	···	···	···	···	···	···	Pf28 H I
23596	0.132	···	···	···	···	···	···	···	···	···	Pf27 H I
23665	0.167	···	···	···	···	···	···	···	···	···	Pf26 H I
23739	0.256	···	···	···	···	···	···	···	1.39	···	Pf25 H I
23828	0.395	···	···	···	···	···	···	···	0.971	···	Pf24 H I
23920	0.417	···	···	···	···	···	···	···	1.45	···	Pf23 H I
24031	0.513	···	···	···	···	···	···	···	1.33	···	Pf22 H I
24160	0.657	···	···	···	···	···	···	···	2.46	···	Pf23 H I

[a]These are the measured wavelengths, with a 1 σ error of $\lesssim$ 5Å.

[b]Fluxes are in units of 10^{-14} erg cm^{-2} s^{-1}, and have not been corrected for extinction.

[c]Unidentified lines observed in several other PNe (see text).

TABLE 4

H I PN LINE FLUXES[a]

Wavelength [b] (Å)	IC 2149C	IC 2149E	IC 3568	IC 4593C	IC 4593E	J 320C	J 320N1	J 320P15	M 4-18	Identification
11539	...	...	...	...	...	...	...	...	2.27	?
11581	...	...	...	...	...	...	...	...	5.59	?
11618	...	...	0.145	...	...	0.351	...	...	...	?
11664	...	...	...	...	0.184	...	...	...	...	He I
11798	...	...	...	...	...	...	...	...	...	He I
11892	2.38	0.994	...	...	...	...	...	...	3.36	He I
11986	2.92	1.15	0.178	...	...	...	...	...	8.00	He I
12038	1.19	...	...	...	...	...	...	...	...	?
12057	...	0.594	0.215	...	...	...	...	...	...	?
12112	...	...	...	...	...	...	...	...	1.70	?
12194	...	...	...	...	...	...	...	...	0.429	?
12228	...	...	...	...	...	...	...	...	0.595	?
12440	...	...	...	...	...	...	...	...	0.743	?
12529	1.95	1.17	0.187	...	...	...	...	...	1.59	He I
12566	...	...	...	...	...	...	...	...	1.26	[Fe II]
12784	3.62	3.50	0.829	2.41	0.958	0.446	0.518	0.495	2.93	He I
12817	65.9	65.8	13.8	33.0	14.8	7.82	8.23	8.69	30.6	Pa5 (Pa Beta) H I
12977	...	...	0.165	0.935	...	...	...	...	0.622	He I
12994	...	0.936	0.312	...	...	...	...	...	...	He I
13118	...	0.428	0.127	...	...	...	...	...	...	?
13034	...	...	...	...	...	...	...	...	0.525	?
13155	...	...	...	...	...	...	...	...	0.856	O I

TABLE 4—*Continued*

Wavelength [b] (Å)	IC 2149C	IC 2149E	IC 3568	IC 4593C	IC 4593E	J 320C	J 320N1	J 320P15	M 4-18	Identification
14562	...	...	...	...	...	...	...	...	0.883	?
14640	...	...	...	...	...	...	...	...	0.236	?
14712	...	...	...	...	...	...	...	...	1.32	?
14743	...	...	...	...	...	...	...	...	1.41	?
14881	...	...	...	...	...	...	...	...	0.320	?
14960	...	...	...	...	...	...	...	...	...	Br25 H I
15000	...	...	...	...	...	...	...	...	...	Br24 H I
15033	2.36	0.359	...	...	...	...	...	...	1.02	Br23 H I
15045	...	...	...	1.02	...	...	...	...	...	?
15076	1.22	0.524	0.124	0.502	...	...	...	...	0.851	Br22 H I
15126	...	0.489	0.134	...	...	...	...	...	0.377	Br21 H I
15184	...	0.625	0.0866	0.515	...	0.0813	...	...	0.602	Br20 H I
15254	0.971	0.638	0.157	0.749	...	0.0788	...	...	0.537	Br19 H I
15335	1.16	0.788	0.172	0.922	...	0.0750	...	...	0.574	Br18 H I
15432	0.886	1.13	0.179	1.01	...	0.120	...	...	0.443	Br17 H I
15549	1.41	1.60	0.231	0.636	...	0.148	0.148	...	0.606	Br16 H I
15693	1.87	1.63	0.279	0.779	...	0.202	0.220	...	1.19	Br15 H I
15826	...	...	...	0.500	...	...	...	0.364	0.339	?
15875	3.16	2.17	0.325	1.38	...	0.220	0.234	0.276	1.50	Br14 H I
16020	...	...	...	...	...	...	...	0.168	...	?
16102	2.75	2.24	0.460	1.35	...	0.345	0.256	0.361	1.29	Br13 H I
16165	...	...	...	...	...	...	...	...	0.230	?
16379	...	...	...	0.455	...	...	...	...	...	?
16401	4.27	2.99	0.621	1.77	...	0.330	0.393	0.471	1.43	Br12 H I
16432	...	...	...	...	...	...	...	...	0.490	?
16801	3.52	3.53	0.719	2.28	...	0.471	0.528	0.460	1.89	Br11 H I
16997	1.91	1.58	0.242	1.09	...	...	0.221	...	2.32	He I
17111	0.814	...	...	...	...	...	...	...	...	?
17356	5.66	5.06	1.06	3.08	...	0.661	0.506	0.740	2.71	?
17831	...	...	...	...	...	...	...	...	6.87	?
19446	7.46	8.12	0.412	6.84	3.06	1.10	1.17	1.02	4.17	Br8 H I
19549	...	0.766	0.105	0.322	...	...	...	0.231	0.566	He I
20006	...	...	...	...	0.768	...	...	0.242	...	?
20373	...	...	...	...	...	...	...	...	...	?

TABLE 4—*Continued*

Wavelength [b] (Å)	IC 2149C	IC 2149E	IC 3568	IC 4593C	IC 4593E	J 320C	J 320N1	J 320P15	M 4-18	Identification
20443	...	...	...	...	...	...	...	...	...	He I
20580	11.1	13.2	1.20	4.49	2.16	0.292	0.309	0.330	5.21	He I
20855	...	...	...	...	...	...	...	...	0.446	?
21015	...	...	...	...	...	...	...	...	0.297	?
21089	...	...	...	...	...	...	...	...	0.318	?
21124	1.27	0.732	0.146	0.427	...	...	...	...	0.835	He I
21658	17.3	16.7	3.08	8.74	4.19	1.88	1.88	1.66	7.74	?
21982	...	0.126	...	...	...	...	...	...	...	?
23489	...	...	...	...	...	...	...	...	...	Pf ?
23541	...	0.304	...	...	...	...	...	...	...	Pf28 H I
23596	...	0.205	...	...	...	...	...	...	...	Pf27 H I
23665	...	0.107	...	...	...	...	...	...	...	Pf26 H I
23739	...	0.237	...	...	...	...	...	...	...	Pf25 H I
23828	...	0.338	...	...	...	...	...	...	...	Pf24 H I
23920	...	0.316	...	...	...	...	...	...	...	Pf23 H I
24031	...	0.414	...	...	...	...	...	...	...	Pf22 H I
24160	...	0.255	...	...	...	...	...	...	...	Pf23 H I

[a]These are the measured wavelengths, with a 1 σ error of $\lesssim$ 5Å.
[b]Fluxes are in units of 10^{-14} erg cm^{-2} s^{-1}, and have not been corrected for extinction.
[c]Unidentified lines observed in several other PNe (see text).

TABLE 5

H_2 + H I PN Line Fluxes[a]

Wavelength[b] (Å)	NGC 40	NGC 2440NE	NGC 2440N	NGC 2440T	NGC 6720A	NGC 6720B	NGC 7027T	NGC 7027WT	BD+30° 3639H2	BD+30° 3639N	BD+30° 3639OE	Identification
11621	···	···	5.91	1.15	.361	···	178	10.8	.384	···	.648	?
11650	···	···	···	···	···	···	···	···	.324	2.06	···	?
11665	···	···	0.863	···	···	···	23.4	1.45	.189	.324	.407	?
11748	···	···	···	···	···	···	3.84	.486	.128	3.59	.157	?
11784	···	···	···	···	···	···	1.37	···	···	···	···	?
11822	···	···	···	···	···	···	5.75	···	···	···	···	?
11854	···	···	···	···	.114	···	···	.331	.272	···	.839	H_2 (3,1) S(3)
11892	1.22	···	1.21	.406	.974	···	62.1	9.21	.894	10.5	.561	He I? H_2 (2,0) S(0)
11970	···	···	···	···	···	···	12.0	1.05	···	···	.685	?
11986	···	···	···	···	···	.164	···	···	.190	2.63	···	He I
12038	···	···	···	···	···	···	2.39	.407	···	···	.460	?
12069	···	···	···	···	···	···	3.56	1.29	.361	···	.238	H_2 (3,1) S(2)
12112	···	···	···	···	···	···	1.41	···	···	···	.230	H_2 (8,5) Q(3)
12143	···	···	.724	.298	.0314	···	8.42	2.35	.139	···	.389	H_2 (8,5) Q(3)
12181	···	···	···	···	.0423	···	1.03	···	.0835	···	···	?
12213	···	···	···	···	.0801	···	···	···	···	···	···	H_2 (11,7)O(3)
12258	···	···	···	···	.146	···	.437	···	.190	···	.424	H_2 (4,2) S(5)
12294	···	···	···	···	···	···	1.52	···	.248	···	.0638	?
12329	···	···	···	···	.202	···	5.63	.552	.528	···	.719	H_2 (3,1) S(1)
12383	···	···	···	···	.268	···	2.53	.844	.354	···	.658	H_2 (2,0) Q(1)
12420	···	···	···	···	.111	···	2.69	.344	···	···	.530	H_2 (2,0) Q(2) +(4,2) S(4)
12442	···	···	···	···	.137	···	···	···	···	···	···	?
12469	···	···	···	···	.230	···	···	···	.171	···	.225	H_2 (2,0) Q(3)
12487	···	···	···	···	···	1.37	.415	···	.0955	···	···	H_2 (2,0) Q(3)
12529	.157	···	···	···	.0499	···	15.6	1.22	.201	2.13	.174	He I
12566	.315	.280	.670	.282	.0831	···	7.49	1.89	.724	7.35	.213	[Fe II]

TABLE 5—*Continued*

Wavelength [b] (Å)	NGC 40	NGC 2440NE	NGC 2440N	NGC 2440T	NGC 6720A	NGC 6720B	NGC 7027T	NGC 7027WT	BD+30° 3639H2	BD+30° 3639N	BD+30° 3639OE	Identification
12618	···	···	···	···	.155	···	···	.314	.397	···	.837	H_2 (3,1) S(0) +(9,6) S(1) +(4,2) S(3)
12696	···	···	···	···	.0276	···	···	···	···	···	···	H_2 (8,5) O(3)
12757	···	···	···	···	.144	···	···	···	···	···	···	?
12784	.697	···	.889	.145	.355	···	40.5	3.71	.656	14.0	.193	He I
12817	18.4	.553	21.5	4.94	4.75	···	946	72.6	29.8	811	9.87	Pa5 (Pa Beta) H I
12869	···	···	···	···	.0665	···	···	.172	···	···	···	H_2 (2,0) Q(7)
12912	···	···	···	···	···	···	3.65	···	···	···	···	?
12928	···	···	···	···	.0305	···	···	···	.0514	.819	.243	H_2 (2,0) O(2)
12977	···	···	···	···	.0610	···	···	···	.0468	1.59	···	He I
12994	···	···	···	.558	···	···	77.6	20.8	···	···	···	?
13108	···	···	···	···	···	···	···	.819	.302	···	.651	H_2 (5,3) S(5) +(4,2) S(1)
13155	···	···	···	···	···	···	···	.875	1.34	7.79	.637	O I + H_2 (9,6) Q(1) ?
13237	···	···	···	···	···	···	···	···	···	···	.196	H_2 (3,1) Q(3)
14760	···	···	···	···	···	···	84.4	5.71	···	···	···	?
14881	···	···	···	···	···	···	15.8	2.04	···	···	···	?
14925	···	···	···	···	···	···	···	···	···	···	.468	H_2 (5,3) Q(1)
14976	···	···	···	···	···	···	···	···	···	···	.240	H_2 (5,3) Q(2)
15010	···	···	···	···	···	···	···	···	···	···	.380	H_2 (6,4) S(1)
15033	···	···	···	···	···	···	11.4	···	.272	4.91	···	Br 23 H I
15051	···	···	···	···	···	···	···	···	···	···	.494	H_2 ?
15076	···	···	···	···	···	···	7.82	.926	.453	6.33	···	Br 22 H I
15091	···	···	···	···	···	···	···	···	···	···	.413	H_2 ?
15126	···	···	···	···	···	···	8.94	.890	···	5.31	···	Br21 H I
15142	···	···	···	···	···	···	···	···	.326	···	···	H_2 (5,3) Q(4)
15184	.272	···	···	···	···	···	11.0	1.21	···	7.12	···	Br20 H I
15205	···	···	···	···	···	···	···	···	.421	···	···	H_2 (3,1) O(5)
15221	···	···	···	···	···	···	···	···	···	···	.348	?
15254	.287	···	.182	···	···	···	11.6	1.01	.362	8.00	···	Br19 H I
15335	.289	···	.222	···	···	···	14.5	1.77	.376	10.3	···	Br18 H I
15334	···	···	···	···	···	···	···	···	···	···	.174	?
15432	.312	···	.192	···	···	···	14.3	1.47	.462	10.5	···	Br17 H I
15549	.460	···	.297	···	···	···	18.5	1.79	.459	10.7	···	Br16 H I

TABLE 5—*Continued*

Wavelength [b] (Å)	NGC 40	NGC 2440NE	NGC 2440N	NGC 2440T	NGC 6720A	NGC 6720B	NGC 7027T	NGC 7027WT	BD+30° 3639H2	BD+30° 3639N	BD+30° 3639OE	Identification
15610	···	···	···	···	···	···	···	.269	.420	···	.445	H_2 (7,5) S(3) + (5,3) Q(7)
15693	.377	···	.248	···	···	···	28.7	2.19	.629	14.0	.196	Br15 H I
15875	.656	···	.459	···	···	···	28.7	2.59	.862	18.9	···	Br14 H I
15877	···	···	···	···	···	···	···	···	···	···	.522	H_2 (7,5) S(2)
15976	···	···	···	···	···	···	3.68	···	···	···	···	?
16003	···	···	···	···	···	···	···	···	.326	···	···	?
16020	···	···	···	···	···	···	4.14	.959	···	···	.555	?
16102	.690	···	.578	.144	···	···	33.9	2.95	.839	21.9	···	Br13 H I
16122	···	···	···	···	···	···	···	···	···	···	.922	?
16211	···	···	···	···	···	···	···	···	.271	···	.349	?
16231	···	···	···	···	···	···	···	···	···	···	.238	?
16401	.981	···	.787	.196	···	···	41.9	3.87	1.14	29.2	.568	Br12 H I
16432	···	.297	.528	.205	···	···	···	2.93	.550	6.44	.568	[Fe II]
16584	···	···	···	···	···	···	.719	···	···	···	···	?
16665	···	···	···	···	···	···	.782	···	···	···	···	[Fe II]
16766	···	···	···	···	···	···	···	.928	.765	···	···	?
16801	1.17	···	1.03	.264	···	···	53.3	5.35	1.33	36.8	.694	Br11 H I
16867	···	···	···	···	···	···	···	.441	.119	···	.302	H_2 (1,0) S(9)
16919	···	···	.375	···	···	···	14.5	.972	.0367	···	···	?
16997	.291	···	.269	···	.0923	···	18.4	2.08	···	3.48	.463	He I
17055	···	···	···	···	···	···	2.01	···	···	···	···	?
17111	···	···	···	···	···	···	1.86	···	···	···	···	?
17160	···	···	···	···	···	···	1.27	···	···	···	···	H_2 (7,5) Q(1)
17247	···	···	···	···	.0886	···	.957	···	···	···	···	H_2 (7,5) Q(1)
17280	···	···	···	···	···	···	···	···	···	···	.374	?
17356	1.75	···	1.44	.371	.373	···	71.9	6.31	2.01	49.8	1.11	Br10 H I
17415	···	···	···	···	.102	···	···	.339	···	···	···	?
17435	···	···	···	···	···	···	2.22	···	1.92	···	···	?
17467	···	···	···	···	.843	···	3.04	.883	.527	···	.930	H_2 (1,0) S(7)
17733	···	···	···	···	.0917	···	4.96	···	···	···	···	?
17866	···	···	···	···	.466	···	···	···	···	···	.674	H_2 (1,0) S(6)
17966	···	···	···	···	.110	···	···	···	···	···	···	H_2 (7,5) Q(3)
18154	4.02	···	1.72	···	.794	···	···	···	···	···	···	H I

TABLE 5—*Continued*

Wavelength [b] (Å)	NGC 40	NGC 2440NE	NGC 2440N	NGC 2440T	NGC 6720A	NGC 6720B	NGC 7027T	NGC 7027WT	BD+30° 3639H2	BD+30° 3639N	BD+30° 3639OE	Identification
19446	···	.112	3.40	.831	.598	.103	157	9.31	2.23	40.4	1.24	Br8 H I + H_2 (1,0) S(5)
19549	···	···	···	···	···	···	25.5	···	···	···	···	He I
19570	···	.556	.443	.355	2.18	.748	···	8.2	2.95	5.95	5.20	H_2 (1,0) S(3)
19624	···	···	.123	···	···	···	···	···	.121	···	···	H_2 (8,6) O(2)
19703	···	···	···	···	···	···	···	···	.212	···	.228	H_2 (8,6) O(2)
19868	···	···	···	···	···	···	···	···	.0747	···	···	H_2 (9,7) S(0)
20217	···	···	···	···	···	···	···	···	···	···	.165	H_2 (7,5) O(5)
20275	···	···	···	···	···	···	···	···	···	···	.211	H_2 ?
20334	···	.332	.286	.280	1.52	.265	2.66	2.27	1.21	1.81	2.08	H_2 (1,0) S(2)
20373	···	···	.127	···	···	···	6.30	···	···	···	···	?
20411	···	···	···	···	···	···	···	···	.130	···	.410	H_2 (8,6) O(3)
20580	2.92	.0728	1.30	.273	.404	···	70.5	5.51	.958	55.9	.569	He I
20643	···	···	···	···	.0825	···	2.46	···	.141	···	.074	?
20732	···	0.0564	···	···	.226	···	···	.45	.649	···	.915	H_2 (2,1) S(3)
20847	···	···	···	···	···	···	···	···	.0885	···	···	H_2 (9,7) Q(2)
21001	···	···	···	···	···	···	···	···	.077	···	···	H_2 (9,7) Q(3)
21023	···	···	···	···	···	···	···	.207	···	···	···	?
21086	···	···	···	···	···	···	···	···	.208	···	···	?
21124	.146	···	.236	.0511	···	···	15.8	1.34	.146	1.62	···	He I
21218	.431	.821	.918	.644	4.03	.645	12.2	7.25	3.67	5.35	5.57	H_2 (1,0) S(1)
21268	···	···	···	···	···	···	···	···	···	···	.0886	H_2 ?
21340	···	···	···	···	···	···	···	···	.0741	···	···	?
21380	···	···	···	···	···	···	···	···	.0584	···	···	?
21409	···	···	···	···	···	···	···	.223	···	···	···	?
21462	···	···	···	···	···	···	···	.160	.0891	···	···	?
21542	···	···	···	···	.243	···	···	.223	.376	···	.471	H_2 (2,1) S(2)
21658	6.27	.103	4.44	1.02	1.22	···	238	20.3	5.26	164	1.72	Br7 (Brγ) H I
21822	···	···	···	···	···	···	···	···	.126	···	···	?
21892	···	···	.836	.228	···	···	31.6	1.55	.119	···	···	?
21993	.611	···	···	···	.0883	···	7.27	.913	···	1.69	···	U[c]
22014	···	···	.030	···	.127	···	···	···	.447	···	.408	H_2 (3,2) S(3)
22099	···	···	···	···	···	···	···	···	.113	.399	···	H_2 (8,6) O(5)
22114	···	···	···	···	···	.0548	···	···	···	···	.218	?

TABLE 5—*Continued*

Wavelength [b] (Å)	NGC 40	NGC 2440NE	NGC 2440N	NGC 2440T	NGC 6720A	NGC 6720B	NGC 7027T	NGC 7027WT	BD+30° 3639H2	BD+30° 3639N	BD+30° 3639OE	Identification
22172	···	···	···	.0792	···	···	1.59	.307	···	1.07	···	?
22234	.0905	.243	0.241	.203	.900	.0866	3.83	2.32	1.17	1.69	1.59	H_2 (1,0) S(0)
22426	···	···	···	···	.082	···	1.16	···	···	···	···	H_2 (2,1) S(1)
22479	···	.0737	.106	···	.449	···	.873	.551	.748	.943	.999	H_2 (2,1) S(1)
22542	···	···	···	···	···	···	.974	.143	.086	.719	···	H_2 (9,7) O(3)
22682	.103	···	···	···	···	···	···	···	.115	.620	···	?
22858	···	···	···	···	···	···	19.4	1.13	···	···	.240	U[c]
22959	···	···	···	···	···	···	2.73	···	.190	···	···	?
22872	···	···	···	···	···	···	···	···	···	···	.240	H_2 (3,2) S(2)
23236	···	···	···	···	···	···	1.88	···	···	1.27	···	?
23448	···	···	···	···	···	···	···	···	···	···	.205	H_2 (4,3) S(3) + (9,7) O(4)
23468	···	···	.388	···	···	···	13.5	.631	.145	2.39	···	?
23541	···	···	···	···	···	···	···	···	.367	2.67	···	Pf28 H I
23551	···	···	···	···	.190	···	···	···	···	···	.433	?
23596	···	···	···	···	···	···	···	···	···	1.78	···	Pf27 H I
23665	···	···	···	···	···	···	···	.102	···	1.78	···	Pf26 H I
23739	···	···	···	···	···	···	2.42	.187	···	···	···	Pf25 H I
23828	···	···	···	···	···	···	4.53	.266	···	1.30	···	Pf24 H I
23861	···	···	···	···	···	···	···	···	.413	···	.450	H_2 (3,2) S(1)
23920	···	···	···	···	···	···	4.74	.419	.269	3.53	···	Pf23 H I
24031	···	···	···	···	···	···	3.56	···	···	3.30	···	Pf22 H I
24065	.505	.608	.768	.480	3.47	.757	13.5	9.46	3.78	7.06	5.49	H_2 (1,0) Q(1)
24130	.0442	0.240	.276	.194	1.08	.160	4.91	2.79	1.42	2.97	1.98	H_2 (1,0) Q(2)
24160	···	···	···	···	···	···	···	···	···	2.98	···	Pf23 H I
24231	.451	.488	.621	.279	3.05	.556	10.3	4.96	2.54	4.91	4.57	H_2 (1,0) Q(3)

[a]These are the measured wavelengths, with a 1 σ error of $\lesssim$ 5Å.

[b]Fluxes are in units of 10^{-14} erg cm^{-2} s^{-1}, and have not been corrected for extinction.

[c]Unidentified lines observed in several other PNe (see text).

TABLE 6

H_2 + H I PN LINE FLUXES[a]

Wavelength [b] (Å)	Hb 12 core	Hb 12 3.″7E[c]	Hb 12 3.″7E 2″S[c]	IC 2003	I21282 +5050	M 1-16 core	M 1-16 1″S	M 1-92	M 2-9 Core	M 2-9 N Knot[d]	M 2-9 Lobe O[d]	Vy 2-2	Identification
11621	···	0.0668	0.0751	5.55	···	0.559	1.42	0.399	···	···	···	2.78	?
11665	···	0.0480	0.0491	0.925	···	0.138	0.237	0.854	···	···	···	1.92	?
11687	···	0.0300	0.0400	···	···	···	···	···	···	···	···	···	H_2 (8,5) S(0)
11748	···	···	···	···	···	0.0807	···	1.73	···	···	···	···	?
11784	···	···	···	···	···	0.0847	0.142	0.768	···	···	···	···	?
11822	···	···	···	···	···	···	···	1.51	···	···	···	···	?
11854	···	0.0839	0.0311	···	···	0.0882	···	···	···	···	···	···	H_2 (3,1) S(3)
11892	···	0.0440	0.0300	0.568	···	0.148	0.372	1.32	3.29	0.275	···	2.39	He I, [Fe II], Fe I, H_2 (2,0) S(0)
11970	···	···	···	···	···	0.0901	0.188	···	3.29	···	···	11.0	?
11986	23.55	···	···	···	···	···	···	1.03	···	···	···	···	He I
12038	···	···	···	···	···	···	0.136	0.955	···	···	···	···	?
12069	···	0.0801	0.0560	···	···	···	···	···	···	···	···	···	H_2 (3,1) S(2)
12087	···	···	···	···	···	···	···	0.664	···	···	···	0.984	?
12143	···	···	0.00405	0.476	···	0.0484	···	···	···	···	···	···	H_2 (8,5) Q(3)
12213	···	···	0.0221	···	···	···	···	···	···	···	···	···	H_2 (11,7)O(3)
12258	···	0.0658	0.0131	···	···	···	0.236	···	···	···	···	···	H_2 (4,2) S(5)
12294	4.40	···	···	···	···	···	···	···	···	···	···	···	?
12329	···	0.127	0.072	···	···	···	···	···	···	···	···	···	H_2 (3,1) S(1)
12383	···	0.0839	0.0761	···	···	0.0469	···	···	···	4.05	···	···	H_2 (2,0) Q(1)
12420	···	0.0641	···	···	···	···	···	···	···	···	···	···	H_2 (2,0) Q(2)+(4,2) S(4)
12469	···	0.0658	0.0230	···	···	···	···	···	···	···	···	···	H_2 (2,0) Q(3)
12529	50.2	0.0668	0.0221	···	···	0.0644	0.325	···	6.13	···	···	23.7	He I
12566	4.71	0.204	0.467	···	···	···	···	1.65	18.6	3.85	···	10.0	[Fe II]

TABLE 6—*Continued*

Wavelength [b] (Å)	Hb 12 core	Hb 12 3.″7E[c]	Hb 12 3.″7E 2″S[c]	IC 2003	I21282 +5050	M 1-16 core	M 1-16 1″S	M 1-92	M 2-9 Core	M 2-9 N Knot[d]	M 2-9 Lobe O[d]	Vy 2-2	Identification
12618	···	0.108	0.0401	···	···	···	···	···	···	···	···	···	H_2 (3,1) S(0)+(9,6) S(1) +(4,2) S(3)
12696	···	0.0310	0.0551	···	···	···	···	···	···	···	···	···	H_2 (8,5) O(3)
12740	···	0.00375	0.01305	···	···	···	···	···	···	···	···	···	H_2 (2,0) Q(6)
12784	84.2	0.0610	0.0650	0.920	···	0.216	0.641	···	16.4	···	···	42.7	He I
12817	1365	1.15	0.510	26.3	0.377	3.61	12.2	11.4	447	3.44	0.728	667	Pa5 (Pa Beta) H I
12869	···	···	0.0270	···	···	···	···	···	···	···	···	···	H_2 (2,0) Q(7)
12928	···	···	0.0900	···	···	···	···	···	···	···	···	···	H_2 (2,0) O(2)
12939	···	···	···	···	···	···	···	···	3.72	···	···	2.17	?
12967	···	···	···	···	···	···	···	···	···	···	···	4.76	?
12978	···	···	0.0371	···	···	···	···	···	8.54	···	···	···	H_2 (5,3) S(6)
12983	18.5	···	···	0.678	···	···	···	···	···	···	···	3.92	He I
13108	···	0.156	0.0851	···	···	···	···	···	···	···	···	···	H_2 (5,3) S(5)+(4,2) S(1)
13155	18.2	0.157	0.0851	···	···	···	···	···	29.6	···	···	2.98	O I + H_2 (9,6) Q(1) ?
13184	···	0.105	0.209	···	···	···	···	···	···	···	···	···	?
13237	···	···	0.0491	···	···	···	···	···	···	···	···	···	H_2 (3,1) Q(3)
13266	···	···	0.113	···	···	···	···	···	···	···	···	···	H_2 (5,3) S(4)
14760	···	···	···	2.10	···	0.327	0.659	···	···	···	···	···	?
14925	···	0.0928	0.057	···	···	0.130	···	···	···	···	···	···	H_2 (5,3) Q(1)
14960	5.97	···	···	···	···	···	···	···	···	···	···	···	Br25 H I
14976	···	0.0990	0.0630	···	···	···	···	···	···	···	···	···	H_2 (5,3) Q(2)
14994	5.34	···	···	···	···	···	···	···	···	···	···	···	C I
15010	···	0.1268	0.0810	···	···	···	···	···	···	···	···	···	H_2 (6,4) S(1)
15033	11.3	···	···	···	···	···	···	···	···	···	···	3.93	Br 23 H I
15051	···	···	···	···	···	0.050	···	···	···	···	···	···	H_2 ?
15076	11.6	···	···	···	···	···	···	···	···	···	···	8.23	Br 22 H I
15091	···	0.116	0.0720	···	···	···	···	···	···	···	···	···	H_2 ?
15126	11.3	···	···	···	···	···	···	···	···	···	···	6.00	Br21 H I
15147	···	0.0658	0.0559	···	···	···	···	···	···	···	···	···	H_2 (5,3) Q(4)
15184	12.2	···	···	···	···	···	···	···	3.07	···	···	6.27	Br20 H I
15205	···	0.0668	0.0270	···	···	···	···	···	···	···	···	···	H_2 (3,1) O(5)
15254	13.8	···	···	0.345	···	···	···	···	3.61	···	···	7.31	Br19 H I
15335	18.2	···	···	0.326	···	···	···	···	7.00	···	···	10.1	Br18 H I
15334	···	···	···	···	···	0.132	···	···	···	···	···	···	?

TABLE 6—*Continued*

Wavelength [b] (Å)	Hb 12 core	Hb 12 3.″7E[c]	Hb 12 3.″7E 2″S[c]	IC 2003	I21282 +5050	M 1-16 core	M 1-16 1″S	M 1-92	M 2-9 Core	M 2-9 N Knot[d]	M 2-9 Lobe O[d]	Vy 2-2	Identification
15432	21.4	···	···	0.397	···	···	0.215	···	2.85	···	···	8.65	Br17 H I
15549	···	···	···	0.562	···	0.102	0.239	···	6.35	···	···	10.9	Br16 H I
15567	···	0.0290	0.0341	···	···	···	···	···	···	···	···	···	?
15610	···	0.130	0.0770	···	···	···	···	···	···	···	···	···	H_2 (7,5) S(3) + (5,3) Q(7)
15693	29.2	···	···	0.757	···	0.176	0.348	···	8.10	···	···	13.6	Br15 H I
15875	36.4	···	···	0.790	···	0.203	0.354	···	13.1	···	···	17.6	Br14 H I
15877	···	0.0781	0.0660	···	···	···	···	···	···	···	···	···	H_2 (7,5) S(2)
15920	···	0.0321	···	···	···	···	···	···	···	···	···	···	?
16003	···	0.0791	0.108	···	···	···	···	0.683	2.63	0.341	···	···	[Fe II]
16102	46.8	0.0641	0.045	0.770	···	0.216	0.402	1.17	10.7	0.143	···	18.9	Br13 H I
16149	···	0.0962	0.072	···	···	···	···	···	···	···	···	···	H_2 (6,4) Q(3)
16204	···	0.0781	···	···	···	···	···	···	···	···	···	···	?
16231	···	···	···	···	···	···	0.177	0.352	···	···	···	···	?
16269	···	0.0471	···	···	···	···	···	···	···	···	···	···	H_2 (6,4) Q(4)
16401	56.2	···	···	1.23	···	0.301	0.503	1.33	15.3	···	···	25.4	Br12 H I
16432	···	0.160	0.581	···	···	···	0.141	2.30	10.1	4.73	···	8.63	[Fe II]
16584	···	···	···	···	···	0.0846	···	···	···	···	···	···	?
16750	···	0.0740	0.152	···	···	···	···	···	···	···	···	···	H_2 (6,4) O(2)
16801	66.3	0.149	0.116	1.21	···	0.504	0.541	1.27	49.3	···	···	32.1	Br11 H I + [Fe II]?
16867	···	0.829	···	···	···	···	···	···	23.0	···	···	···	H_2 (1,0) S(9) + [Fe II]?
16919	···	···	···	···	···	0.101	0.263	···	···	···	···	···	?
16997	35.5	···	···	···	···	···	···	···	8.21	···	···	17.6	He I
17111	···	···	···	···	···	···	···	···	1.75	0.154	···	···	[Fe II]?
17280	···	0.0757	0.0491	···	···	···	···	···	···	···	···	···	?
17317	···	0.0750	0.048	···	···	···	···	···	···	···	···	···	H_2 (6,4) O(3)
17352	···	0.165	0.0851	···	···	···	···	···	···	···	···	···	H_2 (7,5) Q(2)
17356	91.4	···	···	2.14	···	0.674	0.894	1.49	37.2	···	···	44.9	Br10 H I
17415	···	···	···	···	···	···	···	0.485	40.5	···	···	···	[Fe II]?
17435	···	···	···	···	···	···	···	···	···	···	···	2.44	?
17446	5.02	···	···	···	···	···	···	···	···	···	···	···	C I
17459	···	0.0849	0.072	···	···	···	···	···	···	···	···	···	H_2 (1,0) S(7)
19446	···	···	···	2.28	···	0.753	2.27	5.22	77.7	0.935	0.728	84.1	Br8 H I + H_2 (2,1) S(5)
19541	28.9	···	···	···	···	···	···	···	···	0.209	···	17.3	He I
19570	···	0.224	0.187	···	0.913	0.0897	0.330	5.87	23.0	0.132	3.59	···	H_2 (1,0) S(3), [Fe II]?

TABLE 6—*Continued*

Wavelength [b] (Å)	Hb 12 core	Hb 12 3.″7E[c]	Hb 12 3.″7E 2″S[c]	IC 2003	I21282 +5050	M 1-16 core	M 1-16 1″S	M 1-92	M 2-9 Core	M 2-9 N Knot[d]	M 2-9 Lobe O[d]	Vy 2-2	Identification
19703	···	0.0559	···	···	···	···	···	···	···	···	···	···	H_2 (8,6) O(2)
19868	···	0.0331	···	···	···	···	···	···	···	···	···	···	H_2 (9,7) S(0)
20217	···	0.0972	0.0270	···	···	···	···	···	···	···	···	···	H_2 (7,5) O(5)
20334	···	0.129	0.0491	···	···	0.109	0.228	···	···	0.0748	1.61	···	H_2 (1,0) S(2)
20437	···	0.0621	0.0300	···	···	···	···	7.63	···	···	···	···	H_2 (8,6) O(3)
20580	294	0.278	0.142	1.12	···	0.491	0.919	···	12.0	0.506	···	143	He I
20656	···	0.0569	0.0320	···	···	···	···	···	···	···	···	···	H_2 (3,2) S(5)
20732	···	0.0880	0.0870	···	···	···	···	···	···	···	0.432	···	H_2 (2,1) S(3)
20847	···	0.0259	0.0260	···	···	···	···	···	···	···	···	···	H_2 (9,7) Q(2)
21001	···	0.031	···	···	···	···	···	···	···	···	···	···	H_2 (9,7) Q(3)
21124	19.8	···	···	0.344	···	0.0848	0.160	···	···	···	···	10.5	He I
21218	···	0.341	0.150	0.217	0.813	0.434	0.638	2.37	···	0.165	5.2	5.47	H_2 (1,0) S(1)
21284	···	0.0467	···	···	···	···	···	···	···	···	···	···	H_2 ?
21302	···	···	···	···	···	···	···	1.64	···	···	···	···	?
21409	···	···	···	···	···	···	0.102	···	···	···	···	···	?
21542	···	0.0699	···	···	···	···	···	···	···	···	0.167	···	H_2 (2,1) S(2)
21658	314	0.338	0.177	6.55	0.187	1.80	2.54	4.54	109.5	1.10	0.265	156	Br7 (Brγ) H I
21822	···	···	···	···	···	···	···	···	···	···	···	1.02	?
21892	···	···	···	1.02	···	0.208	0.235	···	···	···	···	0.664	?
21993	2.51	···	···	···	···	···	···	···	···	···	···	1.01	U[e]
22014	···	0.0880	0.0500	···	···	···	···	···	···	···	0.250	···	H_2 (3,2) S(3)
22099	···	0.0379	0.0200	···	···	···	0.0776	···	···	···	···	···	H_2 (8,6) O(5)
22184	···	0.017	0.0240	···	···	···	···	···	···	···	···	2.63	?
22234	···	0.122	0.0780	···	0.166	0.205	0.193	···	···	···	1.35	1.51	H_2 (1,0) S(0)
22426	···	···	···	···	···	···	···	···	···	···	···	1.31	H_2 (2,1) S(1)
22479	···	0.159	0.0710	···	···	···	0.150	···	···	0.033	0.572	···	H_2 (2,1) S(1)
22542	···	0.0290	0.0290	···	···	···	···	···	···	···	···	···	H_2 (9,7) O(3)
22682	···	0.0201	···	···	···	···	···	···	···	···	···	···	?
22858	1.88	···	···	0.874	···	···	···	···	···	···	···	2.09	U[e]
22872	···	0.0460	0.0380	···	···	···	···	···	···	···	···	···	H_2 (3,2) S(2)
22973	···	···	···	···	···	···	···	6.45	···	···	···	···	CO
23236	···	···	···	···	···	···	···	4.15	···	···	···	···	CO
23318	···	···	···	···	···	···	···	···	···	···	···	0.818	Pf H I
23360	···	···	···	···	···	···	···	···	···	···	···	0.752	Pf H I

TABLE 6—*Continued*

Wavelength [b] (Å)	Hb 12 core	Hb 12 3.″7E[c]	Hb 12 3.″7E 2"S[c]	IC 2003	I21282 +5050	M 1-16 core	M 1-16 1"S	M 1-92	M 2-9 Core	M 2-9 N Knot[d]	M 2-9 Lobe O[d]	Vy 2-2	Identification
23400	···	···	···	···	···	···	···	···	···	···	···	1.09	Pf H I
23448	···	0.0501	···	0.328	···	···	···	···	···	···	0.0988	···	H_2 (4,3) S(3) + (9,7) O(4)
23468	···	···	···	···	···	···	0.350	···	···	···	···	···	?
23475	···	···	···	···	···	···	···	···	···	···	···	3.26	Pf H I
23541	3.45	···	···	···	···	···	···	···	···	···	···	2.01	Pf28 H I
23551	···	0.089	···	···	···	···	···	5.06	···	···	0.177	···	CO, H_2 (2,1) S(0)
23596	3.14	···	···	···	···	···	···	···	···	···	···	1.69	Pf27 H I
23665	3.45	···	···	···	···	···	···	···	···	···	···	2.02	Pf26 H I
23739	3.14	···	···	···	···	···	···	···	···	···	···	2.19	Pf25 H I
23828	4.40	···	···	···	···	···	···	···	···	···	···	3.79	Pf24 H I
23861	···	0.133	0.0489	···	···	···	···	···	···	···	0.426	···	H_2 (3,2) S(1)
23920	5.34	···	···	0.145	···	···	···	···	···	···	···	3.80	Pf23 H I
24031	5.65	···	···	0.101	···	···	···	···	···	···	···	4.21	Pf22 H I
24065	···	0.389	0.149	0.243	1.39	0.963	1.03	3.00	···	0.165	5.20	6.36	H_2 (1,0) Q(1)
24130	···	0.154	0.0590	···	0.326	0.391	0.285	2.73	···	0.110	1.77	2.17	H_2 (1,0) Q(2)
24160	···	···	···	···	···	···	···	···	···	···	···	4.10	Pf23 H I
24231	···	0.251	0.136	···	0.841	0.475	0.663	···	···	0.165	3.69	2.96	H_2 (1,0) Q(3)

[a]These are the measured wavelengths, with a 1 σ error of $\lesssim$ 5Å.
[b]Fluxes are in units of 10^{-14} erg cm^{-2} s^{-1}, and have not been corrected for extinction.
[c]See Hora & Latter 1996 for an explanation of slit positions
[d]See Hora & Latter 1994 for an explanation of slit positions
[e]Unidentified lines observed in several other PNe (see text).

TABLE 7

H_2 - DOMINATED PN, H II REGION LINE FLUXES[a]

Wavelength [b] (Å)	NGC 2346	AFGL 618 2.4"E	AFGL 618 core	AFGL 2688lobe[c]	AFGL 2688torus[c]	J 900 jet	J 900 lobe	K4-45	M 1-78	Identification
11621	···	1.13	0.708	···	···	···	···	···	···	?
11650	···	0.0797	0.198	···	···	···	···	···	···	?
11748	0.157	0.296	···	···	···	···	···	···	···	?
11854	0.125	0.507	0.635	···	···	···	···	···	···	H_2 (3,1) S(3)
11876	···	···	0.440	···	···	···	···	···	···	? H_2
11930	···	0.196	···	···	···	···	···	···	···	? H_2
11970	···	0.214	···	···	···	···	···	···	···	?
12038	···	0.331	···	···	···	···	···	···	···	?
12069	···	0.479	···	···	···	···	···	···	···	H_2 (3,1) S(2)
12112	···	0.191	···	···	···	···	···	···	···	H_2 (8,5) Q(3)
12258	···	0.194	···	···	···	···	···	···	···	H_2 (4,2) S(5)
12329	···	0.364	0.456	···	···	···	···	···	···	H_2 (3,1) S(1)
12383	···	0.500	0.625	···	···	···	···	···	···	H_2 (2,0) Q(1)
12420	···	···	0.335	···	···	···	···	···	···	H_2 (2,0) Q(2)+(4,2) S(4)
12469	···	0.530	0.560	···	···	···	···	···	···	H_2 (2,0) Q(3)
12529	···	···	0.205	···	···	···	···	···	1.77	He I
12566	···	1.04	1.06	···	···	···	···	···	1.69	[Fe II]
12618	···	0.443	0.594	···	···	···	···	···	···	H_2 (3,1) S(0)+(9,6) S(1) +(4,2) S(3)
12784	0.697	···	···	···	···	···	···	···	5.37	He I
12817	0.258	1.92	6.17	···	···	0.106	···	···	94.9	Pa5 (Pa Beta) H I

TABLE 7—*Continued*

Wavelength [b] (Å)	NGC 2346	AFGL 618 2.4"E	AFGL 618 core	AFGL 2688lobe[c]	AFGL 2688torus[c]	J 900 jet	J 900 lobe	K4-45	M 1-78	Identification
12869	···	0.265	···	···	···	···	···	···	···	H_2 (2,0) Q(7)
12977	···	···	···	···	···	···	···	···	1.01	He I
13155	···	···	0.496	···	···	···	···	···	1.78	O I + H_2 (9,6) Q(1) ?
14881	···	0.212	···	···	···	···	···	···	···	?
15033	···	···	···	···	···	···	···	···	1.45	Br 23 H I
15076	···	···	···	···	···	···	···	···	1.93	Br 22 H I
15126	···	···	···	···	···	···	···	···	1.83	Br21 H I
15190	···	···	···	···	···	···	···	···	2.01	?
15205	···	0.149	···	···	···	···	···	···	···	H_2 (3,1) O(5)
15257	···	···	···	···	···	···	···	···	2.00	?
15280	···	0.122	···	···	···	···	···	···	···	?
15334	···	0.120	0.375	···	···	···	···	···	2.85	?
15432	···	···	···	···	···	···	···	···	3.22	Br17 H I
15549	···	···	···	···	···	···	···	···	4.26	Br16 H I
15877	···	···	0.149	···	···	···	···	···	6.14	H_2 (7,5) S(2) + Br 14 H I
16003	···	···	0.162	···	···	···	···	···	···	?
16102	···	···	···	···	···	···	···	···	7.97	Br 13 H I
16401	···	···	0.440	···	···	···	···	···	10.1	Br 12 H I
16432	···	1.07	1.04	···	···	···	···	···	3.45	[Fe II]
16766	···	0.198	···	···	···	···	···	···	···	?
16798	···	···	0.718	···	···	···	···	···	14.7	Br11 H I
16867	···	0.605	0.808	···	0.420	···	···	···	···	H_2 (1,0) S(9)
17002	···	···	···	···	···	···	···	···	6.68	He I
17131	···	0.465	0.514	···	0.228	···	···	···	···	H_2 (1,0) S(8)
17356	···	···	0.910	···	···	···	···	···	22.2	Br10 H I
17467	0.412	2.41	3.09	1.31	1.80	···	···	···	···	H_2 (1,0) S(7) + (7,5) Q(3)
17866	···	1.38	2.02	0.73	1.20	···	···	···	···	H_2 (1,0) S(6)
19443	0.159	0.489	1.60	0.803	0.720	···	···	···	44.0	Br 8 H I
19541	0.092	···	···	···	···	···	···	···	6.45	He I
19570	0.831	17.1	18.5	8.76	13.2	0.621	0.688	···	···	H_2 (1,0) S(3)
19675	···	0.135	0.171	···	···	···	···	···	···	H_2 ?
20028	···	0.428	···	···	0.228	···	···	···	···	H_2 (2,1) S(4)
20334	0.794	4.67	5.15	2.41	3.84	0.237	0.247	···	1.29	H_2 (1,0) S(2)
20580	···	···	0.325	···	···	0.0316	···	···	75.7	He I

TABLE 7—*Continued*

Wavelength [b] (Å)	NGC 2346	AFGL 618 2.4"E	AFGL 618 core	AFGL 2688lobe[c]	AFGL 2688torus[c]	J 900 jet	J 900 lobe	K4-45	M 1-78	Identification
20643	···	0.189	···	···	···	0.0185	···	···	···	?
20732	0.169	1.43	1.61	1.02	1.20	0.0460	···	···	···	H_2 (2,1) S(3)
21124	···	0.0933	···	···	···	0.0309	···	···	5.08	He I
21218	2.07	13.1	17.2	7.30	12.0	0.537	0.484	1.41	5.23	H_2 (1,0) S(1)
21409	···	···	···	···	···	0.0397	···	···	···	?
21440	···	···	0.409	···	···	···	···	···	0.969	?
21542	0.0855	0.561	0.657	···	0.384	···	···	···	···	H_2 (2,1) S(2)
21658	0.0804	0.217	2.79	···	···	···	···	···	111	Br7 (Brγ) H I
21892	···	···	0.206	···	···	···	···	···	···	?
22014	···	0.310	0.318	···	0.204	···	···	···	···	H_2 (3,2) S(3)
22172	···	···	0.451	···	···	···	···	···	2.79	?
22234	0.444	2.90	3.81	1.61	2.64	0.112	0.154	···	1.71	H_2 (1,0) S(0)
22426	···	···	0.354	···	···	···	···	···	1.17	H_2 (2,1) S(1)
22479	0.169	1.42	1.71	···	0.996	0.0752	0.0837	···	···	H_2 (2,1) S(1)
22858	···	···	···	···	···	···	···	···	0.796	U[c]
22959	···	···	1.21	···	···	···	···	···	···	CO
23236	···	0.352	1.15	···	···	···	···	···	···	CO
23448	···	···	···	···	···	···	···	···	···	H_2 (4,3) S(3) + (9,7) O(4)
23484	···	···	···	···	···	···	···	···	2.36	?
23512	···	0.287	···	···	···	···	···	···	···	?
23536	···	···	1.47	···	···	···	···	···	1.62	Pf 28 H I
23551	···	0.371	···	···	0.312	···	···	···	···	?
23596	···	···	···	···	···	···	···	···	1.26	Pf 27 H I
23664	···	···	···	···	···	···	···	···	1.30	Pf 26 H I
23736	···	···	···	···	···	···	···	···	1.62	Pf 25 H I
23819	···	···	···	···	···	···	···	···	2.41	Pf 24 H I
23861	···	0.255	···	···	0.336	···	···	···	···	H_2 (3,2) S(1)
23916	···	···	···	···	···	···	···	···	2.12	Pf 23 H I
24065	1.36	12.4	17.4	5.77	9.72	0.295	0.256	1.57	9.90	H_2 (1,0) Q(1) + Pf 22 H I
24130	0.445	3.96	5.47	2.41	3.60	0.195	0.205	0.828	4.18	H_2 (1,0) Q(2)
24231	1.11	11.1	14.5	5.33	9.96	0.298	0.359	1.24	8.03	H_2 (1,0) Q(3)

[a]These are the measured wavelengths, with a 1 σ error of $\lesssim$ 5Å.

[b]Fluxes are in units of 10^{-14} erg cm^{-2} s^{-1}, and have not been corrected for extinction.

[c]See Hora & Latter 1994 for an explanation of slit positions.

[d]Unidentified lines observed in several other PNe (see text).

TABLE 8

H_2 EXCITATION ANALYSIS RESULTS

Object/Position	UV Excitated	$T_{ex}(J)$[1] (K)	2-1 S(1)/1-0 S(1)	O/P[2]	A_V[3] (mag)
NGC 40	No?[4]	2100±700	....		0
NGC 2346	Yes	1260±200	0.08	2.2±0.5	0
NGC 2440T	Yes?[5]	2020±200	....	2.2±0.4	0
NGC 2440N	Yes	1065±200	0.12	2.6±0.2	0
NGC 2440NE	No?	2010±100	0.09	2.5±0.2	0
NGC 6720A	Yes	1245±100	0.11	2.6±0.4	1±1
NGC 6720B	No?[3]	2000±200	....	3.0±0.5	0
NGC 7026	—[6]	....	....		...
NGC 7027T	Yes	800±200	0.07	2.9±0.7	0
NGC 7027WT	Yes	1325±200	0.08	3.0±0.2	0
AFGL 618C	Yes	1865±300	0.10	3.0±0.5	2±1
AFGL 618E	Yes	2130±300	0.11	3.0±0.5	2±2
AFGL 2688	No	2300±100	0.09	3.0±0.4	5+10/-5
BD+30°3639N	Yes[5]	1255±300	0.18	2.8±0.5	6
BD+30°3639E	Yes	1350±200	0.18	2.7±0.2	2±1
BD+30°3639H2	Yes	1070±100	0.18	2.3±0.2	6±5
Hb 12 2.4E	Yes	1395±450	0.47	1.7±0.2	3.7+1.5/-1.0
Hb 12 2.4E 1.0S	Yes	1395±500	0.47		3.7+1.5/-1.0
IC 2003	—	....	....		...
I21282+5050	No?[4]	700±400	....		4
J 900J	No	2200±100	0.14		0
J 900L	No	2500±100	0.17		0
M 1-16C	Yes	600±100	....	3.0±0.5	3
M 1-16S	Yes	630±100	0.24	3.0±0.5	0
M1-92	No?[4]	450+650/-450	....		0
M 2-9N	—	....	0.20		5
M 2-9L	Yes	1220±50	0.11	2.8±0.2	5+7/-5
Vy 2-2	Yes	730±200	0.24		1

[1]For UV excited spectra $T_{ex}(J)$ is the rotational excitation temperature. For collisionally excited spectra $T_{ex}(J) = T_{ex}(v)$.

[2]Listed only for those objects with enough lines well detected to make an estimate of the O/P ratio.

[3]Value of visual attenuation used to deredden the H_2 spectra for the excitation analysis (as determined from the H_2 lines only and using a standard interstellar extinction law; Rieke & Lebofsky 1985). Entries with errors shown are determined to greater accuarcy than those without, which should be considered highly uncertain. In no case does the value of A_V change the basic results of the analysis.

[4]v = 1 detections only.

[5]v = 8 transition(s) detected.

[6]— means there are not enough lines detected to make an excitation analysis.